

Final Report

**Protection of Reinforced Concrete Bridge Substructures using
Submerged Bulk Anodes
(BD 546-3)**

submitted to

**Florida Department of Transportation Research Center
605 Suwannee Street
Tallahassee, Florida 32399**

submitted by

**Francisco Presuel-Moreno
Center for Marine Materials
Department of Ocean Engineering
Florida Atlantic University – Sea Tech Campus
101 North Beach Road
Dania Beach, Florida 33004**

**William H. Hartt
Hartt & Associates, Inc.
20914 Morada Court
Boca Raton, Florida 33433**

January 25, 2009

Disclaimer

The opinions, findings, and conclusions expressed in this publication are those of the author and not necessarily those of the State of Florida Department of Transportation.

SI* (MODERN METRIC) CONVERSION FACTORS

APPROXIMATE CONVERSIONS TO SI UNITS

Symbol	When You Know	Multiply By	To Find	Symbol
LENGTH				
in	inches	25.4	millimeters	mm
ft	feet	0.305	meters	m
yd	yards	0.914	meters	m
mi	miles	1.61	kilometers	km
AREA				
in ²	square inches	645.2	square millimeters	mm ²
ft ²	square feet	0.093	square meters	m ²
yd ²	square yard	0.836	square meters	m ²
ac	acres	0.405	hectares	ha
mi ²	square miles	2.59	square kilometers	km ²
VOLUME				
fl oz	fluid ounces	29.57	milliliters	mL
gal	gallons	3.785	liters	L
ft ³	cubic feet	0.028	cubic meters	m ³
yd ³	cubic yards	0.765	cubic meters	m ³
NOTE: volumes greater than 1000 L shall be shown in m ³				
MASS				
oz	ounces	28.35	grams	g
lb	pounds	0.454	kilograms	kg
T	short tons (2000 lb)	0.907	megagrams (or "metric ton")	Mg (or "t")
TEMPERATURE (exact degrees)				
°F	Fahrenheit	5 (F-32)/9 or (F-32)/1.8	Celsius	°C
ILLUMINATION				
fc	foot-candles	10.76	lux	lx
fl	foot-Lamberts	3.426	candela/m ²	cd/m ²
FORCE and PRESSURE or STRESS				
lbf	poundforce	4.45	newtons	N
lbf/in ²	poundforce per square inch	6.89	kilopascals	kPa

APPROXIMATE CONVERSIONS FROM SI UNITS

Symbol	When You Know	Multiply By	To Find	Symbol
LENGTH				
mm	millimeters	0.039	inches	in
m	meters	3.28	feet	ft
m	meters	1.09	yards	yd
km	kilometers	0.621	miles	mi
AREA				
mm ²	square millimeters	0.0016	square inches	in ²
m ²	square meters	10.764	square feet	ft ²
m ²	square meters	1.195	square yards	yd ²
ha	hectares	2.47	acres	ac
km ²	square kilometers	0.386	square miles	mi ²
VOLUME				
mL	milliliters	0.034	fluid ounces	fl oz
L	liters	0.264	gallons	gal
m ³	cubic meters	35.314	cubic feet	ft ³
m ³	cubic meters	1.307	cubic yards	yd ³
MASS				
g	grams	0.035	ounces	oz
kg	kilograms	2.202	pounds	lb
Mg (or "t")	megagrams (or "metric ton")	1.103	short tons (2000 lb)	T
TEMPERATURE (exact degrees)				
°C	Celsius	1.8C+32	Fahrenheit	°F
ILLUMINATION				
lx	lux	0.0929	foot-candles	fc
cd/m ²	candela/m ²	0.2919	foot-Lamberts	fl
FORCE and PRESSURE or STRESS				
N	newtons	0.225	poundforce	lbf
kPa	kilopascals	0.145	poundforce per square inch	lbf/in ²

*SI is the symbol for the International System of Units. Appropriate rounding should be made to comply with Section 4 of ASTM E380.
(Revised March 2003)

Technical Report Documentation Page

1. Report No.	2. Government Accession No.	3. Recipient's Catalog No.	
4. Title and Subtitle Protection of Reinforced Concrete Bridge Substructures using Submerged Bulk Anodes		5. Report Date January, 2009	
		6. Performing Organization Code FAU-OE-CMM-08-3	
7. Author(s) Francisco Presuel-Moreno and William H. Hartt		8. Performing Organization Report No.	
9. Performing Organization Name and Address Center for Marine Materials Florida Atlantic University – Sea Tech Campus 101 North Beach Road Dania Beach, Florida 33004		10. Work Unit No. (TRAIS)	
		11. Contract or Grant No. BD 546-3	
12. Sponsoring Agency Name and Address Florida Department of Transportation 605 Suwannee Street, MS 30 Tallahassee, FL 32399		13. Type of Report and Period Covered Final Report October 1, 2004 – December 31, 2008	
		14. Sponsoring Agency Code	
15. Supplementary Notes			
16. Abstract Reinforced concrete bridge substructures in Florida coastal waters have historically experienced deterioration as a consequence of embedded steel corrosion and resultant concrete cracking and spalling. Ultimately, this deterioration leads to added maintenance costs, reduced service life, and unsafe conditions unless intervention measures are instituted. Galvanic anode cathodic protection (CP), as affected by thermally sprayed zinc for cast-in-place substructure components and zinc mesh jackets for precast ones, is being employed to control this corrosion and extend useful service life. For both types of systems, a submerged bulk zinc anode (SBA) is included to polarize the reinforcement below the waterline and thereby reduce current drain from the lower portion of the thermal spray or zinc mesh. The objective of this research was to determine the extent to which SBAs alone provide protection to the above waterline region of bridge substructures. If adequate or even partial protection is afforded by this means, then considerable cost savings could be realized because of the reduced expense and ease of installation of SBAs compared to zinc thermal spray and CP jackets. To investigate this, two substructure piers on the Bahia Honda Bridge and two on the Niles Channel Bridge, both in the Florida Keys, that were comprised of cast-in-place footers and columns were instrumented with SBAs alone and monitored to determine the level of protection that resulted. For the former bridge, zinc was the SBA type and for the latter magnesium. It was determined that the entire footer reinforcement received protection and that polarization extended up the columns to a certain degree, more so for magnesium than zinc anodes. In addition, the substructures and resultant polarization from the SBAs were modeled using Boundary Element Analysis and two numerical methods. The model results were compared with the field measurements, and the two data sets were determined to be in general agreement. It was concluded that SBAs have utility for extending the useful service life of reinforced concrete bridge substructure elements.			
17. Key Word Bridge substructures, concrete, sea water, corrosion, galvanic anodes, cathodic protection, zinc, magnesium		18. Distribution Statement No restrictions. This document is available to the public through NTIS, Springfield, VA 22161	
19. Security Classif. (of this report) Unclassified	20. Security Classif. (of this page) Unclassified	21. No. of Pages	22. Price

ACKNOWLEDGEMENTS

The authors are indebted to ConcorrFlorida, Inc. and to the FDOT State Materials Office for logistical support during the field portion of this study and, in particular Mr. Rodney Powers, Ivan Lasa, Ronald Simmons, and Dennis Baldi. The assistance of Mr. George Jones of this laboratory is also acknowledged.

EXECUTIVE SUMMARY

Premature deterioration of concrete bridge substructures in coastal locations as a consequence of sea water (chloride) exposure and corrosion of reinforcing steel has been recognized for several decades as a formidable technological challenge and costly maintenance issue. In response to this, the Florida Department of Transportation (FDOT) has now developed more stringent and comprehensive guidelines for materials selection and design such that bridge substructures build within the past ten or so years are expected to experience relatively maintenance-free service for the design life, which may be 75-100 years. At the same time, however, the State has a significant inventory of older bridges for which chloride induced reinforcing steel corrosion followed by concrete cracking and spalling has occurred; and it is necessary that these be maintained cost effectively in a serviceable condition until functionality has expired.

Cathodic protection (CP) is the only proven technology for which long-term service data exist that can control reinforcing steel corrosion in chloride contaminated concrete. Because of this, a series of studies have been performed over the course of the past several decades to identify the most cost effective, practical approach(s) to marine bridge substructure cathodic protection. On the basis of these, the FDOT now widely employs galvanic anode CP in the form of zinc mesh lined fiberglass jackets for precast components and thermally sprayed zinc for cast-in place ones; and these have been judged to extend service life. However, because preliminary research and field trials indicated unacceptably high current drain from the lower elevation region of both the Zn mesh in jackets and thermal spray zinc due to relatively low resistivity of wet concrete and the large amount of reinforcement in the submerged zone, one or more zinc submerged bulk anodes (ZnSBAs) are included on each substructure element. These polarize the submerged portion of the substructure components and significantly reduce the current drain. Consequently, system life is extended compared to what would otherwise be the case.

Field data that have been collected over the past decade or so have indicated that the ZnSBAs may be providing some corrosion protection to higher than anticipated elevations above the waterline. This has prompted several questions including:

1. What level of protection is being afforded by ZnSBAs to the above waterline zone?
2. To what elevation does this protection or partial protection extend?

3. Can SBAs be employed as a stand-alone corrosion control option and, if so, under what conditions?
4. How much can be gained using magnesium SBAs (MgSBAs) rather than Zn ones, considering that driving voltage for the former is about one-half volt greater than for the latter.

The motivation for answering these questions is compounded by the relatively low cost of SBA installation compared to that for CP jackets and thermal spray. Even if the protection afforded by SBAs is only partial, such an approach could have utility as a temporary corrosion control option or in situations where service life extension for a relatively brief period is warranted.

This research was initiated in response to the above questions for the purpose of better defining the utility of SBAs for affecting cathodic protection to reinforced concrete marine bridge substructures. The project consisted of both a field trial and numerical modeling, the purpose of the latter being to analytically project the extent of polarization for the above waterline reinforcement. The field trials utilized two piers on the Bahia Honda (BH) and Niles Channel (NC) Bridges in the Florida Keys. Reinforcement for the former is black bar and for the latter epoxy-coated. The BH bridge consists of prestressed piles, cast-in-place footers and columns, and an interconnecting precast strut. An arc-spray zinc – ZnSBA system was in the process of being installed on some of the BH substructure units during the time-frame of this project. In this case, preliminary baseline data were acquired and potential and current monitoring probes were installed at different elevations on the footers and columns prior to connection of the ZnSBAs to the reinforcement. This was followed by data collection at different times after connecting to the ZnSBAs (there was no arc-spray zinc on these two substructures).

Piers of the second bridge (NC) consisted of pairs of drill shafts and column on each and an interconnecting strut. Two piers (Pier 2 and Pier 12) were identified that were relatively undamaged. Thermal sprayed Zn (TSZ), but without a SBA, had previously been applied to one column of Pier 12 but not to the other or to the columns of Pier 2. Subsequent to acquisition of baseline potential and concrete resistivity data, two magnesium submerged bulk anodes (MgSBAs), were installed on each of these piers. The choice of magnesium considered that these anodes have approximately one-half volt more negative potential than Zn; and so protection should extended to a higher elevation on the footer/column than with ZnSBAs. Potential and current data were acquired at several times subsequent to connecting the MgSBAs.

The field data that were collected during the project clearly indicated that the SBAs polarized the footer reinforcement of the BH Bridge and drill shaft reinforcement of the NC by a minimum of several hundred millivolts, even at the highest elevation, which approached one meter above mean sea level. However, protection of the column steel on the BH bridge (ZnSBAs) was nil above about 0.3 m from the base (top of the footer). This protection may have been negatively impacted by the fact that the columns had been gunited as a previous repair and that the repair material was of relatively high resistivity and disbanded over much of the relevant column surface area such that CP current was precluded from reaching these higher column reinforcement elevations. For the NC bridge pier with TSZ, the drill shafts were protected; but polarization of the column steel above the drill shaft was modest to nil, presumably because the Zn served as a current drain. Polarization of columns on the pier with MgSBAs only was in some cases to a meter or more above the top of the footer; however, the data were difficult to interpret because of apparent lack of reinforcement electrical continuity.

The analyses consisted of Boundary Element Modeling (BEM) using Beasy™ software for the BH bridge and two finite difference methods for the NC. By this, models of the footer and column on each bridge was generated from the construction drawings; and the extent to which the SBAs polarized the reinforcing steel was projected. Good agreement between the field data and model results was obtained.

It is concluded that SBAs have utility for corrosion control of Cl⁻ contaminated concrete bridge substructures in marine environments with partial protection potentially extending to as high as two meters or more above the mean waterline. This elevation to which polarization is affected should depend upon the level of chloride contamination and concrete resistivity. For the present investigation, this elevation may have been greater if, first, data acquired from columns of the BH bridge had been from sound rather than disbanded gunite repairs and, second, electrical continuity had been affected for the NC bridge. A more comprehensive field and numerical modeling program should be initiated to 1) build upon the findings of this study, 2) investigate the effectiveness of this protection concept for other types of substructure elements, and 3) develop methods whereby SBAs can be utilized as a stand-alone protection option for columns with expiring TSZ.

TABLE OF CONTENTS

	<u>page no.</u>
EXECUTIVE SUMMARY	vi
BACKGROUND AND INTRODUCTION	1
PROJECT SCOPE	6
FIELD STUDY	10
Bahia Honda Bridge	10
Procedures	10
Results	15
Niles Channel Bridge	28
Procedures	28
Results	32
West (Gulf Side) Footer/Column, Pier 2	32
East (Atlantic Side) Footer/Column, Pier 2	42
West (Gulf Side) Footer/Column, Pier 12	51
East (Atlantic Side) Footer/Column, Pier 12	57
NUMERICAL MODELING	70
Bahia Honda Bridge	70
Niles Channel Bridge	73
General	73
2D Finite Difference Model	74
System Dimensions	74
Concrete Properties	75
Electrochemical Variables	76
2D FD Computational Procedure	76
1-D Model Description and Implementation	77
Results	77
CONCLUSIONS	80
Bahia Honda Bridge	80
Niles Channel Bridge	81
Summarizing	81
REFERENCES	83

LIST OF FIGURES

	<u>page no.</u>
Figure 1: Photograph of a cracked and spalled marine bridge piling	1
Figure 2: Seven Mile Bridge pier with thermal spray zinc applied to the two columns and strut	3
Figure 3: Schematic illustration of a zinc mesh jacket	3
Figure 4: Photograph of a zinc mesh jacket installation (courtesy of D. Leng)	4
Figure 5: Photograph of an installed zinc mesh jacket	4
Figure 6: Schematic illustration of a thermal spray Zn/SBA GACP system on a substructure	5
Figure 7: General view of the Bahia Honda Bridge	6
Figure 8: Photograph of a footer/column/strut unit on the Bahia Honda Bridge	7
Figure 9: Photograph of the Niles Channel Bridge taken from the old bridge and looking towards Key West	8
Figure 10: Photograph of a typical pier on the Niles Channel Bridge	8
Figure 11: Photograph of the threaded stainless steel ground connection rod on the column of Pier 40W-East	10
Figure 12: Photograph of Pier 40W-East of the Bahia Honda Bridge subsequent to drilling the four pairs of probe core holes	11
Figure 13: Photograph of a monitoring probe prior to embedment	12
Figure 14: Photograph of two core holes with positioned reinforcing steel probes	12
Figure 15: Photograph of the junction box installation and probe wiring on Pier 40W-East	13
Figure 16: Photograph of the upper two core holes, grouted wire routing slots, and junction box on Pier 40W-East subsequent to installation	13
Figure 17: Photograph of Pier 40W-East upon completion of probe installation, wiring, and grouting	14
Figure 18: Photograph of Pier 39W-East upon completion of probe installation, wiring, and grouting	14

LIST OF FIGURES (continued)

	<u>page no.</u>
Figure 19: Free corrosion potential versus elevation for footer and column on each of the two piers. Elevation is referenced to the bottom of the footer	16
Figure 20: Schematic representation of the corrosion potential (ϕ_{corr}) and potential-current kinetics relationships for steel in concrete	17
Figure 21: Footer and column reinforcing steel potential data for Pier 40W-East as a function of elevation for each of the three site visits. Elevation is referenced to the bottom of the footer	19
Figure 22: Footer and column reinforcing steel potential data for Pier 39W-East as a function of elevation for each of the three site visits. Elevation is referenced to the bottom of the footer	20
Figure 23: Schematic illustration of the potential shift of footer and column reinforcement that is expected to accompany SBA activation	21
Figure 24: Resistivity versus elevation data for various positions on Pier 40W-East of the Bahia Honda Bridge as acquired during the May, 2005 site visit(top of the footer is at approximately 0.6 m elevation).....	23
Figure 25 Resistivity versus elevation data for Pier 40W-East of the Bahia Honda Bridge as measured during each of the three site visits (top of the footers at approximately 0.6 elevation).....	23
Figure 26: Polarized potential data for reinforcement and probes (isolated, connected, and depolarized) for Pier 40W-East	24
Figure 27: Polarized potential data for reinforcement and probes (isolated, connected, and depolarized) for Pier 39W-East	25
Figure 28: Plot of 1) isolated and 2) connected and depolarized probe potentials according to elevation for both piers at the time of the February, 2005 site visit. Average values for the reinforcement on this same pier are also indicated. Elevation is referenced to the bottom of the footer	26
Figure 29: Schematic illustration of the probe potential shift that accompanies coupling to pier reinforcement	27
Figure 30: Plot of probe current density versus elevation	28
Figure 31: Photograph of a 22.6 kg pier type Mg anode as-received	29

LIST OF FIGURES (continued)

	<u>page no.</u>
Figure 32: Schematic illustration of the MgSBA installation scheme	30
Figure 33: Photograph of Pier 2 subsequent to MgSBA installation	30
Figure 34: Plan view schematic illustration of a pier on the Niles Channel Bridge showing the orientations at which potential and resistivity measurements were made	31
Figure 35: Free corrosion potential data for the west footer/column of Pier 2 as acquired during the August 7 and 8, 2007 site visit	33
Figure 36: Average free corrosion potential data as a function of elevation from Figure 35	33
Figure 37: Plot of current-on potentials at each measurement elevation on the west footer/column of Pier 2 for each of the site visits in comparison to the free corrosion values	35
Figure 38: Comparison of current-on and current-off potentials for the west footer/column of Pier 2	38
Figure 39: Magnitude of polarization after 369 days activation as a function of elevation for the west footer/column of Pier 2	38
Figure 40: Magnitude of depolarization as a function of elevation after 132 and 369 days activation	40
Figure 41: Resistivity data acquired on the west footer/column of Pier 2 during the 8/07 site visit	42
Figure 42: Average resistivity data as acquired on the west footer/column of Pier 2 during different site visits	43
Figure 43: Free corrosion potential data for the east footer/column of Pier 2 as acquired during the August 7 and 8, 2007 site visit	44
Figure 44: Average free corrosion potential data for the east footer/column of Pier 2 as acquired during the August 7 and 8, 2007 site visit	45
Figure 45: Plot of current-on potentials at each measurement elevation on the west footer/column of Pier 2 for each of the site visits in comparison to the free corrosion values	47
Figure 46: Comparison of current-on and current-off potentials for the east footer/column of Pier 2	48

LIST OF FIGURES (continued)

	<u>page no.</u>
Figure 47: Magnitude of depolarization as a function of elevation after 132 and 369 days activation for the east footer/column of Pier 2	50
Figure 48: Resistivity data as acquired on the east footer/column of Pier 2 on August 7, 2007 (top of the drill shaft is at approximately 0.75 m elevation).....	52
Figure 49: Average resistivity data as acquired during each of the four site visits (top of the drill shaft is at approximately 0.75 m elevation).....	52
Figure 50: Free corrosion potential data for the east footer/column of Pier 12 as acquired during the August 7, 2007 site visit	53
Figure 51 Plot of current-on potentials at each measurement elevation on the west footer/column of Pier 12 for each of the site visits in comparison to the free corrosion values	55
Figure 52: Comparison of current-on and current-off potentials for the west footer/column of Pier 12	57
Figure 53: Magnitude of depolarization as a function of elevation after 132 and 369 days activation for the west footer/column of Pier 12	59
Figure 54: Free corrosion potential data for the east footer/column of Pier 12 as acquired during the August 7, 2007 site visit	61
Figure 55 Plot of current-on potentials at each measurement elevation for the east footer/column of Pier 12 for each of the site visits in comparison to the free corrosion values	63
Figure 56: Comparison of current-on and current-off potentials for the east footer/column of Pier 12	65
Figure 57: Magnitude of depolarization as a function of elevation after 132 and 369 days activation for the east footer/column of Pier 12	67
Figure 58: Resistivity data as acquired on the east footer/column of Pier 12 on December 18, 2007	68
Figure 59: Average resistivity data as acquired on the east footer/column of Pier 12 during each of three site visits	69
Figure 60: Assumed polarization curve for steel and anode that were employed in the BEM analysis	71

LIST OF FIGURES (continued)

	<u>page no.</u>
Figure 61: Beasy modeling results for potential on a footer and column concrete of the Bahia Honda Bridge	71
Figure 62: BEM model of the footer and column reinforcement and the submerged bulk anodes on a pier of the Bahia Honda Bridge	72
Figure 63: Enlarged view of the color coded potential scale from Figures 61 and 62	72
Figure 64: Comparison of the BEM potential versus elevation projection with the field survey results	73
Figure 65: Comparison of the BEM potential versus elevation projections for a MgSBA and ZnSBA	74
Figure 66. Resistivity and diffusivity profiles assumed for the 2D FD model. Active and passive regions are also indicated	75
Figure 67. Resistivity profiles used with the 1D model	78
Figure 68: Comparison of 1D model results and experimental potential values after four hours of energizing the system (the average field measurement results are indicated by the series with symbols and connecting line)	78
Figure 69 Potential profiles 2D FD vs experimental potential profiles (squares indicate experimental values)	79

LIST OF TABLES

	<u>page no.</u>
Table 1: Comparison of electrochemical properties for Zn and Mg bulk anodes	9
Table 2: Listing of free corrosion potentials as recorded during the 8/04 site visit: (a) Pier 39W-East and (b) Pier 40W-East	15
Table 3: Listing of the reinforcement polarized potentials as a function of elevation for Pier 40W-East as recorded during the 2/05 site visit (elevation measured from the bottom of the footer)	18
Table 4: Listing of the reinforcement polarized potentials as a function of elevation for Pier 40W-East as recorded during the 5/05 site visit (elevation measured from the bottom of the footer)	18
Table 5: Listing of reinforcement polarized potentials as a function of elevation for Pier 39W-East as measured during the 2/05 site visit	19
Table 6: Listing of reinforcement polarized potentials as a function of elevation for Pier 39W-East as recorded during the 5/05 site visit	20
Table 7: Resistivity data for various elevations and orientations that were on pier 40W-East as acquired during the May, 2005 site visit	22
Table 8: Average resistivity as measured during each of the three site visits	22
Table 9: Probe potential data as acquired for Pier 40W-East during the (a) 2/05 site visit and (b) 5/05 site visit	24
Table 10: Probe potential data as acquired for Pier 39W-East during the 5/05 site visit	25
Table 11: Listing of probe current densities	27
Table 12: Listing of Niles Channel Bridge site visit dates and tasks performed	31
Table 13: Free corrosion potentials at various elevations from the west (Gulf) footer/column of Pier 2 on August 7, 2007	32
Table 14: Free corrosion potentials at various elevations from the west (Gulf) footer/column of Pier 2 on August 8, 2007	32
Table 15: Current-on potential at each of the measurement orientations and elevations after (a) two hours, (b) 16 days, (c) 132 days, and (d) 369 days activation	34
Table 16: Net current output at different times after anode activation for Pier 2	36

LIST OF TABLES (continued)

	<u>page no.</u>
Table 17: Listing of current-on and current-off potentials for the west footer/column of Pier 2 after (a) 16, (b) 132, and (c) 369 days activation	37
Table 18: Magnitude of depolarization after (a) 132 days activation and 24 hours depolarization, (b) 132 days activation and 45 days depolarization, (c) 369 days activation and 24 hours depolarization, and (d) 369 days activation and 48 hours depolarization	39
Table 19: Resistivity data acquired from the west footer/column of Pier 2 on: (a) 8/07, (b) 12/07, (c) 2/08, and (d) 8/08	41
Table 20: Free corrosion potentials at various elevations from the east (Atlantic side) footer/column of Pier 2 on August 7, 2007 (no data for the E orientation were recorded)	43
Table 21: Free corrosion potentials at various elevations from the east (Atlantic side) footer/column of Pier 2 on August 8, 2007 (no data for the E orientation were recorded)	44
Table 22: Current-on potential at each of the measurement elevations on the east footer/column of Pier 2 after (a) two hours, (b) 16 days, (c) 132 days, and (d) 369 days activation	45
Table 23: Listing of current-on and current-off potentials for the east footer/column of Pier 2 after (a) 16, (b) 132, and (c) 369 days activation	47
Table 24: Magnitude of depolarization after (a) 132 days activation and 24 hours depolarization, (b) 132 days activation and 45 days depolarization, (c) 369 days activation and 24 hours depolarization, and (d) 369 days activation and 48 hours depolarization	49
Table 25: Resistivity data acquired from the east footer/column of Pier 2 on (a) 8/07, (b) 12/07, (c) 2/08, and (d) 8/08	51
Table 26: Free corrosion potentials at various elevations from the west (Gulf side) footer/column of Pier 12 as measured on August 7, 2007	53
Table 27: Current-on potential at each of the measurement orientations/elevations on the west footer/column of Pier 12 after (a) four hours, (b) 16 days, (c) 132 days, and (d) 369 days activation	54

LIST OF TABLES (continued)

	<u>page no.</u>
Table 28: Listing of current-on and current-off potentials for the west footer/column of Pier 12 after (a) 16, (b) 132, and (c) 369 days activation	56
Table 29: Magnitude of depolarization after (a) 132 days activation and 24 hours depolarization, (b) 132 days activation and 45 days depolarization, (c) 369 days activation and 24 hours depolarization, and (d) 369 days activation and 48 hours depolarization	58
Table 30: Resistivity data acquired from the west footer/column of Pier 12 on each of the three site visits for which measurements were made along with the overall average: (a) 12/07, (b) 2/08, and (c) 8/08	60
Table 31: Free corrosion potentials at various elevations from the east (Atlantic side) footer/column of Pier 12 acquired on August 7, 2007	61
Table 32: Current-on potential at each of the measurement elevations on the east footer/column of Pier 12 after (a) four hours, (b) 16 days, (c) 132 days, and (d) 369 days activation	62
Table 33: Listing of current-on and current-off potentials for the east footer/column of Pier 12 after (a) 16, (b) 132, and (c) 369 days activation	64
Table 34: Magnitudes of depolarization after (a) 132 days activation and 24 hours depolarization, (b) 132 days activation and 45 days depolarization, (c) 369 days activation and 24 hours depolarization, and (d) 369 days activation and 48 hours depolarization	65
Table 35: Resistivity data acquired from the east footer/column of Pier 12 on each of the three site visits for which measurements were made along with the overall average: (a) 12/07, (b) 2/08, and (c) 8/08	67
Table 36: Net current output at different times after anode activation for Pier 12	67
Table 37: Kinetic constants for the corrosion reactions	76

BACKGROUND AND INTRODUCTION

Premature deterioration of Florida marine bridge substructures as a consequence of sea water (chloride) exposure and reinforcing steel corrosion has been recognized for several decades as a formidable technological challenge and costly problem. The deterioration sequentially involves the following steps:

1. Progressive Cl⁻ ingress into the concrete until a critical concentration of this species is achieved at the reinforcement depth.
2. Breakdown of the normally protective passive film on the reinforcement and initiation of active corrosion.
3. Accumulation of solid corrosion products in the concrete pore space adjacent to the steel-concrete interface to the point where the concrete tensile strength is reached and cracking occurs.
4. Continued steel cross section loss and progression and interconnection of concrete cracks to the point where concrete spalling results.

Figure 1 shows a photograph of a cracked and spalled prestressed piling and exposed, corroding reinforcement.



Figure 1: Photograph of a cracked and spalled marine bridge piling.

In response to this problem, the Florida Department of Transportation (FDOT) has now developed

more stringent and comprehensive guidelines for materials selection and design such that bridge substructures build within the past ten or so years are expected to be relatively maintenance-free for the design life, which may be 75-100 years. At the same time, however, the State has a significant inventory of older bridges for which chloride induced reinforcing steel corrosion and concrete cracking and spalling have occurred; and it is necessary that these be maintained cost effectively in a serviceable condition until functionality has expired.

Cathodic protection (CP) has been recognized for some 25-plus years as the only method for which long-term service experience exists whereby active corrosion of reinforcing steel in chloride contaminated concrete can be controlled. Nationwide, such CP has been mostly of the impressed current (IC), as opposed to galvanic anode (GA), type because of the relatively high resistivity of concrete and, consequently, the high driving voltage that is normally required to affect adequate polarization of the reinforcing steel. Even with Impressed Current Cathodic Protection (ICCP), anodes must normally be distributed as throwing power; that is, the lateral distance beyond an anode to which current can be delivered, is limited. However, ICCP has shortcomings, which include the following:

1. There must be a source of electrical power.
2. Systems are susceptible to rectifier failure.
3. Excessive polarization may cause hydrogen embrittlement and brittle fracture in the case of prestressed components.
4. System reliability is such that periodic monitoring by trained personnel is required.

These factors either do not apply or are of less significance in the case of Galvanic Anode Cathodic Protection (GACP) systems; however, the fact that driving voltage for these is limited to the native potential difference between the galvanic anode and reinforcement may result in inadequate protection, particularly for high concrete resistivity applications.^{1,2} Also important are, first, a tendency for resistive corrosion products and for moisture depletion to develop in concrete near the anode-concrete interface and, second, limited anode service life due to its corrosion. Specific galvanic anode types that have been investigated include 1) thermally sprayed Zn with or without a humectant,^{1,2,3,4,5,6,7} 2) a thermally sprayed Al-Zn-In alloy,⁸ 3) Zn strip with hydrogel adhesive,⁹ 4) surface mounted penny and expanded Zn sheet,^{4,10,11} 5) Zn mesh with fiberglass jacket,¹² and 6) Zn anode in chemically enhanced mortar.¹³

While there have been studies and applications of GACP for northern bridge decks,¹⁴ the greater utility has been in marine substructure applications. Here, corrosion and concrete cracking and spalling are most advanced in the splash zone where concrete remains wet and of relatively low resistivity. At

present, the various research and development efforts pertaining to the above anode options have largely converged to the system of choice for cast-in-place substructure components being thermally sprayed Zn and for precast pilings Zn mesh lined, grout filled fiberglass jackets. Figure 2 shows a photograph of a pier at the Seven Mile Bridge to which thermal spray zinc has been applied. Note, in this case, that the Zn has been sprayed directly upon the exposed reinforcement (column on the right) without need for concrete repair. Likewise, Figure 3 is a schematic illustration of a zinc mesh jacket; and Figure 4 shows a jacket being installed. A finished, installed CP jacket is shown in Figure 5.



Figure 2: Seven Mile Bridge pier with thermal spray zinc applied to the two columns and strut.

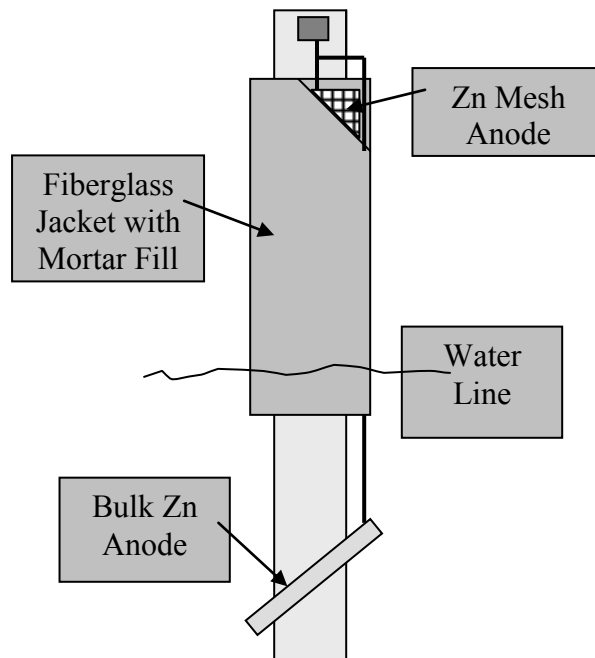


Figure 3: Schematic illustration of a zinc mesh jacket.



Figure 4: Photograph of a zinc mesh jacket installation (courtesy of D. Leng).



Figure 5: Photograph of an installed zinc mesh jacket.

An additional feature of substructure GACP via either thermal spray or jackets is the inclusion of a submerged Zn bulk anode (ZnSBA) as a system component. The purpose of the ZnSBA is to polarize the

below waterline reinforcing steel and thereby reduce current drain and premature depletion of the lower portion of the galvanic anode, either thermal spray or mesh Zn. Figure 6 provides a schematic illustration of a thermal spray-ZnSBA system on a pier that consists of prestressed pilings and a cast-in-place footer and column.

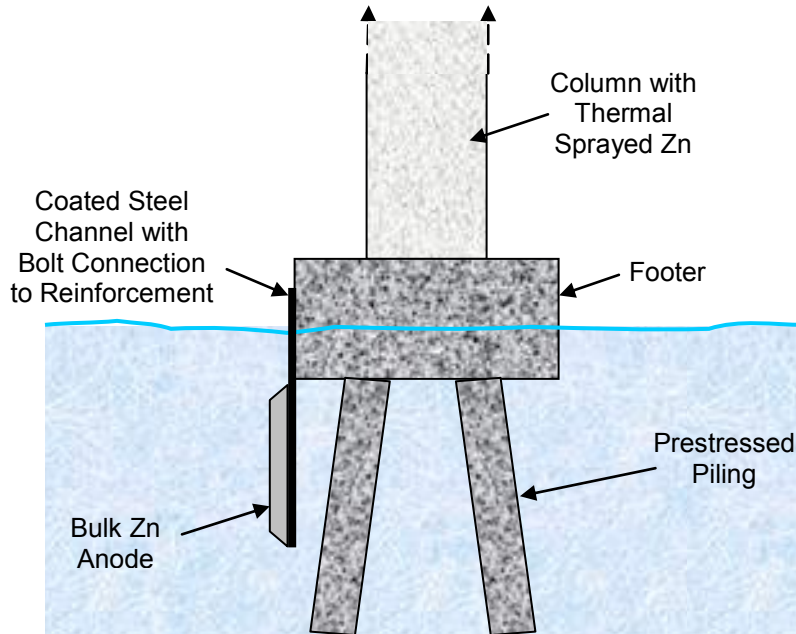


Figure 6: Schematic illustration of a thermal spray Zn/SBA GACP system on a substructure.

The present study was undertaken to better understand the extent to which SBAs, as a stand alone protection source, provide above waterline polarization of reinforcing steel and, where possible, to quantify the role of influential variables. While SBAs, in and of themselves, may not necessarily serve as an all-encompassing CP option, they could provide at least partial protection to a portion of the Cl⁻ contaminated splash zone and possibly more elevated regions and thereby serve as a low cost life extension option.

PROJECT SCOPE

The present research consisted of two components. The first of these involved field assessment of both ZnSBAs, as have been employed previously in conjunction with thermally sprayed zinc (TSZ), and, as a new consideration, magnesium SBAs (MgSBAs). The former were installed on two piers of the Bahia Honda Bridge (BH), upon which a thermal spray Zn-ZnSBA CP system was in the process of being applied and the latter on two piers of the Niles Channel (NC) Bridge. The former bridge (BH) was constructed in 1972 and consists to two approximately 2.4 km long dual lane roadways that extend over essentially open sea water in the lower Florida Keys. The substructure in the center spans consists of pilings/footer/column pairs connected to one another by a strut. The reinforcing steel (black bar) in the columns has corroded and caused concrete cracking and spalling on most piers. For the columns, this damage is concentrated at the lower elevations; and the spalls have been previously repaired by conventional guniting. Visible damage of the footers was limited to an occasional upper corner that has spalled.

A critical determinant in selecting this bridge was that a contractor was in the process of installing a TSZn-ZnSBA CP system on a number of piers at the time that this study initiated. Figure 7 shows a perspective view of the bridge, and Figure 8 is a photograph of a typical substructure unit on which TSZ had been recently applied to the column and strut. Three coated steel channels, each of which supports a



Figure 7: General view of the Bahia Honda Bridge.



Figure 8: Photograph of a footer/column/strut unit on the Bahia Honda Bridge.

ZnSBA, can be seen mounted on the face of the left footer. The now-abandoned Old Bahia Honda Bridge, which is 90-plus years old, is in the background of the latter photograph. For the new bridge, footers are 2.44 m wide (perpendicular to the roadway) by 3.66 m long by 1.52 m high and are reinforced with a cage of 25 mm diameter (#8) bars and a horizontal mat of the same size bars above the top of the prestressed pilings. Design clear cover over the cage bars is 100 mm (4.0 in). The tidal range was estimated to be from near the footer bottom to mid-height. The columns are 0.91 m in diameter and are reinforced with 12 mm diameter (#4) hoop bars on 0.31 m (12 in.) centers and 11 equally spaced 32 mm diameter (#10) vertical bars. Design clear cover over the outer hoop bars is 75 mm (3.0 in.).

The Niles Channel Bridge (NC), on the other hand, is located several miles to the Key West side of the BH and was constructed in 1981, consists of a single lane in both directions, and is approximately 1.3 km long. The superstructure is of segmental box construction, and the substructure is comprised of piers with pairs of drill shafts and columns and an interconnecting strut. The contractor had the option of either precasting the struts or casting in place, and it is not known which construction method was used. The reinforcement is epoxy-coated (ECR). Conventional repairs had been made and TSZ applied to some columns. Only two piers (numbers 2 and 12) were identified as having minimal or no corrosion induced damage, and these were selected for application of MgSBAs. Also, TSZ had previously been applied to the west column of Pier 12, although not the east one; however, there was no SBA. Figure 9 shows a

perspective photograph of the bridge and Figure 10 of an individual pier (number 5). Columns of this particular pier have been previously treated with TSZ. Diameter of the drill shafts was 1.37 m (4'6") and for the columns 1.07 m (3'6"). The reinforcement cage, which was common to both footer and column,



Figure 9: Photograph of the Niles Channel Bridge taken from the old bridge and looking towards Key West.

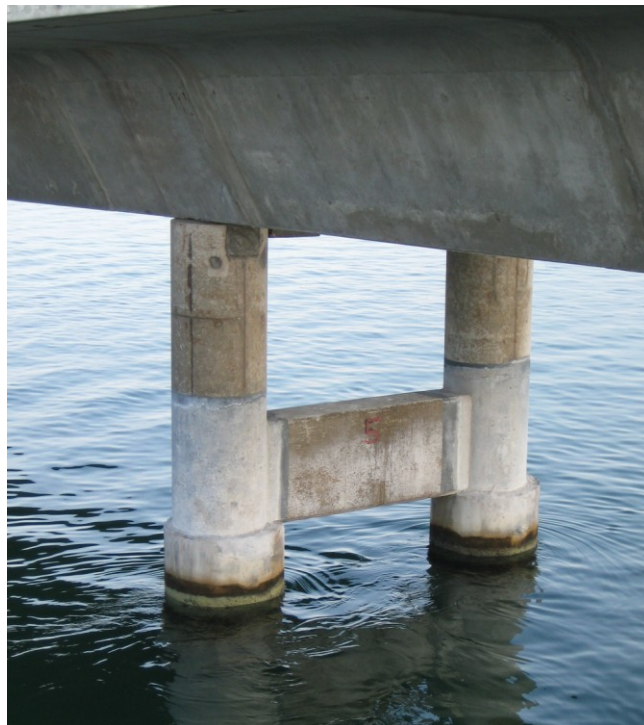


Figure 10: Photograph of a typical pier on the Niles Channel Bridge.

consisted of nine equally spaced 34.9 mm (#11) vertical bars and outer hoop bars for which diameter and spacing is unknown. Design cover for the footers was 152 mm (6.0”) and for the columns 102 mm (4.0”). As such, the columns on the NC amounted to a smaller diameter extension of the footers, whereas these components were more distinct for the BH.

MgSBAs have not been previously employed in conjunction with CP of reinforced concrete substructures on marine bridges. Table 1¹⁵ compares electrochemical properties of Mg and Zn anodes in sea water and indicates the potential advantage of the former over the latter. Thus, while efficiency for Mg is but slightly greater than one-half of that for Zn, current capacity, which is the more important parameter in that this reflects current delivered per unit weight, is about 40 percent greater. However, for reinforcing steel in concrete, where concrete resistivity can be the factor that limits protection, the fact that driving voltage for Mg is approximately one-half volt greater than for Zn is particularly advantageous, especially in situations where the challenge is to deliver current to as high an elevation as possible above water line portion of columns.

Table 1: Comparison of electrochemical properties for Zn and Mg bulk anodes.

	Potential, mV Ag/AgCl	Current Capacity, A-hr/kg	Efficiency, %
Zinc (MIL-A-18001 J)	-1,000 to -1,050	770-820	99
Magnesium (H-1 alloy)	-1,400 to -1,600	1,100	55

The second aspect of the study involved modeling of substructure polarization as affected by the SBAs. Boundary Element Modeling (BEM) was employed for the BH Bridge using commercially available Beasy™ software, whereas two finite difference modeling methods were used for the NC. With regard to the latter, previous studies by Presuel-Moreno et al.¹⁶ and Sagüés et al.¹⁷ applied both a finite difference two dimensional (2-D) model, which accommodated combined activation and concentration cathodic polarization behavior, and a simplified one-dimensional (1-D) model. Both of these methods were employed in the present study. The 2-D model closely replicated the geometry of the footer-column but was computationally demanding, whereas the 1-D model was simplified but required fewer such resources. To the extent possible, field data and modeling results were compared.

FIELD STUDY

Bahia Honda Bridge

Procedures

This bridge was first visited in August, 2004, at which time a contractor was in the process of Zn spraying the columns and struts on a number of piers and installing ZnSBAs. Previously, the east side footer and column of the west bridge on Piers 39 and 40 (designated 39W-East and 40W-East, respectively) had been identified for purposes of this study. By prior arrangement, TSZ was not applied to these piers; but ZnSBAs had been mounted but remained electrically isolated from the steel at the time of this initial visit. Both of these columns had been gunited during repairs that took place during 1986-1987 (no unrepaired components were available at the time of the present study).

Steel potential was measured using a Ag/AgCl reference electrode placed upon a moist sponge at the elevation of interest and a Fluke multimeter. The ground connection was via a threaded stainless steel rod that the contractor had previously fastened into the column reinforcement. Figure 11 shows a photograph of this on Pier 40W-East. Surveys performed by FDOT personnel prior to the contractor beginning the CP installation confirmed reinforcement electrical continuity throughout the columns and footers on individual piers. Concrete resistivity was measured using a CNS Farnell-RM MKII Model U95 four pin meter with a 5 cm (2.0 in.) pin spacing. Readings were taken with the probe in the horizontal orientation. Once a first reading was made, the probe was rotated 180°; and a second reading acquired.



Figure 11: Photograph of the threaded stainless steel ground connection rod on the column of Pier 40W-East.

Reported values are the average of the two at each position. Both measurements (potential and resistivity) were made along five equally spaced vertical lines on the east footer face and three lines spaced about 0.5 m apart on the east-most (Atlantic) side of the columns of the two piers. The two outermost of the five vertical lines on the footers were labeled “KW” and “Mia” according to their facing Key West and Miami, respectively, whereas the middle one was labeled “E” reflecting its orientation, and the two intermediate ones “KW/E” and “E/Mia” according to the lines to either side.

In order to measure the magnitude of current density once the ZnSBAs were connected, reinforcing steel probes were installed in individual 76 mm diameter core holes on each of the east columns on the two piers. Elevations of the core hole pairs on 40W-East were 1.40, 1.65, 2.16, and 2.67 m relative to the bottom of the footer and on 39W-East 1.40 and 2.16 m. The lowest elevation core hole pair was near the top of the footer and the 1.65 m holes on 40W-East were near the bottom of the column. Figure 12 shows a photograph of the 40W-East pier subsequent to coring the holes. The probes were 64 mm lengths of 16 mm diameter (#5) reinforcing steel to which an electrical lead wire was attached at one end and the connection and a portion of the steel coated with epoxy. Figure 13 is a photograph of one probe, and Figure 14 shows two core holes with probes positioned therein. The cabling from each probe was positioned in grooves that were cut in the concrete; and the wiring was routed to a junction box, where one probe of each pair remained isolated and the second was connected to the reinforcement via the threaded stainless steel rod (Figure 11). As such, the disconnected probe of each pair served as a source of baseline potential data (free corrosion), whereas the connected probe was assumed to undergo the same



Figure 12: Photograph of Pier 40W-East of the Bahia Honda Bridge subsequent to drilling the four pairs of probe core holes.



Figure 13: Photograph of a monitoring probe and connection cable prior to embedment.



Figure 14: Photograph of two core holes with positioned reinforcing steel probes.

polarization as the reinforcement itself at that elevation. This configuration allowed a zero resistance ammeter to be inserted in series between this latter probe and the reinforcement during subsequent site visits such that CP current to the probe could be measured. Also, this same probe could be disconnected and the magnitude of depolarization determined. Both CP current and depolarization are indicators of the extent to which embedded steel is cathodically protected. Figure 15 is a photograph taken during the probe and junction box installation. This shows the probes positioned in the core holes and the wiring

being routed to the junction box. The core holes were backfilled with a ready-mix concrete (small coarse aggregate) to which Cl^- as NaCl was admixed. Figure 16 shows a close-up photograph of the upper two probe pair locations on Pier 40W-East upon completion of installation, and Figure 17 provides a general view. Figure 18 does the same for Pier 39W-East.



Figure 15: Photograph of the junction box installation and probe wiring on Pier 40W-East.



Figure 16: Photograph of the upper two core holes, grouted wire routing slots, and junction box on Pier 40W-East subsequent to installation.



Figure 17: Photograph of Pier 40W-East upon completion of probe installation, wiring, and grouting.



Figure 18: Photograph of Pier 39W-East upon completion of probe installation, wiring, and grouting.

It was intended that the project team would make the ZnSBA-reinforcing steel connection at a later time in such a manner that this could be opened and anode current output and reinforcing steel depolarization measured. However, the contractor subsequently connected the ZnSBAs in a permanent manner such that disconnection was not feasible. The exact date of connection is unknown but was in the October-November, 2004 timeframe. Subsequent visits were made to the site in February and May, 2005 at which time polarized rebar potentials and concrete resistivity were measured at the same locations as for the initial visit. In addition, potential of all probes and depolarization and current for the connected probes were measured.

Results

Table 2 lists free corrosion rebar potentials as a function of elevation for both piers as measured during the initial site visit (August, 2004), Figure 19 provides a plot of these. The trend in each case is similar in that potential was relatively constant and negative over the entire footer elevation (footer height was 1.52 m) but was progressively more positive with increasing height on the columns. The relatively negative potentials for the footer reinforcement are thought to reflect the fact that this concrete was water saturated (or nearly so). As such, corrosion rate of the reinforcement is expected to be nil, which is consistent with the fact that no previous repairs had been made on the footers (unlike the columns) and instances of cracking and spalling were few. Alternatively, it may be that only the lower region of the

Table 2: Listing of free corrosion potentials as recorded during the 8/04 site visit: (a) Pier 39W-East and (b) Pier 40W-East.

Elevation, m	Potential, mV (Ag/AgCl)					
	KW	KW/E	E	E/Mia	Mia	Average
0.64	-509	-500	-496	-505	-495	-501
0.89	-492	-488	-488	-481	-497	-489
1.14	-515	-500	-504	-509	-505	-507
1.40	-519	-511	-500	-491	-527	-510
1.65	-	-402	-409	-396	-	-402
1.96	-	-300	-313	-321	-	-311
2.26	-	-289	-288	-377	-	-318
2.57	-	-275	-280	-288	-	-281
2.87	-	-262	-246	-285	-	-264
3.18	-	-252	-278	-274	-	-268
3.48	-	-198	-180	-215	-	-198
3.78	-	-260	-275	-217	-	-251

(a)

Elevation, m	Potential, mV (Ag/AgCl)					
	KW	KW/E	E	E/Mia	Mia	Average
0.64	-500	-507	-494	-521	-542	-513
0.89	-514	-512	-503	-527	-556	-522
1.14	-514	-519	-521	-517	-525	-519
1.40	-484	-495	-489	-493	-520	-496
1.65	-	-473	-422	-416	-	-437
1.96	-	-420	-401	-403	-	-408
2.26	-	-441	-410	-403	-	-418
2.57	-	-421	-394	-391	-	-402
2.87	-	-388	-372	-371	-	-377
3.18	-	-329	-314	-322	-	-322
3.48	-	-286	-275	-287	-	-283
3.78	-	-205	-284	-218	-	-236

(b)

footers was water saturated and that the relatively negative potentials here cathodically polarize the more elevated footer steel. Figure 20 shows a schematically illustrated polarization diagram that explains the potential difference for active versus passive reinforcing steel in both water saturated and unsaturated concrete and why a relatively positive potential is expected for passive steel in aerated concrete and a less positive one for actively corroding steel. This projects the most negative potential to occur in water saturated concrete because, first, embedded steel is likely to be active due to lack of O₂ availability and, second, concentration polarization of the O₂ electrode for the same reason.

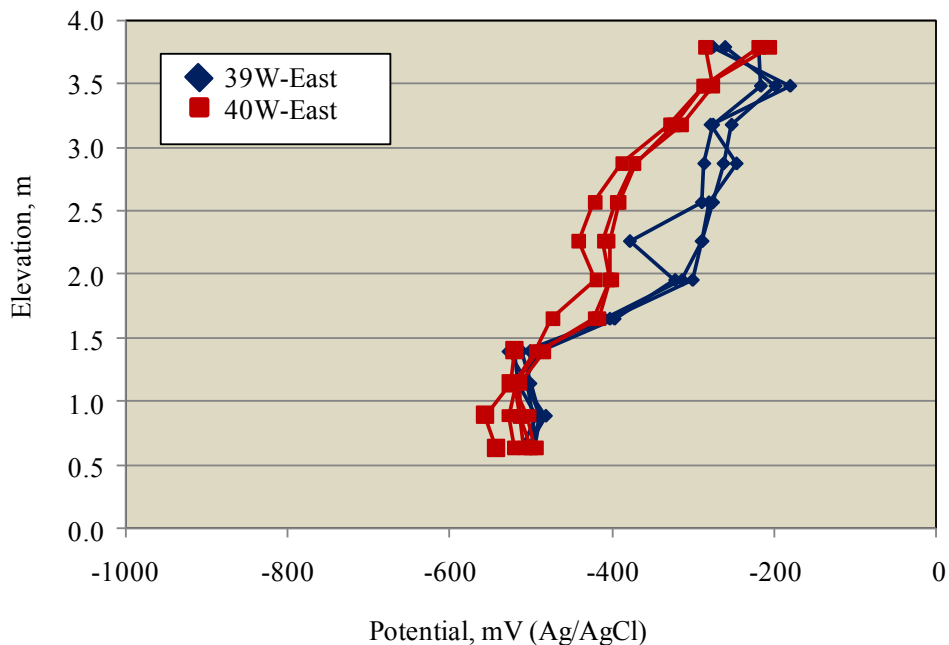


Figure 19: Free corrosion potential versus elevation for the footer and column on each of the two piers. Elevation is referenced to the bottom of the footer.

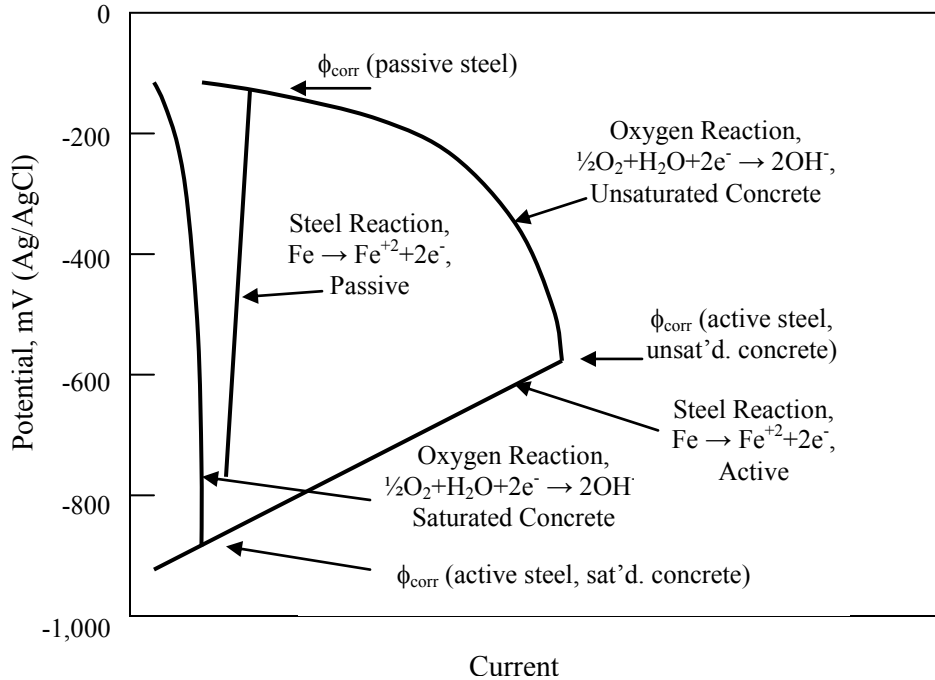


Figure 20: Schematic representation of the corrosion potential (ϕ_{corr}) and potential-current kinetics relationships for steel in concrete.

As noted above, gunite repairs had previously been made on the columns; and this may have affected the corrosion state of the reinforcement in these areas. That this was the case is suggested by the most elevated potential data for the columns (Figure 19), where four of the six readings are more negative than at the next lower elevation, in contrast to the overall trend where potential was progressively more positive the higher the elevation. These highest elevation readings were the only ones on the columns that were taken upon original sound concrete and not from over the repair gunite.

Table 3 lists reinforcement potentials for Pier 40W-East as recorded during the 2/05 site visit and Table 4 does the same for the 5/05 visit. Figure 21 reproduces the data in Figure 19 for Pier 40W-East but with results from the February and May, 2005 site visits (Tables 3 and 4) added, at which times the ZnSBAs were connected to the reinforcement. Likewise, Tables 5 and 6 list reinforcement potentials for Pier 39W-East, as determined at the 2/05 and 5/05 site visits, respectively; and Figure 22 plots these results. In both cases, the polarized potential trends indicate that the footer reinforcement was polarized to the range -830 to -970 $\text{mV}_{\text{AgAgCl}}$ which is close to the measured ZnSBA potential (-975 $\text{mV}_{\text{AgAgCl}}$). As for the freely corroding case, the more positive footer potentials occurred at the higher elevations which is consistent with, first, greater concrete resistivity at higher elevations as documented subsequently, second, there being a greater voltage drop between the higher elevation steel and the ZnSBAs because of the longer, more resistive concrete path and, third, the higher elevation concrete being more aerated such that

greater current should be required to affect the same degree of polarization. Within the bottom 50 cm of the columns a relatively abrupt transition to more positive potentials occurred, which is indicative of reduced polarization and protection. At higher elevations, potentials were more positive than for the originally measured free corrosion values and, as such, indicate a lack of protection. This was particularly true for Pier 40W-East (Figure 21).

Table 3: Listing of the reinforcement polarized potentials as a function of elevation for Pier 40W-East as recorded during the 2/05 site visit (elevation measured from the bottom of the footer).

Elevation, m	Potential, mV(Ag/AgCl)					
	KW	KW/E	E	E/Mia	Mia	Average
0.64	-916	-927	-891	-908	-884	-905
0.89	-881	-893	-862	-884	-849	-874
1.14	-861	-887	-857	-886	-848	-868
1.40	-852	-871	-824	-864	-849	-852
1.65	-	-601	-637	-620	-	-619
1.96	-	-351	-392	-372	-	-372
2.26	-	-270	-313	-294	-	-292
2.57	-	-241	-241	-264	-	-249
2.87	-	-226	-190	-230	-	-215
3.18	-	-178	-184	-188	-	-183
3.48	-	-119	-127	-164	-	-137
3.78	-	-191	-184	-174	-	-183

Table 4: Listing of the reinforcement polarized potentials as a function of elevation for Pier 40W-East as recorded during the 5/05 site visit (elevation measured from the bottom of the footer).

Elevation, m	Potential, mV(Ag/AgCl)					
	KW	KW/E	E	E/Mia	Mia	Average
0.89	-900	-	-925	-	-	-913
1.14	-880	-900	-925	-930	-853	-898
1.40	-830	-880	-890	-875	-832	-861
1.65	-	-460	-660	-630	-	-583
1.96	-	-300	-370	-325	-	-332
2.26	-	-218	-315	-243	-	-259
2.57	-	-206	-185	-191	-	-194
2.87	-	-193	-152	-167	-	-171
3.18	-	-150	-155	-136	-	-147
3.48	-	-78	-98	-112	-	-96
3.78	-	-206	-214	-171	-	-197

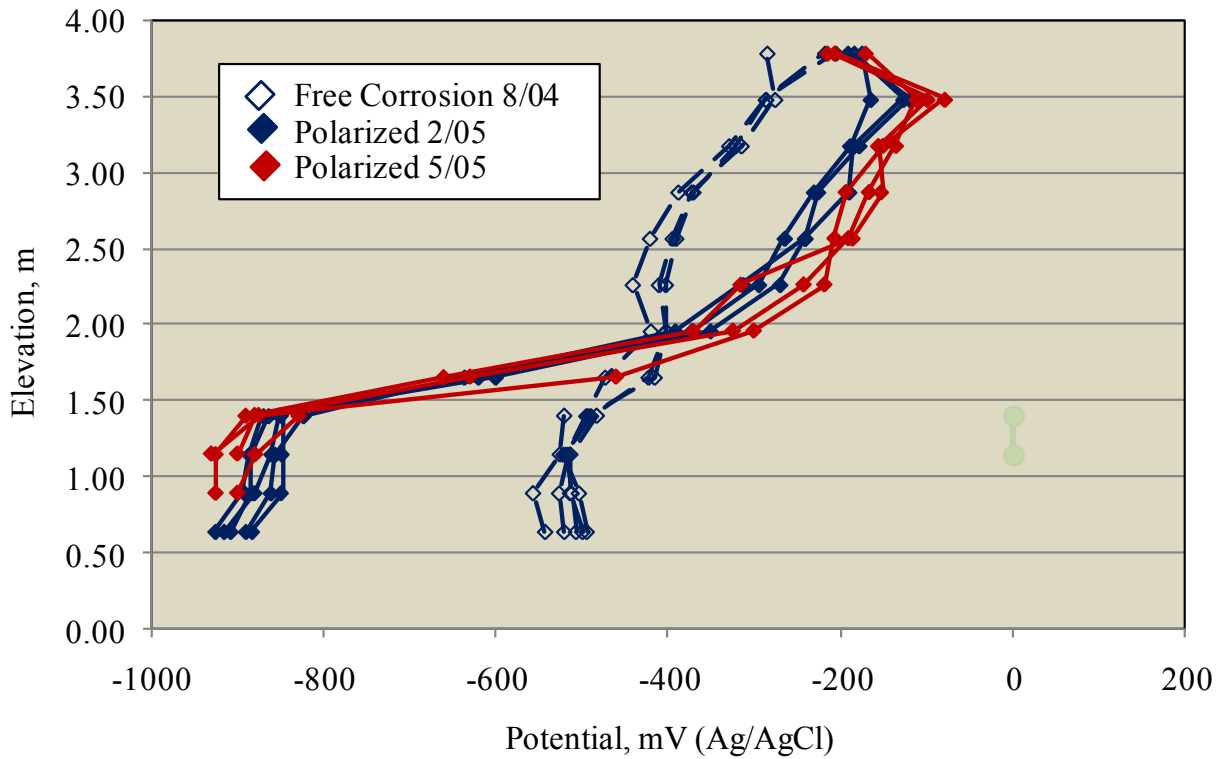


Figure 21: Footer and column reinforcing steel potential data for Pier 40W-East as a function of elevation for each of the three site visits. Elevation is referenced to the bottom of the footer.

Table 5: Listing of reinforcement polarized potentials as a function of elevation for Pier 39W-East as measured during the 2/05 site visit.

Elevation, m	Potential, mV(Ag/AgCl)					
	KW	KW/E	E	E/Mia	Mia	Average
0.64	-916	-927	-891	-908	-884	-905
0.89	-881	-893	-862	-884	-849	-874
1.14	-861	-887	-857	-886	-848	-868
1.40	-852	-871	-824	-864	-849	-852
1.65	-	-601	-637	-620	-	-619
1.96	-	-351	-392	-372	-	-372
2.26	-	-270	-313	-294	-	-292
2.57	-	-241	-241	-264	-	-249
2.87	-	-226	-190	-230	-	-215
3.18	-	-178	-184	-188	-	-183
3.48	-	-119	-127	-164	-	-137
3.78	-	-191	-184	-174	-	-183

Table 6: Listing of reinforcement polarized potentials as a function of elevation for Pier 39W-East as recorded during the 5/05 site visit.

Elevation, m	Potential, mV(Ag/AgCl)					
	KW	KW/E	E	E/Mia	Mia	Average
0.64	-935	-972	-971	-970	-923	-954
0.89	-924	-923	-913	-916	-888	-913
1.14	-910	-917	-915	-903	-862	-901
1.40	-895	-881	-866	-867	-842	-870
1.65	-	-500	-518	-534	-	-517
1.96	-	-367	-352	-377	-	-365
2.26	-	-305	-277	-321	-	-301
2.57	-	-267	-261	-306	-	-278
2.87	-	-235	-206	-231	-	-224
3.18	-	-200	-168	-165	-	-178
3.48	-	-185	-134	-97	-	-139
3.78	-	-136	-154	-68	-	-119

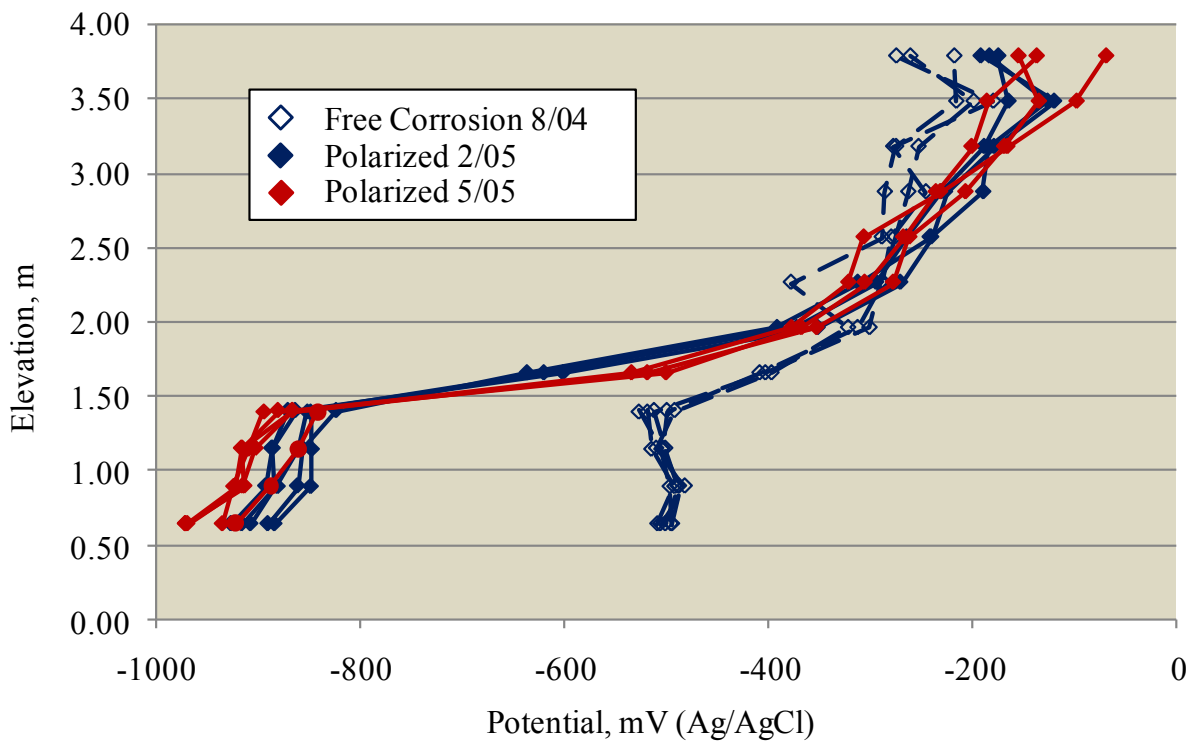


Figure 22: Footer and column reinforcing steel potential data for Pier 39W-East as a function of elevation for each of the three site visits. Elevation is referenced to the bottom of the footer.

Upon connection of the ZnSBAs, it was anticipated that the reinforcement potential would shift to more negative values with the magnitude of this change moderating with increasing elevation. Figure 23 illustrates this schematically. While this anticipated shift occurred for the footer and lower elevation column steel, at higher elevations potentials changed in the opposite direction (more positive). This gives the appearance that CP resulted in anodic polarization here; however, this is thought not to have been the case, as explained below.

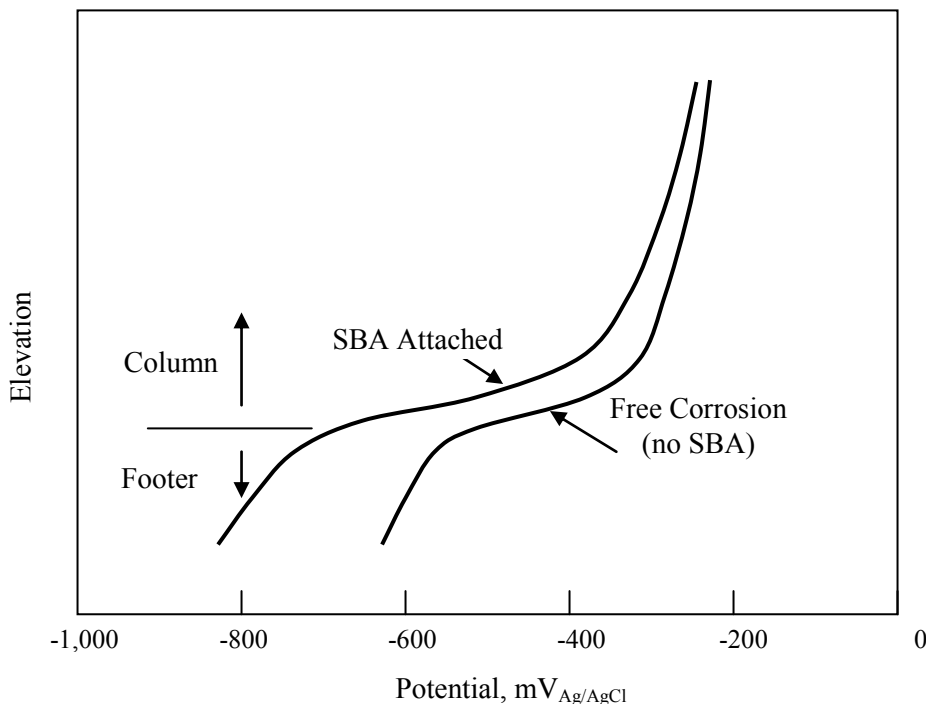


Figure 23: Schematic illustration of the potential shift of footer and column reinforcement that is expected to accompany SBA activation.

Table 7 lists resistivity data that were acquired as a function of elevation for Pier40W-East during the May, 2005 site visit; and Table 8 lists the average resistivities measured at each elevation and site visit. Figures 24 and 25 provide plot these results. The data reveal a trend where resistivity was relatively low for the footer concrete and at the highest level on the column for which readings were taken. Also, while the data in Figure 24 varied with probe position at any given elevation, still the three sets of data conform to a common trend. The elevation range for which resistivity was relatively high corresponds to that of the gunite repair on the column, whereas the lower readings both below and above this were from the original sound concrete. Figure 25 shows the average resistivity results for pier 40W-East at the time of the three visits. Data for Pier 39W-East at the time of the initial visit are also illustrated (resistivity was not measured for this pier during the February and May, 2005 site visits). The fact that column resistivity was higher at the time of the second and third site visits compared to during

Table 7: Resistivity data for various elevations and orientations that were on pier 40W-East as acquired during the May, 2005 site visit.

Elevation, m	Resistivity, kOhm.cm			
	Left	Center	Right	Average
3.78	3.6	6.2	3.0	5.0
3.48	26.4	16.4	2.6	17.3
3.18	17.3	12.7	6.8	21.5
2.87	20.5	18.6	19.8	16.8
2.57	19.5	18.2	20.0	19.3
2.26	19.5	20.8	17.3	17.3
1.96	20.2	18.5	19.3	20.0
1.65	24.3	21.8	16.8	19.8
1.40	4.2	4.4	21.5	6.8
1.14	2.8	2.5	17.3	2.6
0.89	2.6	3.1	5.0	3.0

Table 8: Average resistivity as measured during each of the three site visits.

Elevation, m	Resistivity, kOhm.cm			
	39W-East (8/04)	40W-East (8/04)	40W-East (2/05)	40W-East (5/05)
3.78	0.6	1.0	1.5	2.9
3.48	7.5	3.9	21.1	22.0
3.18	6.7	3.5	17.0	20.0
2.87	6.5	3.1	16.2	19.6
2.57	6.5	3.1	15.7	19.2
2.26	6.3	2.9	14.9	19.0
1.96	5.5	2.8	13.1	18.6
1.65	5.3	2.6	10.3	17.2
1.40	1.0	0.9	10.0	5.1
1.14	1.0	0.9	4.1	4.9
0.89	-	-	1.5	2.6

the initial one probably reflects cooler temperatures or less moisture (or both) at the two latter times. Generally, the resistivity data correlate with potentials in that values for the latter were relatively positive at locations where resistivity was high and vice versa. This probably explains the shift in column steel potentials to more positive values at the times of the second two site visits (see Figures 21 and 22). On this basis, these more positive potentials did not result from connection of the ZnSBAs but instead were a consequence of concrete resistivity having increased.

Table 9 lists probe potential data that were acquired for Pier 40W-East during the two site visits (2/05 and 5/05), and Figure 26 plots these along with the potential profile for the Pier 40W-East reinforcement that was measured on 2/05. Here, the term “isolated” refers to potential of the free

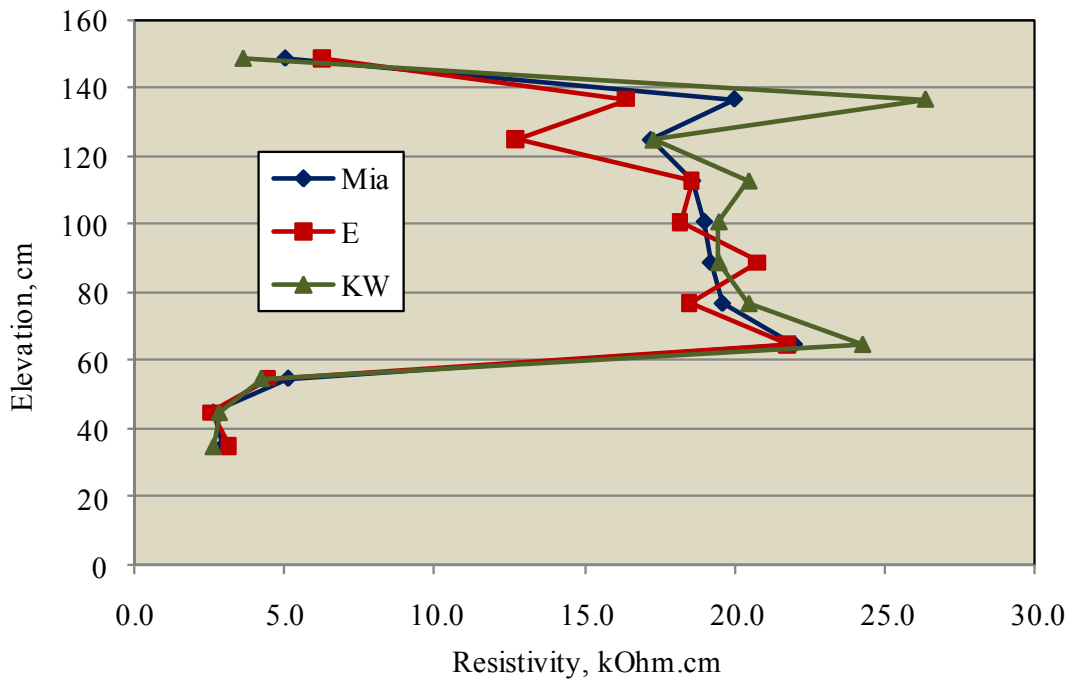


Figure 24: Resistivity versus elevation data for various positions on Pier 40W-East as acquired during the May, 2005 site visit (top of the footer is at approximately 0.6 m elevation).

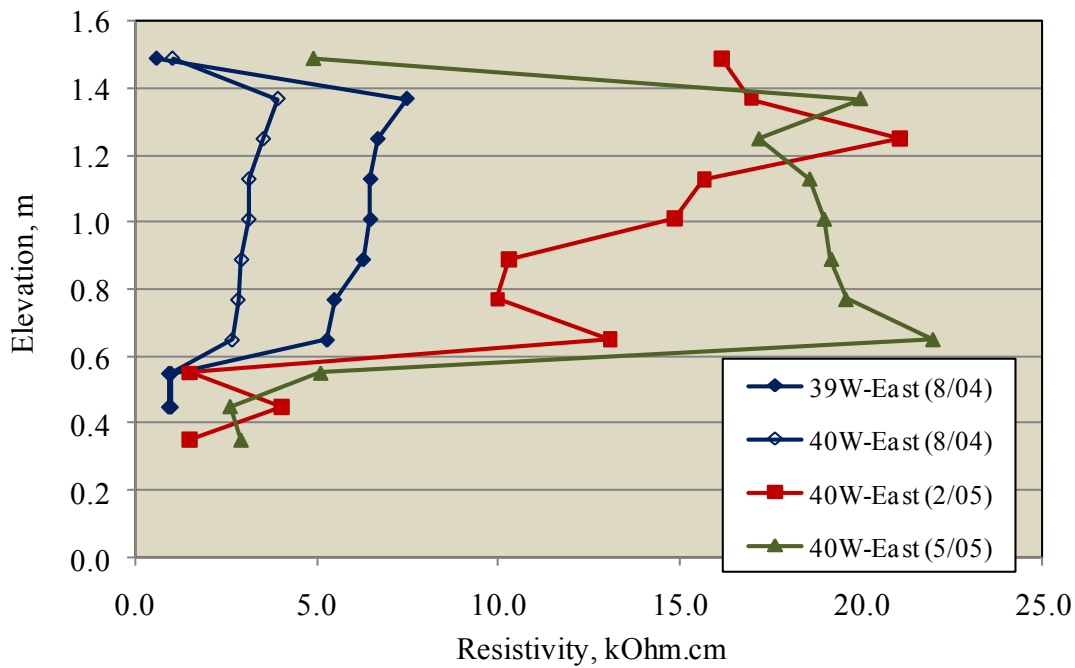


Figure 25 Resistivity versus elevation data for Pier 40W-East as measured during each of the three site visits (top of the footer is at approximately 0.6 m elevation).

corrosion (unconnected) probes. Table 10 and Figure 27 provide the same information for Pier 39W-East. In both cases, potential of the connected probes was essentially the same as for the reinforcing steel; and with exception of the 1.65 m elevation 40W-East probe, isolated probe potentials on both piers were in the range -400 to -200 mV (Ag/AgCl).

Table 9: Probe potential data as acquired for Pier 40W-East during the (a) 2/05 site visit and (b) 5/05 site visit.

Elevation, m	Potential, mV (Ag/AgCl)		
	Isolated	Connected	De-Polarized
1.40	-308	-859	-508
1.65	-425	-604	-448
2.16	-299	-331	-298
2.67	-270	-232	-298

(a)

Elevation, m	Potential, mV(Ag/AgCl)	
	Isolated	Connected
1.40	-280	-857
1.65	-564	-650
2.16	-297	-340
2.67	-217	-265

(b)

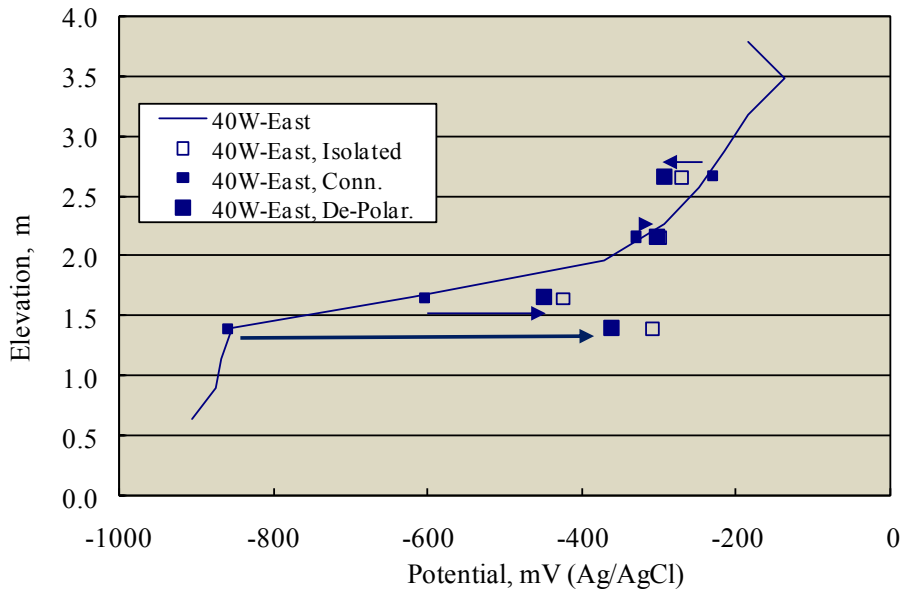


Figure 26: Polarized potential data for reinforcement and probes (isolated, connected, and depolarized) for Pier 40W-East.

Table 10: Probe potential data as acquired for Pier 39W-East during the 5/05 site visit.

Elevation, m	Average Reinforcement Potential, mV (Ag/AgCl)		
	Isolated	Connected	De-Polarized
1.40	-354	-870	-499
2.16	-249	-327	-367

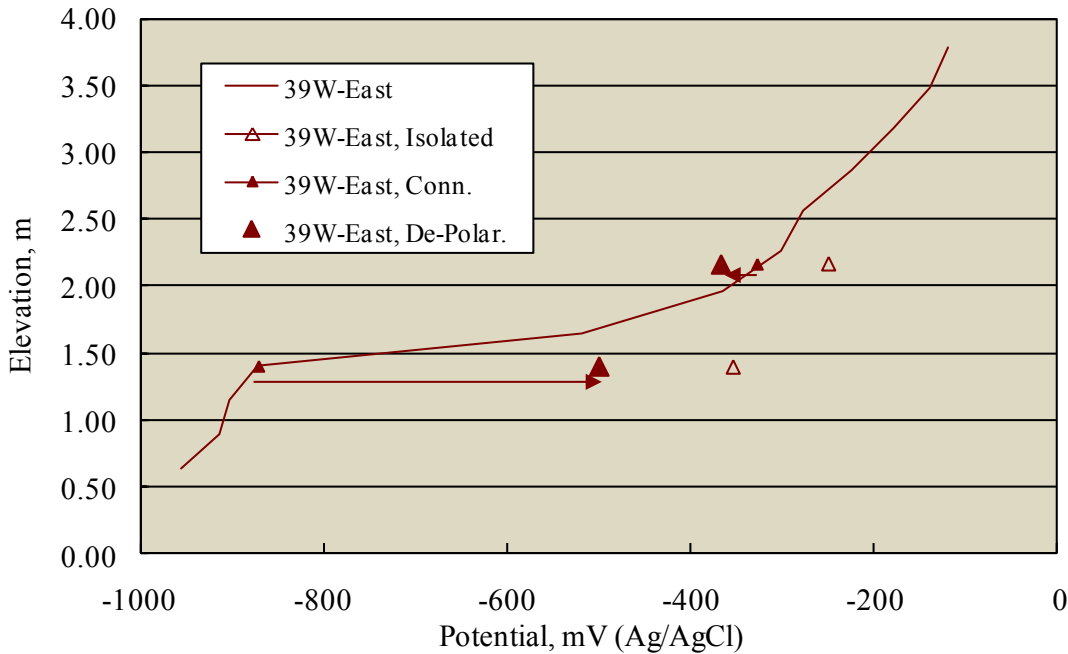


Figure 27: Polarized potential data for reinforcement and probes (isolated, connected, and depolarized) for Pier 39W-East.

Of particular interest in Figures 26 and 27 is the depolarization data from the connected probes. For the three lower elevation probes on Pier 40W-East (elevations 1.40, 1.65, and 2.16 m), the magnitude of depolarization decreased with increasing elevation. Based upon the 100 mV depolarization criterion for protection, the data indicate that protection was affected at the elevation of the lower two probes (depolarizations of 498 and 154 mV, respectively, at the 1.40 and 1.65 m elevations) but was only partial at 2.16 m (depolarization 29 mV). For the highest elevation probe, the depolarization was in the opposite sense (60 mV in the active direction), suggesting that this probe had been anodically polarized. On Pier 39W-East, the lower probe depolarized by 371 mV; but for the upper, depolarization was in the opposite sense by 40 mV suggesting also that it had been anodically polarized. Figure 28 shows these data for the two piers on the same plot, thus better facilitating a direct comparison.

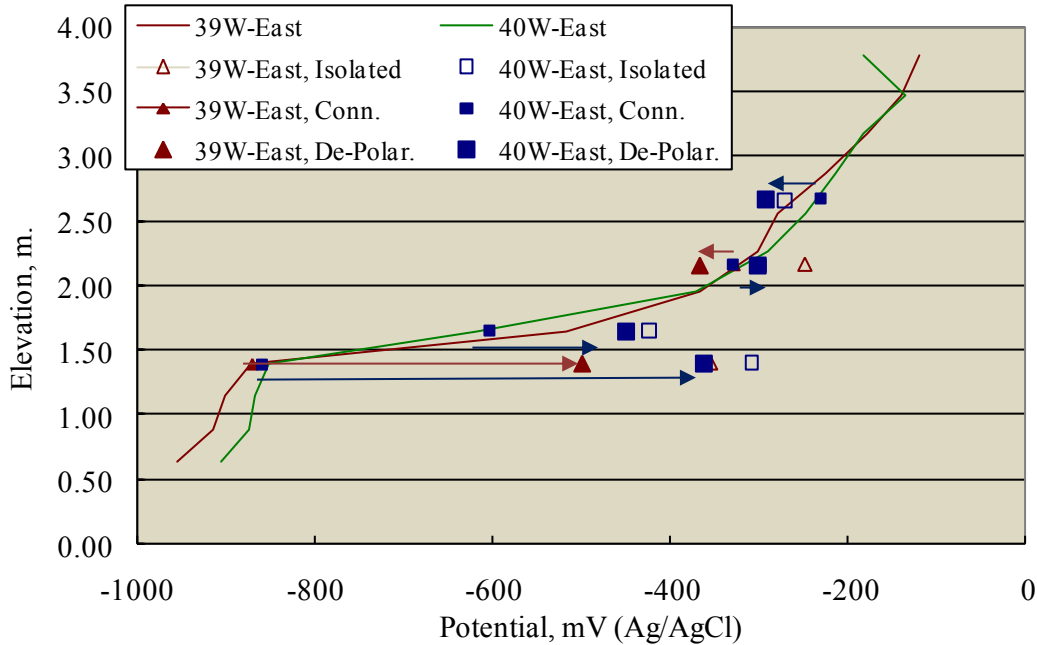


Figure 28: Plot of 1) isolated and 2) connected and depolarized probe potentials according to elevation for both piers at the time of the February, 2005 site visit. Average values for the reinforcement on this same pier are also indicated. Elevation is referenced to the bottom of the footer.

As noted above, comparison of the August, 2004 and February, 2005 potential data suggests that CP from the ZnSBAs induced corrosion of reinforcement at the higher elevations, since potentials here were more positive after CP activation. In rationalizing this, the corrosion state of probes compared to that of the reinforcement was considered. Each probe was exposed in the same, relatively uniform, Cl⁻ admixed concrete irrespective of elevation; and so corrosion state and potential should be determined by [Cl⁻] and the degree of moisture saturation (higher moisture, more negative potential). Potential of all isolated probes, with the exception of the lowest one on Pier 40W-East, is consistent with this trend. However, prior to connection to the ZnSBAs, potential gradient of the reinforcing steel from relatively negative to less negative with increasing elevation is expected to be more pronounced than for the isolated probes since the submerged and splash zone concrete is water saturated and the more negative steel here tends to cathodically polarize the higher elevation steel. At an elevation beyond the range of this polarization, there is an equal chance that potential of an isolated probe will be either active or noble to that of the reinforcement. It follows then that connection of a probe whose native potential is more negative than that of the reinforcement should result in it being anodically polarized and its corrosion rate enhanced. Figure 29 illustrates this schematically. This is thought to explain the apparent “reverse polarization” of the higher elevation probes.

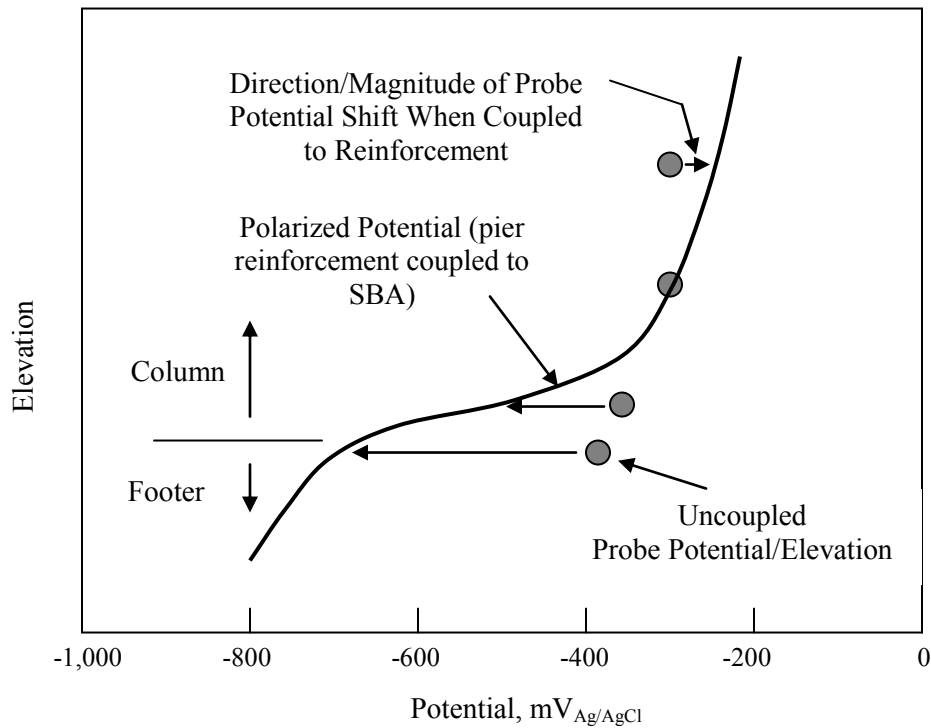


Figure 29: Schematic illustration of the probe potential shift that accompanies coupling to pier reinforcement.

Likewise, Table 11 lists current densities that were determined for both piers by inserting a zero resistance ammeter in series between the coupled probe and reinforcing steel; and Figure 30 plots these results. Data at the time of the 5/05 site visit were not acquired for Pier 39W-East. Note that current density for the 2.16 m 40W-East probe had shifted from positive (cathodic) to negative between the two visits.

Table 11: Listing of probe current densities.

Pier	Date	Elevation, m	Current Density, mA/m ²
40W-East	2/05	2.67	-9.29
		2.16	11.67
		1.65	39.91
		1.40	128.25
40W-East	5/05	2.67	-6.36
		2.16	-3.65
		1.65	12.33
		1.40	147.82
39W-East	2/05	2.16	-6.80
		1.40	17.74

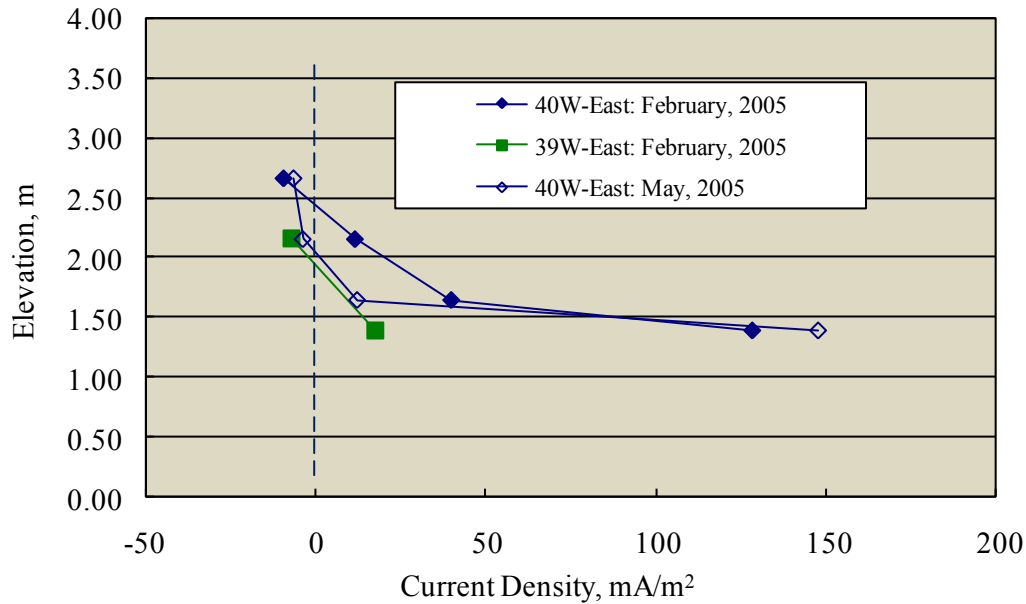


Figure 30: Plot of probe current density versus elevation.

An unavoidable unknown in evaluating the field data is the extent to which the gunite repairs on the two columns affected throwing power of the ZnSBAs and CP performance at the higher elevations. It can be reasoned, however, that since the gunite was disbonded at some locations and elsewhere probably constituted a resistive interface to current flow, polarization on the columns was less than if the concrete had been sound. This is supported by the fact that concrete resistance at the highest elevation, which was above the gunite repair and where the concrete remained sound, was less than that for the gunite (Figures 24 and 25). Thus, while the level of corrosion protection afforded by the ZnSBAs decreased with increasing elevation with the 100 mV criterion extending to 1.5-2.0 m and polarization being nil at 2.0-2.5 m above the bottom of the footers. It is likely this would have extended to a higher elevation if the concrete had been sound.

Niles Channel Bridge

Procedures

An initial inspection of this bridge was performed in March, 2007, at which time Piers 2 and 12 were selected for installation of MgSBAs based upon the finding that these had nil or only minor cracking and no delaminations or spalls. Subsequently, ten 22.6 kg (50 pound) pier type Mg anodes each measuring 38.1 cm (15.0 in.) high by 20.3 cm (8.0 in.) in diameter were obtained from Galvotec Corrosion Services in McAllen, Texas. Figure 31 provides a photograph of one of these as-received and showing that these were cast with a 19 mm diameter galvanized pipe along the anode axis. To facilitate mounting on the



Figure 31: Photograph of a 22.6 kg pier type Mg anode as-received.

bridge, the bottom central region of each anode was excavated to expose the embedded end of the galvanized pipe which terminated about five cm above the anode base. Next, a length of another 19 mm galvanized pipe was threaded onto each end of the embedded pipe via a threaded coupling; and an insulated #6 copper wire was bolted to the pipe that extended from the anode top. This galvanized pipe and wire were then inserted into a 25 mm pvc pipe which was then filled with epoxy. Figure 32 schematically illustrates design of the MgSBA mounting configuration where two anodes were positioned opposite one another on either side of the west (Gulf) end of the strut. The lead wire from each anode was bolted to a stainless steel rod that had been threaded into the column reinforcement. This connection was such that a one Ohm resistor could be inserted into the circuit and voltage drop across the resistor measured, from which net current output from the anode pair could be calculated. Figure 33 is a photograph of Pier 2 subsequent to anode installation. Table 12 provides a listing of the dates of the various site visits and the tasks performed during each.

All potential measurements were made either with a Ag/AgCl or Cu/CuSO₄ reference electrode (in the latter case these were converted to Ag/AgCl for reporting consistency by adding 70 mV to the recorded reading) and a Fluke multimeter; and concrete resistivity was measured using a CNS Farnell-RM MKII Model U95 four pin meter according to the procedure reported above. Both measurements (potential and resistivity) were made on each footer and column face, first with the reference electrode in

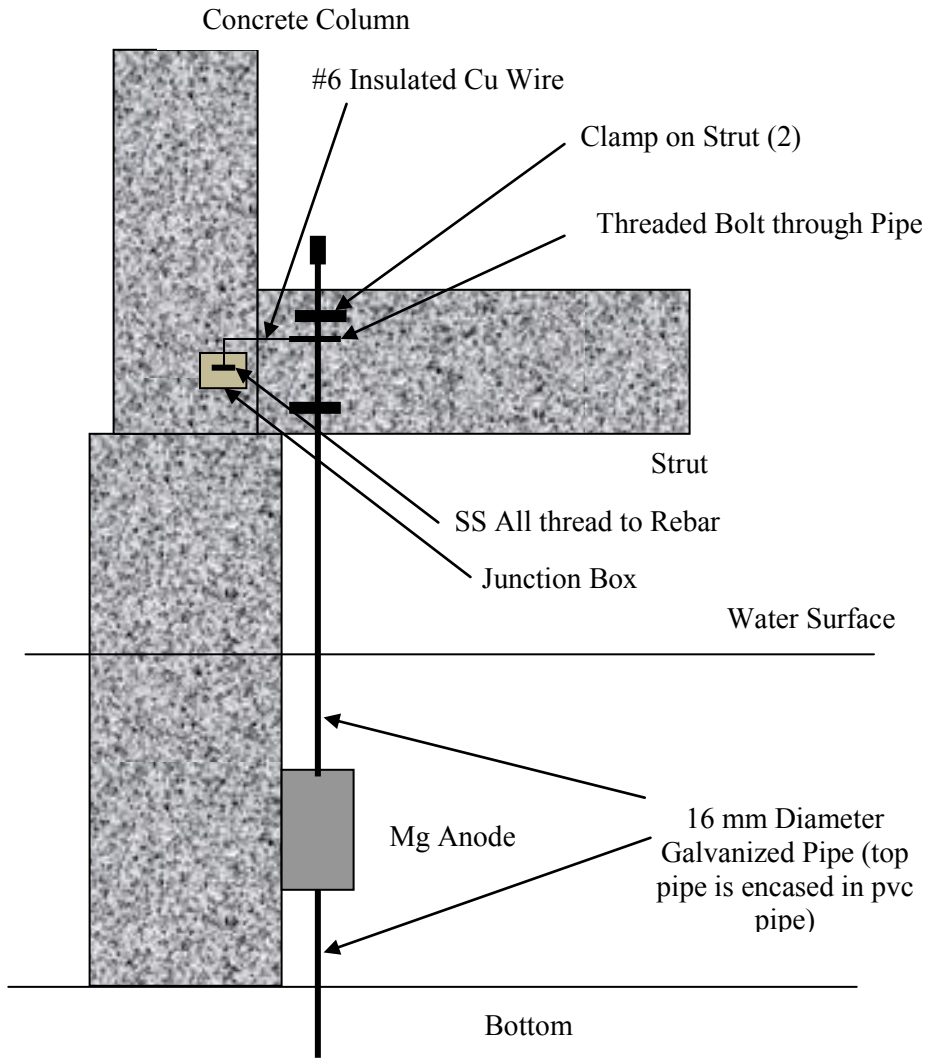


Figure 32: Schematic illustration of the MgSBA installation scheme.



Figure 33: Photograph of Pier 2 subsequent to MgSBA installation.

Table 12: Listing of Niles Channel Bridge site visit dates and tasks performed.

Date	Task
August 7,8, 2007	1. Collect baseline (free corrosion and resistivity) data.
	2. Install anodes.
	3. Collect polarized potential and depolarization data.
August 24, 2007	1. Collect polarized potential and depolarization data.
	2. Collect resistivity data.
December 18, 2007	1. Collect polarized potential and depolarization data.
	2. Collect resistivity data.
February 1, 2008	1. Collect long-term depolarization data.
	2. Collect resistivity data.
August 12-14, 2008	1. Collect polarized potential and depolarization data.
	2. Collect resistivity data.

the water, then at the marine growth line (MGL),^a and at 0.30 m (1.0 ft) intervals above this. Readings were made on three vertical lines spaced 90° apart on each footer/column. These were designated as “Mia,” “W,” and “”KW” for the west (Gulf) side footer/column and “Mia,” “E,” and “”KW” for the east (Atlantic) side footer/column according to orientation, as illustrated in Figure 34. Results for each of the four footer/column pairs are presented below.

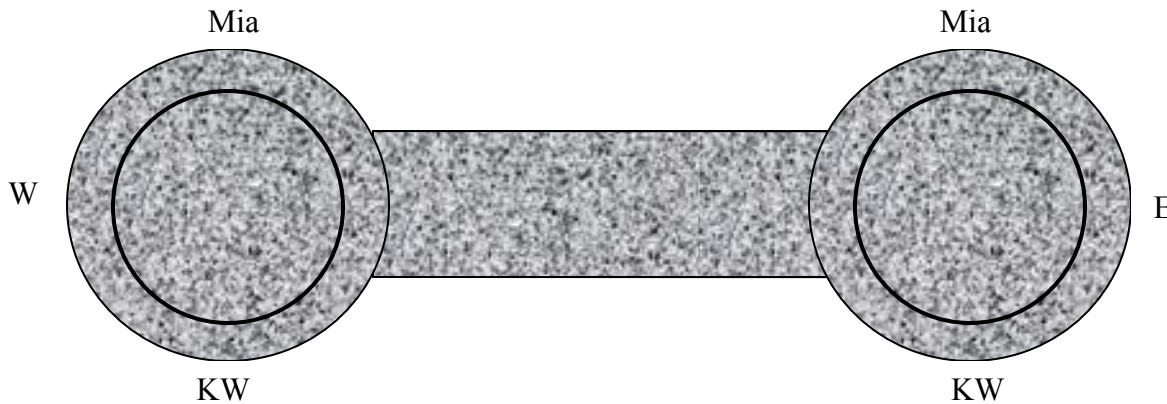


Figure 34: Plan view schematic illustration of a pier on the Niles Channel Bridge showing the orientations at which potential and resistivity measurements were made.

^a In the plots of potential versus elevation presented subsequently, 0 m elevation is with the reference electrode in the water; and the 0.30 m reading is at the MGL, although this was typically higher than 0.30 m above the water line. The third reading at elevation 0.61 m was typically near the top of the footer, and the following reading was on the column.

Results

West (Gulf Side) Footer/Column, Pier 2: Tables 13 and 14 list free corrosion potential at the different elevations and orientations along with the averages as acquired on August 7 and 8, 2007, respectively. Figure 35 plots these data, and Figure 36 does the same for the average value at each elevation. The general trend is one where potential was relatively negative at lower elevations and became progressively more positive with increasing elevation for reasons explained above (see Figure 20). Likewise, Table 15 lists the current-on potential at each measurement elevation and also the average at each elevation as recorded during each of the site visits subsequent to activation; and Figure 37 plots these average values

Table 13: Free corrosion potentials at various elevations from the west (Gulf) footer/column of Pier 2 on August 7, 2007.

Elevation, m	Potential, mV (Ag/AgCl)			
	Mia	W	KW	Average
2.44	-238	-151	-246	-212
2.13	-220	-227	-277	-241
1.83	-255	-221	-294	-257
1.52	-266	-245	-360	-290
1.22	-343	-324	-383	-350
0.91	-371	-355	-380	-369
0.61	-417	-417	-418	-417
0.30	-429	-420	-422	-424
0.00	-457	-447	-459	-454

Table 14: Free corrosion potentials at various elevations from the west (Gulf) footer/column of Pier 2 on August 8, 2007.

Elevation, m	Potential, mV (Ag/AgCl)			
	Mia	W	KW	Average
2.44	-243	-247	-272	-254
2.13	-280	-278	-314	-291
1.83	-308	-308	-311	-309
1.52	-346	-294	-343	-328
1.22	-410	-362	-330	-367
0.91	-445	-407	-392	-415
0.61	-448	-400	-402	-417
0.30	-425	-446	-420	-430
0.00	-478	-459	-459	-465

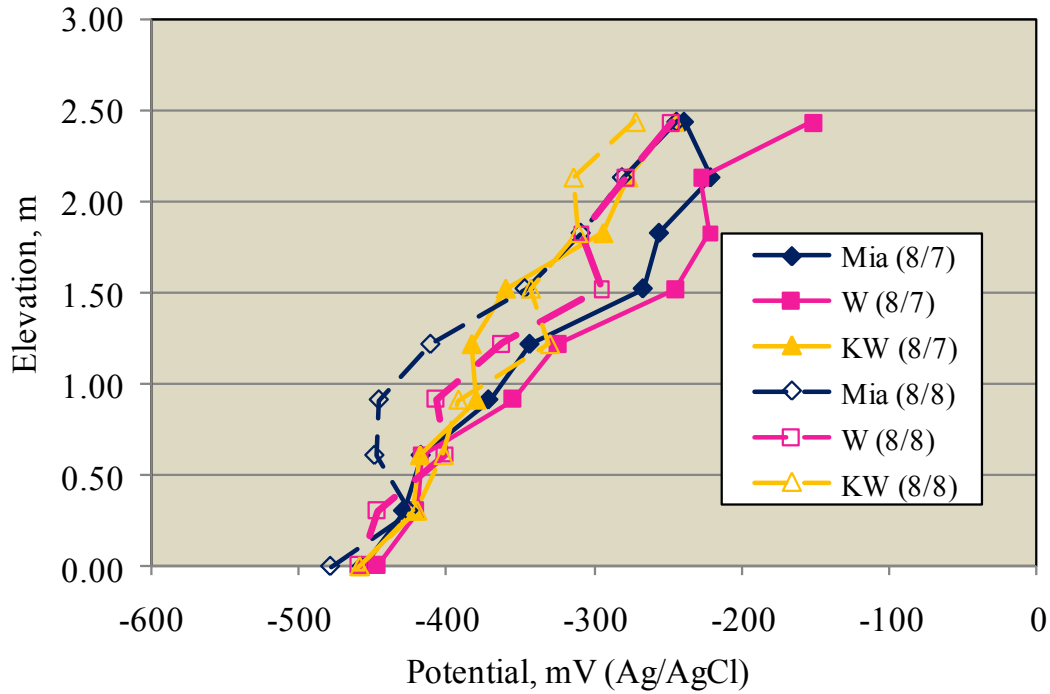


Figure 35: Free corrosion potential data for the west footer/column of Pier 2 as acquired during the August 7 and 8, 2007 site visit.

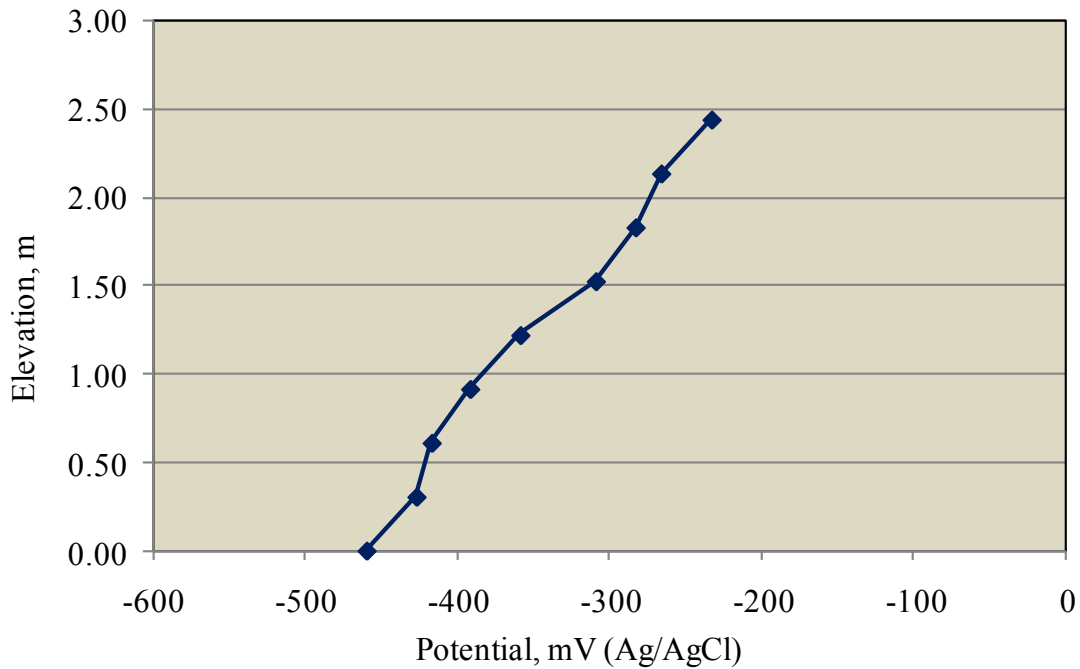


Figure 36: Average free corrosion potential data as a function of elevation from Figure 35.

Table 15: Current-on potential at each of the measurement orientations and elevations after (a) two hours, (b) 16 days, (c) 132 days, and (d) 369 days activation.

Elevation, m	Potential, mV (Ag/AgCl)			
	Mia	W	KW	Average
2.44	-370	-380	-370	-373
2.13	-420	-400	-420	-413
1.83	-440	-460	-450	-450
1.52	-490	-530	-520	-513
1.22	-560	-590	-570	-573
0.91	-590	-660	-660	-637
0.61	-650	-700	-750	-700
0.30	-730	-830	-850	-803
0.00	-1300	-1300	-1310	-1303

(a)

Elevation, m	Potential, mV (Ag/AgCl)			
	Mia	W	KW	Average
2.44	-10	-40	-10	-20
2.13	-50	-30	-60	-47
1.83	-110	-10	-140	-87
1.52	-220	-200	-260	-227
1.22	-330	-350	-380	-353
0.91	-420	-500	-530	-483
0.61	-500	-550	-600	-550
0.30	-680	-790	-770	-747
0.00	-880	-880	-880	-880

(b)

Elevation, m	Potential, mV (Ag/AgCl)			
	Mia	W	KW	average
2.44	-240	-330	-303	-291
2.13	-260	-430	-363	-351
1.83	-330	-530	-447	-436
1.52	-500	-620	-563	-561
1.22	-670	-720	-693	-694
0.91	-780	-840	-790	-803
0.61	-840	-890	-837	-856
0.30	-930	-1000	-953	-961
0.00	-1140	-1110	-1130	-1127

(c)

Elevation, m	Potential, mV (Ag/AgCl)			
	Mia	W	KW	Average
2.44	-477	-471	-448	-465
2.13	-493	-408	-482	-461
1.83	-570	-436	-565	-524
1.52	-643	-530	-672	-615
1.22	-768	-723	-805	-765
0.91	-900	-883	-932	-905
0.61	-974	-1028	-1088	-1030
0.30	-1101	-1132	-1138	-1124
0.00	-1182	-1215	-1239	-1212

(d)

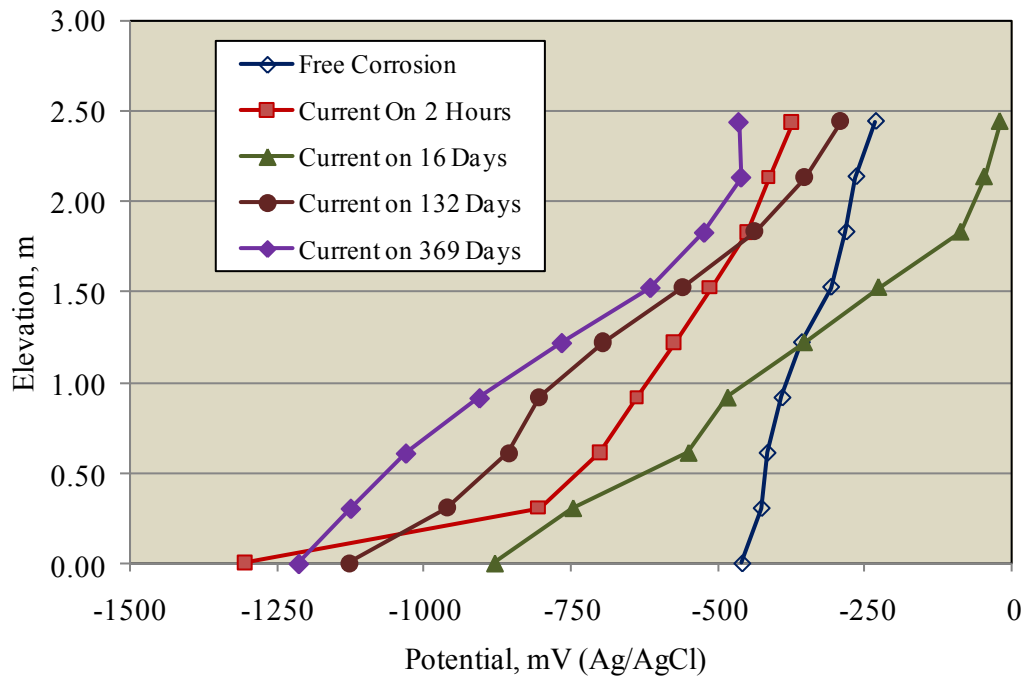


Figure 37: Plot of current-on potentials at each measurement elevation on the west footer/column of Pier 2 for each of the site visits in comparison to the free corrosion values.

as a function of elevation in comparison to the free corrosion potentials (Figure 36).^b With the exception of the 16 days activated data, the general trend is one where current-on potentials, first, were more negative than the free corrosion values, second, became generally more negative with time and, third, exhibited a difference compared to the pre-activation potentials that was greatest at the lowest elevation

^b The time of the August 12, 2008 site visit was 369 days after anodes had been connected, and this is used as the connection time. Doing this disregards the fact that anodes were disconnected between December 18, 2007 and February 1, 2008 (45 days), as explained later.

and became progressively less with increasing elevation. The data at 16 days activation indicate cathodic polarization for the lowest 1.2 m only, and potentials were more positive than the free corrosion values above this. The reason for this exceptional behavior is unknown, although the data are consistent with the operating potential of the anodes having shifted to a more positive value.

Net current output of the two anodes on Pier 2 was measured at the time of each site visit with results being as reported in Table 16. The expected trend is one where current decreases with increasing time to a steady-state value but perhaps varies cyclically with seasonal temperature variations. The exception to this trend is that current after 16 days activation (135 mA) was lower than at 132 and 369 days (182 and 145 mA, respectively).

Table 16: Net current output at different times after anode activation for Pier 2.

Date	Time Since Activation, days	Current, mA
August 8, 2007	0	580
August 24, 2007	16	135
December 18, 2007	132	182
August 12, 2008	369	145

It is generally recognized that current-on potentials do not necessarily reflect the extent to which an electrode is polarized, particularly in high resistive media such as concrete, because of the voltage drop between anode and cathode. Consequently, “instant” current-off potentials were measured at the time of the 16, 132, and 369 days activated site visits using a Miller C1 current interrupter and a 30 seconds on – one second off cycle. Table 17 lists these data at each measurement elevation in comparison to the current-on values and the average of each, and Figure 38 plots the average values versus elevation. This indicates that the difference between the two sets of measurements was negligible for the first two acquisitions except for lower elevations at 16 days activation; however, at the 369 days activation this voltage drop ranged from -88 to -146 mV and was roughly independent of elevation. The reason for this difference in voltage drop for the last compared to the initial two data acquisition times is unclear. Irrespective of this, Figure 39 plots the average magnitude of cathodic polarization as the difference between the 369 day current-off potentials (Table 17c) minus the average free corrosion potentials (Figure 36) versus elevation. This implies that approximately 100 mV polarization was achieved at the highest elevation above the waterline (~2.5 m).

A second measure of the extent of cathodic protection is the magnitude of depolarization at some time after disconnection of the anodes. Table 18 lists the magnitude of these depolarizations at the

Table 17: Listing of current-on and current-off potentials for the west footer/column of Pier 2 after (a) 16, (b) 132, and (c) 369 days activation.

Elevation, m	Potential, mV (Ag/AgCl)							
	Mia		W		KW		Average	
	On	Off	On	Off	On	Off	On	Off
2.44	-10	0	-40	-50	-10	-20	-20	-23
2.13	-50	-40	-30	-50	-60	-50	-47	-47
1.83	-110	-130	-10	-20	-140	-130	-87	-93
1.52	-220	-200	-200	-170	-260	-240	-227	-203
1.22	-330	-310	-350	-310	-380	-350	-353	-323
0.91	-420	-370	-500	-470	-530	-490	-483	-443
0.61	-500	-460	-550	-480	-600	-540	-550	-493
0.30	-680	-600	-790	-670	-770	-660	-747	-643
0.00	-880	-720	-880	-720	-880	-730	-880	-723

(a)

Elevation, m	Potential, mV (Ag/AgCl)							
	Mia		W		KW		Average	
	On	Off	On	Off	On	Off	On	Off
2.44	-340	-330	-240	-230	-330	-320	-303	-293
2.13	-400	-380	-260	-250	-430	-420	-343	-350
1.83	-480	-470	-330	-320	-530	-520	-420	-437
1.52	-570	-560	-500	-490	-620	-610	-533	-553
1.22	-690	-680	-670	-660	-720	-710	-653	-683
0.91	-750	-730	-780	-770	-840	-820	-770	-773
0.61	-780	-770	-840	-830	-890	-870	-827	-823
0.30	-930	-910	-930	-910	-1000	-980	-903	-933
0.00	-1140	-1040	-1140	-1070	-1110	-1050	-1060	-1053

(b)

Elevation, m	Potential, mV (Ag/AgCl)							
	Mia		E		KW		Average	
	On	Off	On	Off	On	Off	On	Off
2.59	-477	-356	-471	-352	-448	-327	-465	-345
2.29	-493	-369	-408	-284	-482	-360	-456	-338
1.98	-570	-447	-436	-310	-565	-440	-498	-399
1.68	-643	-517	-530	-398	-672	-548	-591	-488
1.37	-768	-639	-723	-589	-805	-679	-724	-636
1.07	-900	-768	-883	-746	-932	-798	-861	-771
0.76	-974	-829	-1028	-890	-1088	-945	-1005	-888
0.51	-1101	-950	-1132	-980	-1138	-999	-1081	-976
0.00	-1182	-1019	-1215	-1040	-1239	-1058	-1185	-1039

(c)

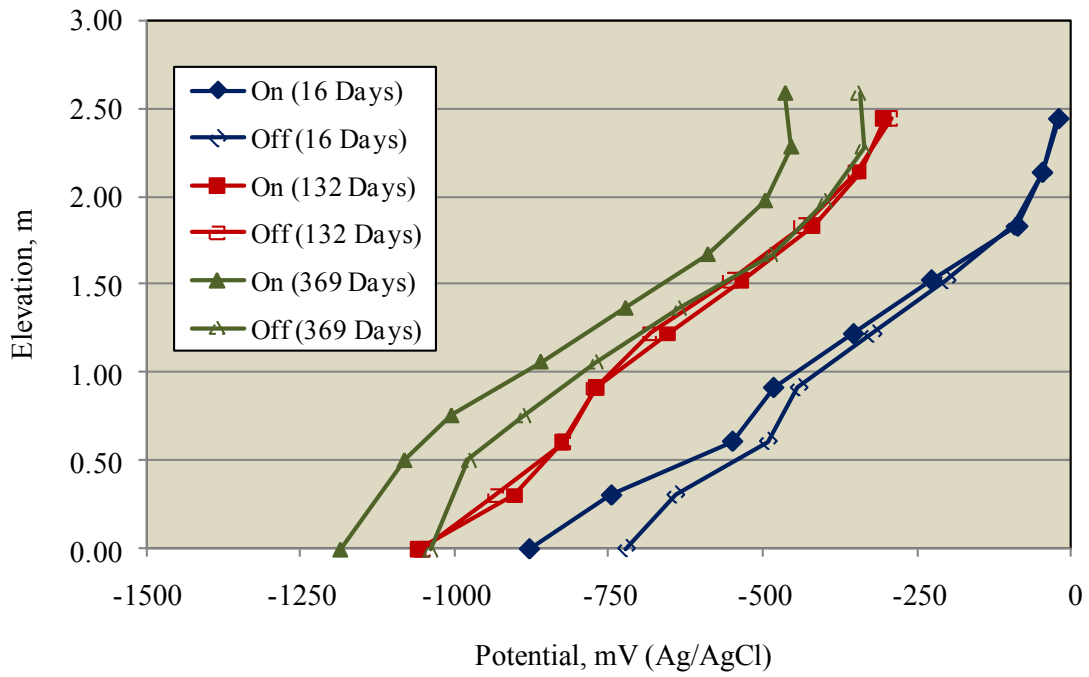


Figure 38: Comparison of current-on and current-off potentials for the west footer/column of Pier 2.

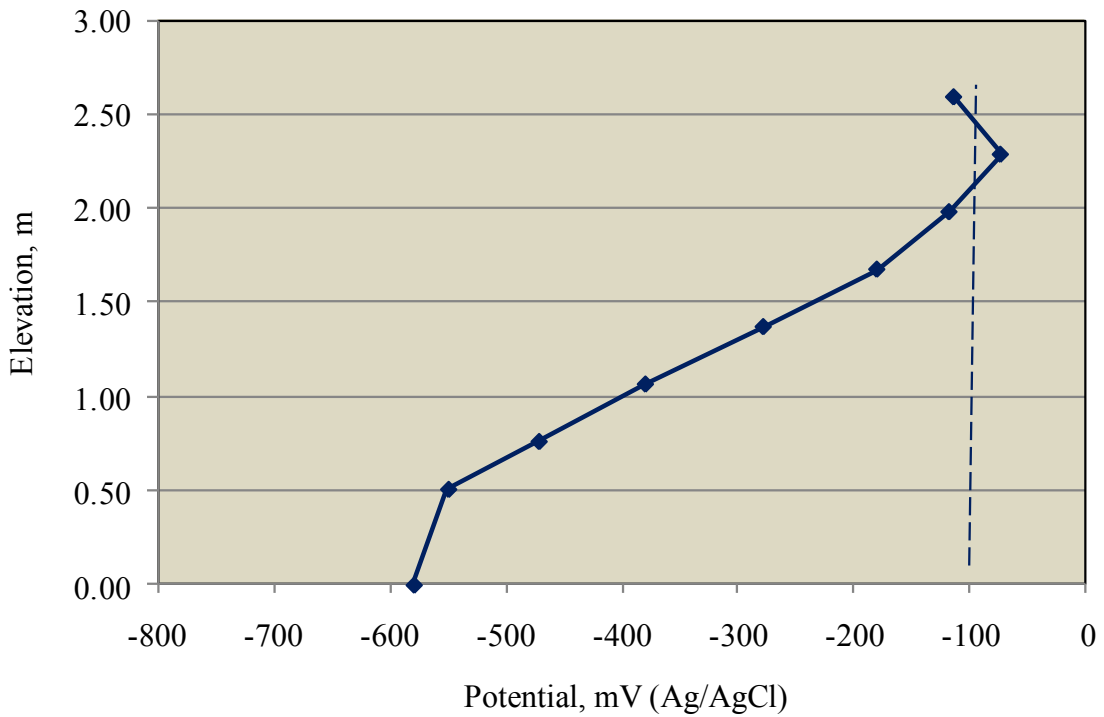


Figure 39: Magnitude of polarization after 369 days activation as a function of elevation for the west footer/column of Pier 2.

various elevations and times of disconnection for the west footer/column of Pier 2 at 132 and 369 days subsequent to activation, and Figure 40 provides a plot of the averages of these data. Clearly, the magnitude of these depolarizations, for which the highest elevation at which 100 mV occurred was about 1.3 m, are less than indicated by the polarized values reported in Figure 39. This may reflect, at least in part, a relatively moist state of the concrete, such that depolarization required longer times than even 45 days; however, even after this time, depolarization was nil at the higher elevations (132 days activation data), whereas the polarization data (Figure 39) indicate about a 100 mV potential shift to 2.5 m. In this regard the polarization and depolarization results appear at odds with one another. A possible reason for this are discussed subsequently.

Table 19 lists concrete resistivity data from the west footer/column of Pier 12 as measured during

Table 18: Magnitude of depolarization after (a) 132 days activation and 24 hours depolarization, (b) 132 days activation and 45 days depolarization, (c) 369 days activation and 24 hours depolarization, and (d) 369 days activation and 48 hours depolarization.

Elevation, m	Depolarization, mV			
	Mia	W	KW	Average
2.44	10	40	10	20
2.13	20	30	-20	10
1.83	0	60	-30	10
1.52	-20	40	-40	-7
1.22	-50	-20	-30	-33
0.91	-60	-50	-60	-57
0.61	-30	-60	-50	-47
0.30	-80	-50	-90	-73
0.00	-70	-90	-70	-77

(a)

Elevation, m	Depolarization, mV			
	Mia	W	KW	Average
2.44	-20	20	10	17
2.13	-20	10	-20	20
1.83	-60	-10	-30	-7
1.52	-90	-40	-40	-53
1.22	-140	-130	-30	-123
0.91	-180	-190	-60	-173
0.61	-150	-200	-50	-173
0.30	-230	-260	-90	-253
0.00	-240	-270	-70	-253

(b)

Elevation, m	Depolarization, mV			
	Mia	W	KW	Average
2.59	-20	-20	-21	-20
2.29	-20	-29	-223	-91
1.98	-11	-22	-18	-17
1.68	0	-33	-34	-22
1.37	-52	-36	-56	-48
1.07	-52	-63	-80	-65
0.76	-59	-93	-115	-89
0.51	-60	-105	-95	-87
0.00	-50	-66	-84	-67

(c)

Elevation, m	Depolarization, mV			
	Mia	W	KW	Average
2.59	-29	-35	-29	-31
2.29	-22	-34	-33	-30
1.98	-29	-28	-31	-29
1.68	-35	-40	-41	-39
1.37	-67	-50	-76	-64
1.07	-74	-80	-110	-88
0.76	-89	-116	-126	-110
0.51	-95	-120	-111	-109
0.00	-110	-109	-115	-111

(d)

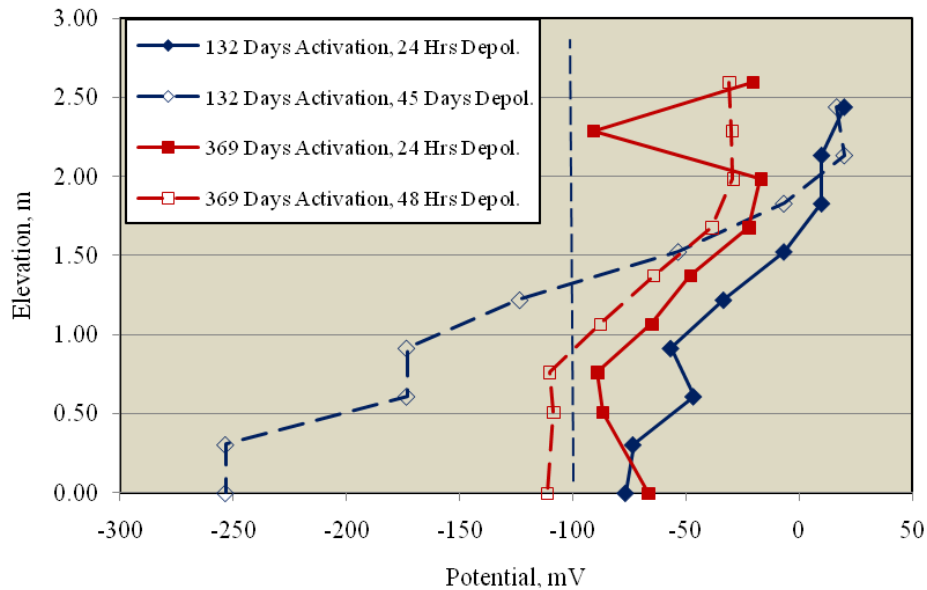


Figure 40: Magnitude of depolarization as a function of elevation after 132 and 369 days activation.

each of the four site visits. Figure 41 plots these data for the three orientations from the 8/07 site visit, and Figure 42 plots the average resistivity measured during each visit versus elevation. The results indicate that resistivity was relatively low on the footer and increased progressively on average with

Table 19: Resistivity data acquired from the west footer/column of Pier 2 on: (a) 8/07, (b) 12/07, (c) 2/08, and (d) 8/08.

Elevation, m	Resistivity, kOhm.cm			
	Mia	W	KW	Average
2.44	26.3	23.8	23.3	24.5
2.13	13.6	20.5	16.4	16.8
1.83	11.1	18.8	12.6	14.2
1.52	7.2	12.6	9.0	9.6
1.22	7.3	9.1	8.1	8.2
0.91	8.8	3.5	5.8	6.0
0.61	0.9	0.9	1.4	1.1
0.30	1.0	5.7	2.0	2.9
0.00	0	0.0	0.0	0.0

(a)

Elevation, m	Resistivity, kOhm.cm			
	Mia	W	KW	Average
2.44	32.4	39.1	42.8	38.1
2.13	32.6	32.3	30.3	31.7
1.83	20.1	25.4	20.0	21.8
1.52	12.5	18.7	9.4	13.5
1.22	11.0	7.2	5.8	8.0
0.91	-	-	-	-
0.61	1.3	1.8	2.4	1.8
0.30	4.0	3.0	3.2	3.4

(b)

Elevation, m	Resistivity, kOhm.cm			
	Mia	W	KW	Average
2.44	33.0	35.0	40.0	36.0
2.13	33.0	33.0	30.0	32.0
1.83	33.0	33.0	20.0	28.7
1.52	33.0	22.0	10.0	21.7
1.22	33.0	7.0	7.0	15.7
0.91	33.0	7.0	5.0	15.0
0.61	33.0	4.0	4.0	13.7
0.30	33.0	6.0	5.0	14.7

(c)

Elevation, m	Resistivity, kOhm.cm			
	Mia	W	KW	Average
2.44	59.5	34.5	60.5	51.5
2.13	22.3	38.5	29.5	30.1
1.83	23.5	15.7	26.9	22.0
1.52	14.6	17.1	19.0	16.9
1.22	11.0	21.8	8.4	13.7
0.91	9.1	9.6	5.3	8.0
0.61	7.7	4.0	7.5	6.4
0.30	1.0	1.3	1.5	1.3

(d)

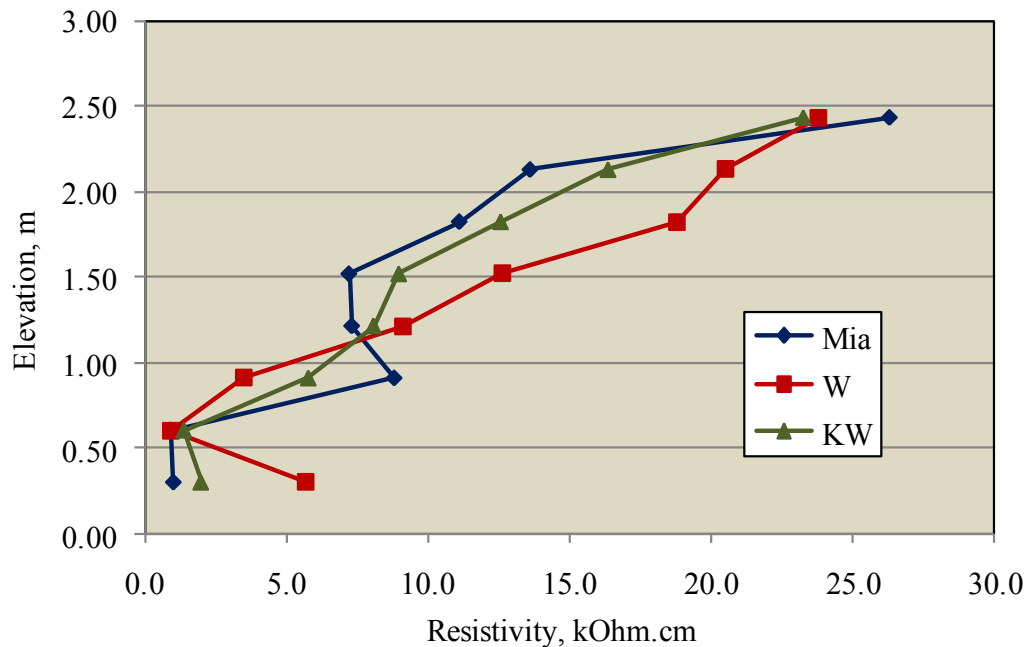


Figure 41: Resistivity data acquired on the west footer/column of Pier 2 during the 8/07 site visit.

increasing elevation, consistent with the concrete being progressively more dry with increasing height.

East (Atlantic Side) Footer/Column, Pier 2: Tables 20 and 21 list free corrosion potential at the different elevations and orientations along with the averages as acquired on August 7 and 8, 2007, respectively. Figure 43 plots these data and Figure 44 the average at each elevation. The trend is generally similar as reported above for the west footer/column of this same pier (potential was relatively negative at lower elevations and became progressively more positive with increasing elevation, Figures 35 and 36).

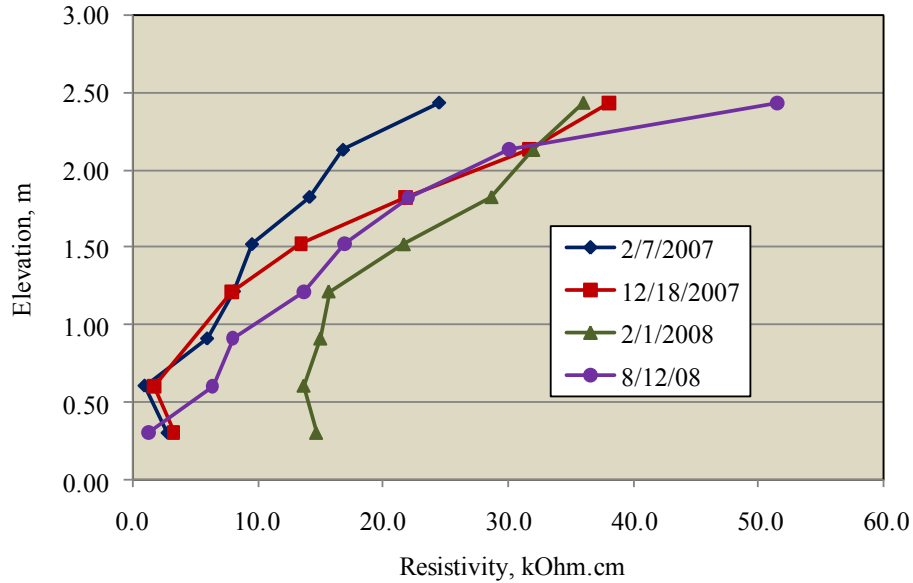


Figure 42: Average resistivity data as acquired on the west footer/column of Pier 2 during different site visits.

Table 20: Free corrosion potentials at various elevations from the east (Atlantic side) footer/column of Pier 2 on August 7, 2007 (no data for the E orientation were recorded).

Elevation, m	Potential, mV (Ag/AgCl)			
	Mia	E	KW	Average
2.44	-51	-	-183	-117
2.13	-92	-	-180	-136
1.83	-140	-	-191	-166
1.52	-222	-	-250	-236
1.22	-266	-	-376	-321
0.91	-430	-	-433	-432
0.61	-316	-	-445	-381
0.30	-440	-	-425	-433
0.00	-300	-	-459	-380

Likewise, Table 22 lists the current-on potential at each measurement elevation and also the average at each elevation as recorded during each of the site visits subsequent to activation. Figure 45 plots these average values as a function of elevation in comparison to the free corrosion potentials (Figure 44). As for the west footer/column of this pier, the 16 days activated data exhibit the least polarization with this extending only to about 0.7 m above the waterline. A second distinction is that polarization after 132 days exceeded that at 369 days, which contrasts with, first, expectation as explained above and, second, the west footer/column data (Figure 37).

Table 21: Free corrosion potentials at various elevations from the east (Atlantic side) footer/column of Pier 2 on August 8, 2007 (no data for the E orientation were recorded).

Elevation, m	Potential, mV (Ag/AgCl)			
	Mia	E	KW	Average
2.44	-210	-	-180	-195
2.13	-227	-	-182	-205
1.83	-281	-	-196	-239
1.52	-357	-	-287	-322
1.22	-380	-	-354	-367
0.91	-400	-	-420	-410
0.61	-443	-	-426	-435
0.30	-417	-	-400	-409
0.00	-458	-	-459	-459

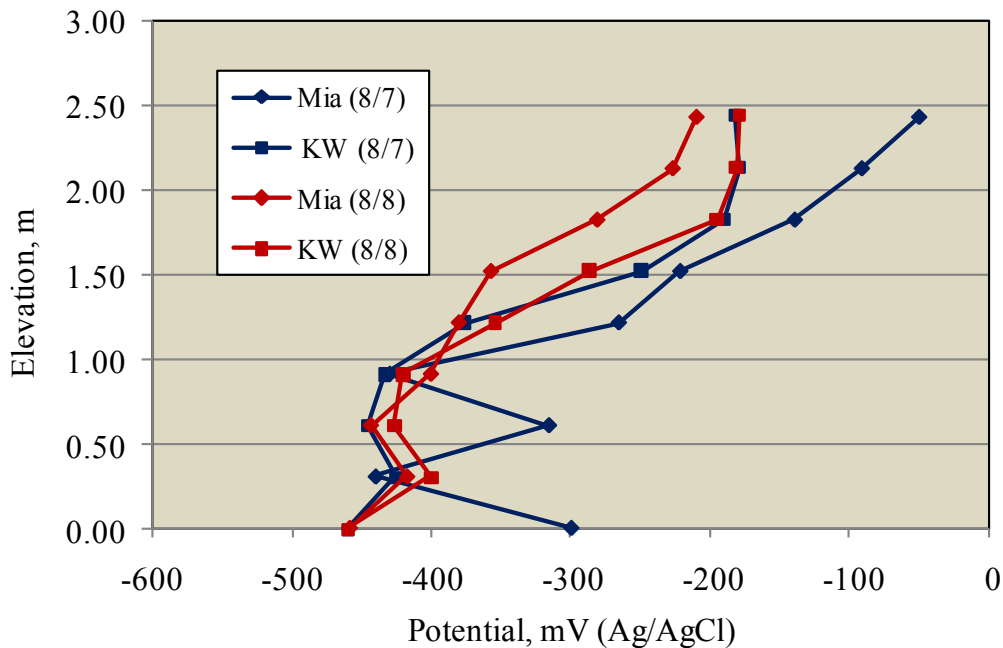


Figure 43: Free corrosion potential data for the east footer/column of Pier 2 as acquired during the August 7 and 8, 2007 site visit.

Table 23 lists the instant-off potential at each measurement elevation in comparison to the current-on values and the average of each, and Figure 46 plots the average values versus elevation. This indicates that the difference between the two sets of on-off measurements was distinct at each of the site visits with data after 132 days polarization being more negative than at 369 days, which contrasts with expectation as explained above. Also, the current off potentials at 132 days polarization are more negative than the

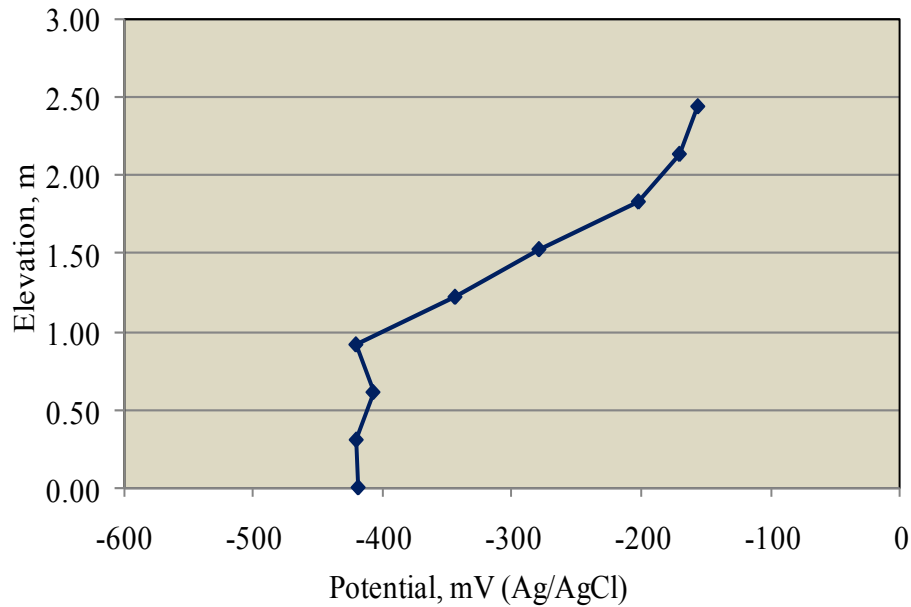


Figure 44: Average free corrosion potential data for the east footer/column of Pier 2 as acquired during the August 7 and 8, 2007 site visit.

current on ones, which contradicts expectation. However, the research team is confident that the data were recorded correctly; and a possible explanation is presented subsequently.

Table 24 lists the magnitude of depolarizations for this footer/column at the various elevations and times of disconnection subsequent to activation, and Figure 47 provides a plot of the averages of these data. Most of the 24 and 48 hour data show some depolarization to the highest elevation (2.5 m);

Table 22: Current-on potential at each of the measurement elevations on the east footer/column of Pier 2 after (a) two hours, (b) 16 days, (c) 132 days, and (d) 369 days activation.

Elevation, m	Potential, mV (Ag/AgCl)			
	Mia	E	KW	Average
2.44	-270	-	-250	-260
2.13	-330	-	-260	-295
1.83	-430	-	-310	-370
1.52	-550	-	-430	-490
1.22	-700	-	-550	-625
0.91	-820	-	-660	-740
0.61	-850	-	-740	-795
0.30	-930	-	-810	-870
0.00	-1320	-	-1320	-1320

(a)

Elevation, m	Potential, mV (Ag/AgCl)			
	Mia	E	KW	Average
2.44	-150	-40	-40	-77
2.13	-110	-60	-100	-90
1.83	-240	-120	-130	-163
1.52	-300	-200	-180	-227
1.22	-340	-310	-260	-303
0.91	-450	-400	-300	-383
0.61	-500	-510	-390	-467
0.30	-710	-660	-650	-673
0.00	-870	-870	-870	-870

(b)

Elevation, m	Potential, mV (Ag/AgCl)			
	Mia	E	KW	Average
2.44	-710	-760	-730	-733
2.13	-760	-770	-770	-767
1.83	-810	-840	-810	-820
1.52	-890	-910	-860	-887
1.22	-960	-1000	-870	-943
0.91	-1080	-1100	-980	-1053
0.61	-1170	-1190	-1000	-1120
0.30	-1250	-1270	-1090	-1203
0.00	-1450	-1480	-1470	-1467

(c)

Elevation, m	Potential, mV (Ag/AgCl)			
	Mia	E	KW	Average
2.44	-455	-488	-430	-458
2.13	-468	-496	-462	-475
1.83	-524	-515	-522	-520
1.52	-590	-580	-564	-578
1.22	-689	-677	-614	-660
0.91	-778	-759	-688	-742
0.61	-897	-890	-744	-844
0.30	-1040	-1014	-763	-939
0.00	-1121	-1108	-1024	-1084

(d)

however, magnitude of the 45 days depolarization exceeds 100 mV only to about 1.3 m; and above about 1.5 m the data indicate that the reinforcement anodically depolarized. These differences along with other apparent discrepancies (reversed on-off potentials (Figure 46)) may have been due to lack of ECR electrical continuity, since this can result in local anodic sites. Making electrical contact with the

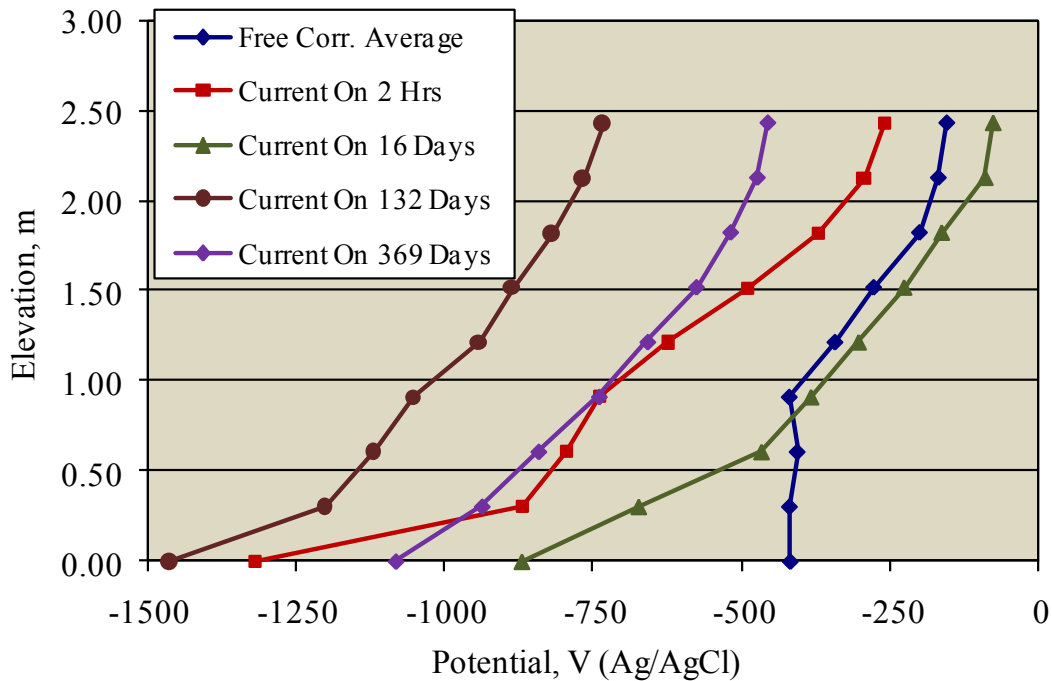


Figure 45: Plot of current-on potentials at each measurement elevation on the west footer/column of Pier 2 for each of the site visits in comparison to the free corrosion values.

reinforcement was difficult because of the large cover; however, two bars on the east column of Pier 2 were located by drilling and contact was made using a probe. The voltage between each of these bars and the ground connection on the west column was 1.6 and 1.7 mV. Based upon the generally accepted

Table 23: Listing of current-on and current-off potentials for the east footer/column of Pier 2 after (a) 16, (b) 132, and (c) 369 days activation.

Elevation, m	Potential, mV (Ag/AgCl)							
	Mia		E		KW		Average	
	On	Off	On	Off	On	Off	On	Off
2.44	-150	-100	-40	-10	-40	20	-77	-30
2.13	-110	-70	-60	-20	-100	50	-90	-13
1.83	-240	-180	-120	-80	-130	-80	-163	-113
1.52	-300	-240	-200	-160	-180	-130	-227	-177
1.22	-340	-280	-310	-270	-260	-210	-303	-253
0.91	-450	-390	-400	-350	-300	-250	-383	-330
0.61	-500	-440	-510	-460	-390	-340	-467	-413
0.30	-710	-610	-660	-580	-650	-560	-673	-583
0.00	-870	-720	-870	-750	-870	-720	-870	-730

(a)

Elevation, m	Potential, mV (Ag/AgCl)							
	Mia		E		KW		Average	
	On	Off	On	Off	On	Off	On	Off
2.44	-660	-730	-690	-770	-640	-740	-663	-747
2.13	-700	-780	-700	-780	-690	-780	-683	-780
1.83	-740	-810	-770	-860	-740	-840	-737	-837
1.52	-790	-870	-840	-920	-820	-920	-800	-903
1.22	-800	-880	-930	-1000	-890	-990	-870	-957
0.91	-910	-980	-1030	-1100	-1010	-1100	-947	-1060
0.61	-930	-990	-1120	-1190	-1100	-1190	-1043	-1123
0.30	-1020	-1100	-1200	-1280	-1180	-1270	-1103	-1217
0.00	-1400	-1430	-1410	-1450	-1380	-1430	-1270	-1437

(b)

Elevation, m	Potential, mV (Ag/AgCl)							
	Mia		E		KW		Average	
	On	Off	On	Off	On	Off	On	Off
2.59	-525	-350	-558	-382	-500	-327	-528	-353
2.29	-538	-363	-566	-394	-532	-357	-541	-371
1.98	-594	-420	-585	-415	-592	-416	-572	-417
1.68	-660	-486	-650	-478	-634	-458	-626	-474
1.37	-759	-586	-747	-575	-684	-511	-697	-557
1.07	-848	-674	-829	-652	-758	-579	-782	-635
0.76	-967	-795	-960	-787	-814	-638	-874	-740
0.51	-1110	-926	-1084	-905	-833	-651	-961	-827
0.00	-1191	-1000	-1178	-984	-1094	-900	-1127	-961

(c)

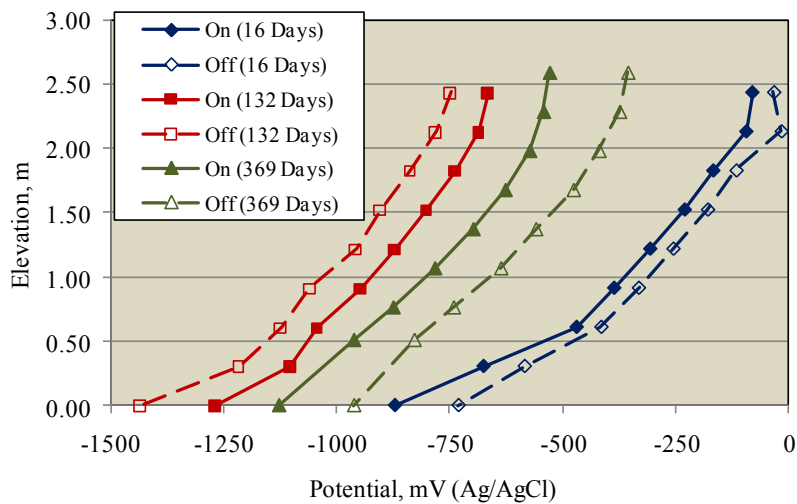


Figure 46: Comparison of current-on and current-off potentials for the east footer/column of Pier 2.

Table 24: Magnitude of depolarization after (a) 132 days activation and 24 hours depolarization, (b) 132 days activation and 45 days depolarization, (c) 369 days activation and 24 hours depolarization, and (d) 369 days activation and 48 hours depolarization.

Elevation, m	Depolarization, mV			
	Mia	E	KW	Average
2.59	10	-40	20	-3
2.29	-10	-50	0	-20
1.98	-10	-40	-10	-20
1.68	-40	-50	-20	-37
1.37	-50	-70	-40	-53
1.07	-110	-120	10	-73
0.76	-100	-100	-80	-93
0.51	-20	-90	-50	-53
0.00	-80	-90	-60	-77

(a)

Elevation, m	Depolarization, mV			
	Mia	E	KW	Average
2.59	170	130	120	140
2.29	70	60	90	73
1.98	60	40	90	63
1.68	20	20	40	27
1.37	-30	-30	-10	-23
1.07	-180	-260	-210	-217
0.76	-260	-320	-370	-317
0.51	-240	-330	-370	-313
0.00	-250	-260	-240	-250

(b)

Elevation, m	Depolarization, mV			
	Mia	E	KW	Average
2.59	-75	-39	-3	-39
2.29	92	-39	4	19
1.98	86	-25	-14	16
1.68	38	-27	-13	-1
1.37	36	-49	-29	-14
1.07	126	-73	-34	6
0.76	172	-132	-202	-54
0.51	-72	-95	-90	-86
0.00	-109	-67	-82	-86

(c)

Elevation, m	Depolarization, mV			
	Mia	E	KW	Average
2.59	-39	-47	-7	-31
2.29	-25	-54	14	-22
1.98	-13	-26	-9	-16
1.68	-12	-46	-29	-29
1.37	-24	-57	-43	-41
1.07	-50	-92	-65	-69
0.76	-119	-171	-226	-172
0.51	-140	-102	-151	-131
0.00	-141	-95	-100	-112

(d)

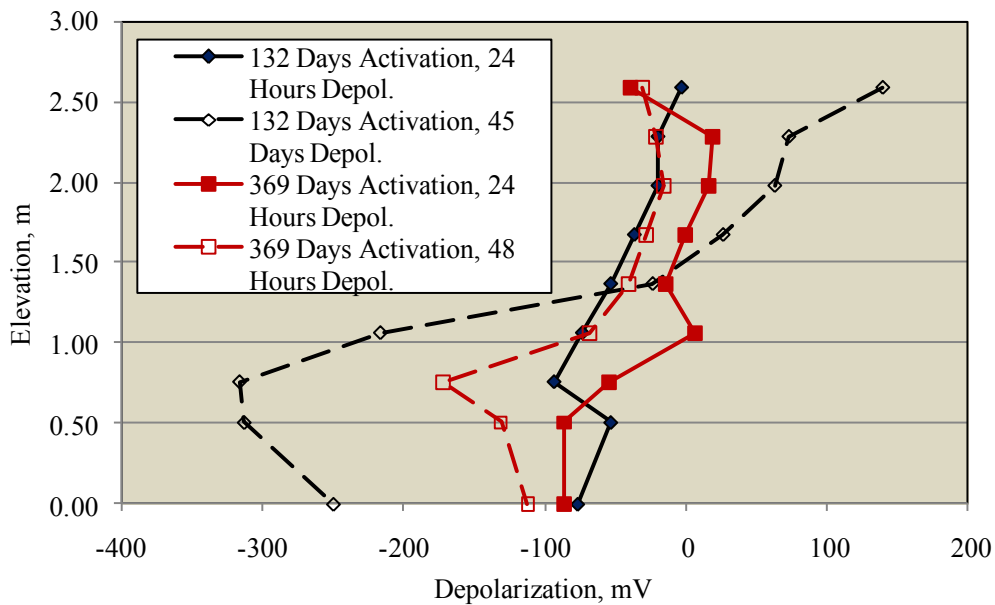


Figure 47: Magnitude of depolarization as a function of elevation after 132 and 369 days activation for the east footer/column of Pier 2.

criterion that voltages greater than 0.3 mV indicate discontinuity, it was concluded that at least these two bars but probably others were not in the cathodic protection circuit. The fact that the electronic portion of this circuit required that current from the east foot/column steel return to ground through the strut probably caused or at least contributed to this.

Table 25 lists concrete resistivity data for the west footer/column of Pier 12 as measured during each of the four site visits. Figure 48 plots the August, 2007 results for each orientation as a function of elevation; and Figure 49 does the same for the average resistivity measured during each site visit. The results indicate that resistivity generally was relatively low on the footer and increased with increasing

elevation, consistent with the concrete being progressively more dry with increasing height.

West (Gulf Side) Footer/Column, Pier 12: Table 26 provides free corrosion potential data at the different elevations and orientations along with the averages as acquired on August 7, 2007; and Figure 50 plots these results. Because TSZ had previously been applied to the column, approximately 75 mm diameter

Table 25: Resistivity data acquired from the east footer/column of Pier 2 on (a) 8/07, (b) 12/07, (c) 2/08, and (d) 8/08.

Elevation, m	Resistivity, kOhm.cm			
	Mia	E	KW	Average
2.44	34.2	26.0	-	30.1
2.13	26.8	27.1	29.5	27.8
1.83	20.8	39.1	27.8	29.2
1.52	8.3	22.5	20.0	16.9
1.22	5.7	7.1	8.3	7.0
0.91	9.4	4.8	5.1	6.4
0.61	1.4	1.2	1.2	1.3
0.30	2.9	3.9	4.1	3.6

(a)

Elevation, m	Resistivity, kOhm.cm			
	Mia	E	KW	Average
2.44	34.4	28.2	31.0	31.2
2.13	24.3	24.8	23.0	24.0
1.83	16.2	15.6	10.0	13.9
1.52	10.1	10.2	7.0	9.1
1.22	11.1	9.6	9.1	9.9
0.91	-	-	-	-
0.61	1.5	1.1	1.2	1.3
0.30	5.0	1.5	2.1	2.9

(b)

Elevation, m	Resistivity, kOhm.cm			
	Mia	E	KW	Average
2.44	-	31.0	-	31.0
2.13	25.0	29.0	32.0	28.7
1.83	16.0	25.0	21.0	20.7
1.52	11.0	15.0	12.0	12.7
1.22	13.0	13.0	8.0	11.3
0.91	8.0	8.0	10.0	8.7
0.61	3.0	3.0	8.0	4.7
0.30	5.0	6.0	3.0	4.7

(c)

Elevation, m	Resistivity, kOhm.cm			
	Mia	E	KW	Average
2.44	62.9	65.2	67.7	65.3
2.13	25.3	25.9	22.4	24.5
1.83	24.7	22.5	15.5	20.9
1.52	11.6	18.3	10.7	13.5
1.22	8.4	10.4	7.4	8.7
0.91	7.9	7.8	6.8	7.5
0.61	4.9	3.9	5.2	4.7
0.30	1.5	1.1	0.8	1.1

(d)

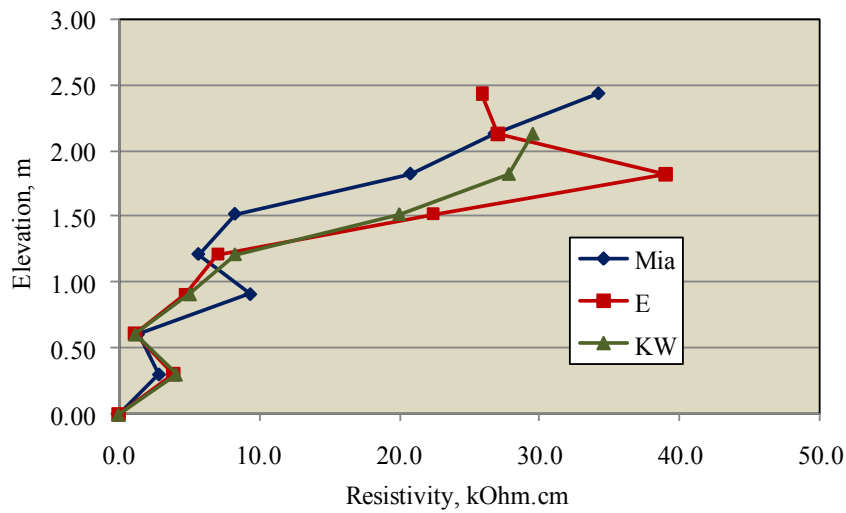


Figure 48: Resistivity data as acquired on the east footer/column of Pier 2 on August 7, 2007 (top of the drill shaft is at approximately 0.75 m elevation).

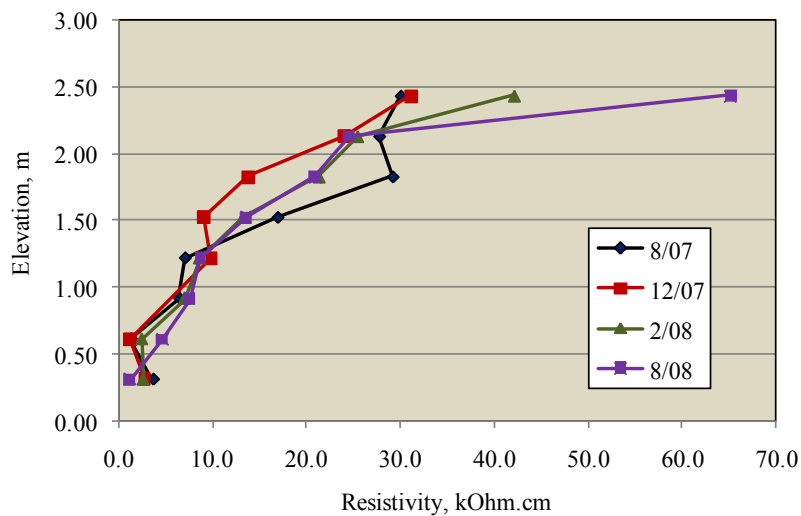


Figure 49: Average resistivity data as acquired during each of the four site visits Figure 48: Resistivity data as acquired on the east footer/column of Pier 2 on August 7, 2007 (top of the drill shaft is at approximately 0.75 m elevation).

Table 26: Free corrosion potentials at various elevations from the west (Gulf side) footer/column of Pier 12 as measured on August 7, 2007.

Elevation, m	Potential, mV (Ag/AgCl)			
	Mia	W	KW	Average
2.90	-370	-460	-440	-423
2.59	-400	-370	-380	-383
2.29	-510	-350	-400	-420
1.98	-530	-360	-410	-433
1.68	-420	-400	-430	-417
1.37	-450	-480	-560	-497
1.07	-530	-540	-530	-533
0.76	-540	-540	-530	-537
0.51	-520	-	-	-520
0	-540	-550	-550	-547

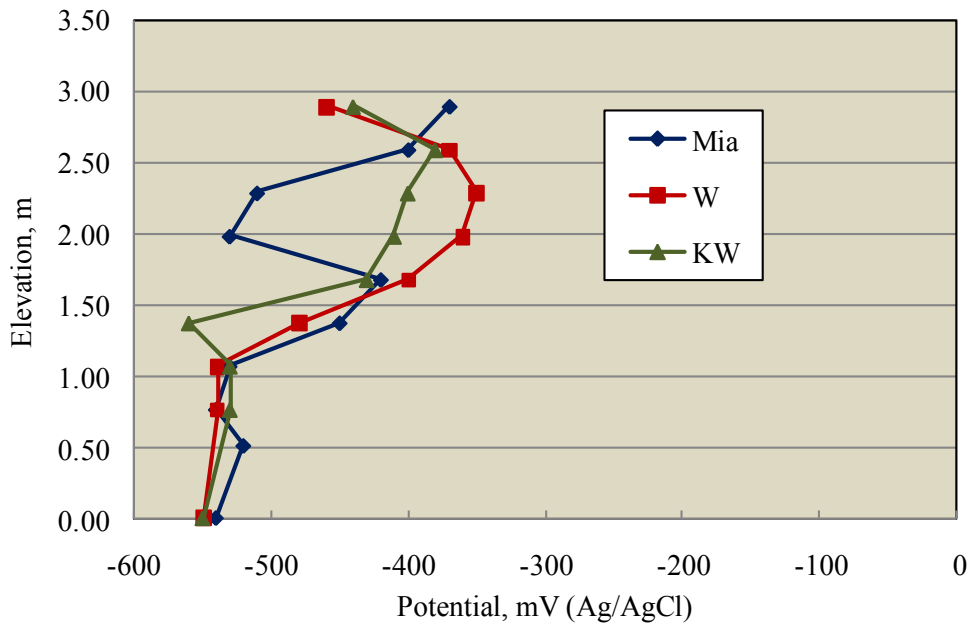


Figure 50: Free corrosion potential data for the east footer/column of Pier 12 as acquired during the August 7, 2007 site visit.

holes were drilled through this coating at the measurement locations so the reference electrode could contact the concrete directly. The general trend in Figure 50 is the same as determined for Pier 2 (potential was more positive at increasing elevation); however, the Pier 12 west column free corrosion potentials are generally more positive than for Pier 2, consistent with some polarization being provided here by the TSZ.

Table 27 lists the current-on potential at each measurement elevation and also the average at each elevation as recorded during the site visits subsequent to activation. Figure 51 plots the average values of these data as a function of elevation in comparison to the free corrosion potentials (Figure 50). This reveals minimal polarization for the 16 day data and that polarization at other times was nil above 1.2 to 2 m. As such, the MgSBAs affected less apparent polarization here than occurred for Pier 2. This is attributed to the TSZ serving as a current sink such that current density on the reinforcement was proportionally reduced. The highest elevation to which any cathodic polarization was affected was 2 m (369 days data). Such a rational assumes, however, that the initial free corrosion potentials remain applicable at the later times.

Table 27: Current-on potential at each of the measurement orientations/elevations on the west footer/column of Pier 12 after (a) four hours, (b) 16 days, (c) 132 days, and (d) 369 days activation.

Elevation, m	Potential, mV (Ag/AgCl)			
	Mia	W	KW	Average
2.90	-200	-150	-200	-183
2.59	-250	-210	-220	-227
2.29	-350	-180	-230	-253
1.98	-350	-230	-260	-280
1.68	-400	-290	-310	-333
1.37	-370	-400	-530	-433
1.07	-550	-550	-600	-567
0.76	-640	-600	-710	-650
0.51	-860	-710	-780	-783
0.00	-1310	-1310	-1250	-1290

(a)

Elevation, m	Potential, mV (Ag/AgCl)			
	Mia	W	KW	Average
2.90	40	-	-	40
2.59	-10	-	-	-10
2.29	-130	-	-40	-85
1.98	-110	-	-50	-80
1.68	-150	-	-40	-95
1.37	-170	-	-190	-180
1.07	-320	-	-350	-335
0.76	-430	-	-450	-440
0.51	-610	-	-600	-605
0.00	-800	-	-730	-765

(b)

Elevation, m	Potential, mV (Ag/AgCl)			
	Mia	W	KW	Average
2.90	-	-260	-250	-255
2.59	-180	-240	-360	-260
2.29	-150	-380	-370	-300
1.98	-170	-360	-	-265
1.68	-400	-480	-470	-450
1.37	-380	-740	-660	-593
1.07	-480	-740	-840	-687
0.76	-720	-760	-900	-793
0.51	-830	-890	-1000	-907
0.00	-1050	-1120	-1080	-1083

(c)

Elevation, m	Potential, mV (Ag/AgCl)			
	Mia	W	KW	Average
2.90	-	-	-	-
2.59	-400	-321	-	-361
2.29	-265	-283	-345	-298
1.98	-405	-460	-400	-422
1.68	-453	-586	-448	-496
1.37	-515	-600	-639	-585
1.07	-666	-803	-730	-733
0.76	-899	-887	-950	-912
0.51	-1025	-926	-1040	-997
0.00	-	-	-	-

(d)

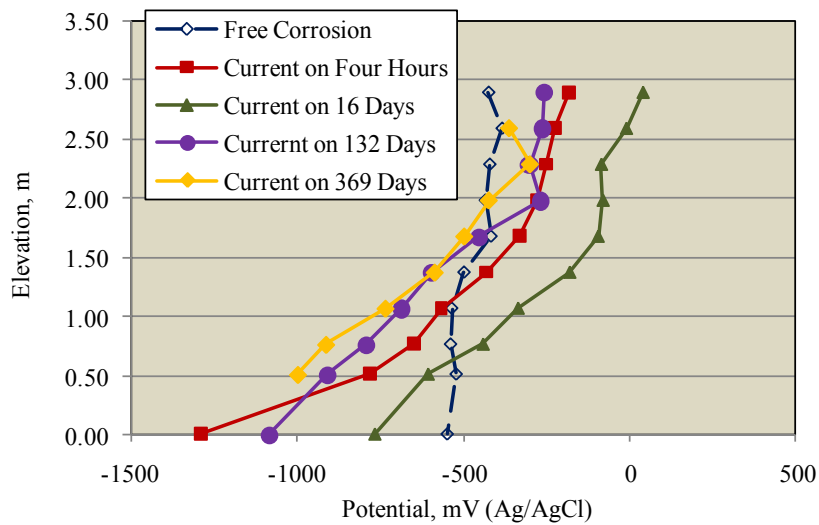


Figure 51 Plot of current-on potentials at each measurement elevation on the west footer/column of Pier 12 for each of the site visits in comparison to the free corrosion values.

Table 28 lists the instant-off potential at each measurement elevation in comparison to the current-on values and the average of each, and Figure 52 plots the average values versus elevation. This indicates that the difference between the on and off measurements was small or nil at the time of the initial two site visits but ranged from -81 to -137 mV and was relatively independent of elevation after 369 days activation. This is in general agreement with the Pier 2 data.

Table 29 lists the magnitudes of depolarization for this footer/column at the various elevations and disconnection periods subsequent to activation, and Figure 53 provides a plot of the averages of these data. The 132 days activation data indicate 100 mV depolarization to about 1-1.5 m, whereas the 369 days results show some depolarization to the highest measurement location. The trend reversals and

Table 28: Listing of current-on and current-off potentials for the west footer/column of Pier 12 after (a) 16, (b) 132, and (c) 369 days activation.

Elevation, m	Potential, mV (Ag/AgCl)					
	Mia		KW		Average	
	On	Off	On	Off	On	Off
2.59	-10	0	-	-	10	0
2.29	-130	-120	-40	-40	-85	-80
1.98	-110	-110	-50	-50	-80	-80
1.68	-150	-140	-40	-30	-95	-85
1.37	-170	-150	-190	-190	-180	-170
1.07	-320	-300	-350	-340	-335	-320
0.76	-430	-410	-450	-430	-440	-420
0.51	-610	-550	-600	-570	-605	-560
0.00	-800	-680	-730	-630	-765	-655

(a)

Elevation, m	Potential, mV (Ag/AgCl)							
	Mia		W		KW		Average	
	On	Off	On	Off	On	Off	On	Off
2.90	-	-	-260	-240	-250	-240	-255	-240
2.59	-180	-180	-240	-230	-360	-350	-260	-253
2.29	-150	-150	-380	-370	-370	-360	-300	-293
1.98	-170	-170	-0.36	-0.35	-	-	-85	-85
1.68	-400	-400	-0.48	-0.47	-470	-460	-290	-287
1.37	-380	-370	-0.74	-0.73	-660	-650	-347	-340
1.07	-480	-480	-0.74	-0.73	-840	-830	-440	-437
0.76	-720	-720	-0.76	-0.75	-900	-890	-540	-537
0.51	-830	-820	-0.89	-0.88	-1000	-990	-610	-604
0.00	-1050	-1050	-1.12	-1.07	-1080	-1060	-710	-704

(b)

Elevation, m	Potential, mV (Ag/AgCl)							
	Mia		W		KW		Average	
	On	Off	On	Off	On	Off	On	Off
2.59	-400	-346	-321	-213	-	-	-361	-280
2.29	-265	-155	-283	-161	-345	-230	-298	-182
1.98	-405	-325	-460	-355	-400	-327	-422	-336
1.68	-453	-337	-586	-450	-448	-337	-496	-375
1.37	-515	-413	-600	-498	-639	-480	-585	-464
1.07	-666	-485	-803	-680	-730	-622	-733	-596
0.76	-899	-780	-887	-770	-950	-839	-912	-796
0.51	-1025	-897	-926	-806	-1040	-1005	-997	-903
0.00	-	-	-	-	-	-	-	-

(c)

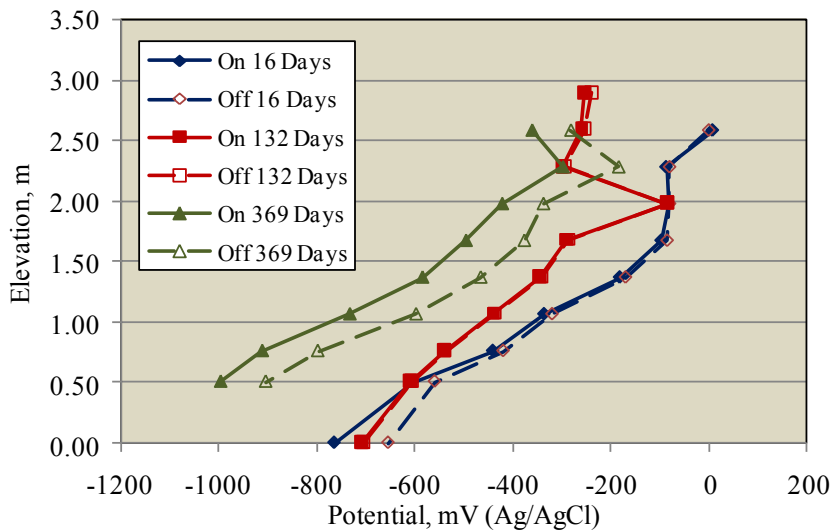


Figure 52: Comparison of current-on and current-off potentials for the west footer/column of Pier 12.

positive depolarizations (132 days activation) suggest a lack of electrical continuity of the rebars, as mentioned above.

Table 30 lists concrete resistivity data from the west footer of Pier 12, as measured during the three site visit for which data were acquired. The data are from the footer only because the TSZ precluded measurements on the column.

East (Atlantic Side) Footer/Column, Pier 12: Table 31 provides free corrosion potential data at the different elevations and orientations along with the averages as acquired on August 7, 2007; and Figure 54 plots these results. The general trend is the same as determined for the Pier 2 footer/columns (potential was more positive at increasing elevation) but are more negative at the column elevations than

for the west footer/column of this pier (Figure 50).

Table 29: Magnitude of depolarization after (a) 132 days activation and 24 hours depolarization, (b) 132 days activation and 45 days depolarization, (c) 369 days activation and 24 hours depolarization, and (d) 369 days activation and 48 hours depolarization.

Elevation, m	Depolarization, mV			
	Mia	W	KW	Average
2.59	-20	0	-130	-50
2.29	-10	-160	-30	-67
1.98	10	20	370	133
1.68	-30	-130	10	-50
1.37	-10	-270	-190	-157
1.07	-20	-90	-210	-107
0.76	-60	-80	-120	-87
0.51	-90	-170	-180	-147
0.00	-90	-100	-90	-93

(a)

Elevation, m	Depolarization, mV			
	Mia	W	KW	Average
2.90	-	50	-40	5
2.59	-10	10	-110	-37
2.29	60	30	-10	27
1.98	160	130	430	240
1.68	-40	170	40	57
1.37	150	-80	20	30
1.07	70	-160	-210	-100
0.76	-130	-180	-250	-187
0.51	-170	-290	-300	-253
0.00	-280	-300	-290	-290

(b)

Elevation, m	Depolarization, mV			
	Mia	W	KW	Average
2.59	-189	-86	-54	-110
2.29	-34	-63	-60	-52
1.98	-148	-107	-62	-106
1.68	-91	-175	4	-87
1.37	-103	-159	-51	-104
1.07	-65	-177	-42	-95
0.76	-106	-112	-77	-98
0.51	-137	-91	-171	-133

(c)

Elevation, m	Depolarization, mV			
	Mia	W	KW	Average
2.59	-206	-57	39	-75
2.29	-69	-22	95	1
1.98	-146	-99	-48	-98
1.68	-79	-192	15	-85
1.37	-118	-170	-80	-123
1.07	-155	-215	-30	-133
0.76	-118	-110	-90	-106
0.51	-103	-105	-145	-118

(d)

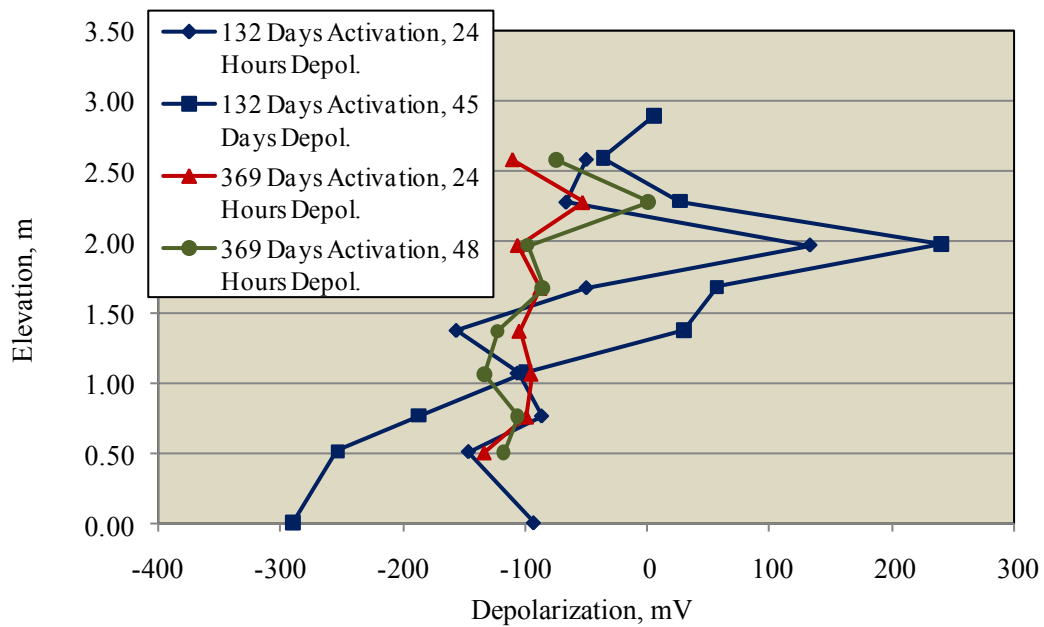


Figure 53: Magnitude of depolarization as a function of elevation after 132 and 369 days activation for the west footer/column of Pier 12.

Table 32 lists the current-on potential at each measurement elevation and also the average at each elevation as recorded during the site visits subsequent to activation. Figure 55 plots the average values of these data as a function of elevation in comparison to the free corrosion potentials (Figure 54). This reveals minimal polarization for the 16 day data and that polarization was nil above about 1-1.5 m, consistent with what was reported above for other footer/columns at this site visit. On the other hand, the 369 days activation data indicate almost 100 mV polarization at the highest elevation. It can be reasoned that, like the west footer/column of this pier, current that was drained by the TSZ reduced what was available to the east footer/column.

Table 30: Resistivity data acquired from the west footer/column of Pier 12 on each of the three site visits for which measurements were made along with the overall average: (a) 12/07, (b) 2/08, and (c) 8/08.

Elevation, m	Resistivity, kOhm.cm			
	Mia	W	KW	Average
2.44	-	-	-	-
2.13	-	-	-	-
1.83	-	-	-	-
1.52	-	-	-	-
1.22	-	-	-	-
0.91	-	-	-	-
0.61	11.7	3.7	1.5	5.6
0.30	15.5	5.6	1.5	7.5

(a)

Elevation, m	Resistivity, kOhm.cm			
	Mia	W	KW	Average
2.44	-	-	-	-
2.13	-	-	-	-
1.83	-	-	-	-
1.52	-	-	-	-
1.22	-	-	-	-
0.91	-	-	-	-
0.61	11.7	3.7	1.5	5.6
0.30	15.5	5.6	1.5	7.5

(b)

Elevation, m	Resistivity, kOhm.cm			
	Mia	W	KW	Average
2.44	-	-	-	-
2.13	-	-	-	-
1.83	-	-	-	-
1.52	-	-	-	-
1.22	-	-	-	-
0.91	-	-	-	-
0.61	11.7	3.7	1.5	5.6
0.30	15.5	5.6	1.5	7.5

(c)

Table 31: Free corrosion potentials at various elevations from the east (Atlantic side) footer/column of Pier 12 acquired on August 7, 2007.

Elevation, m	Potential, mV (Ag/AgCl)			
	Mia	E	KW	Average
2.54	-150	-240	-240	-210
2.24	-290	-310	-300	-300
1.93	-330	-330	-350	-337
1.63	-340	-370	-380	-363
1.32	-370	-410	-400	-393
1.02	-500	-500	-510	-503
0.71	-490	-510	-500	-500
0.41	-520	-510	-520	-517
0.00	-540	-550	-550	-547

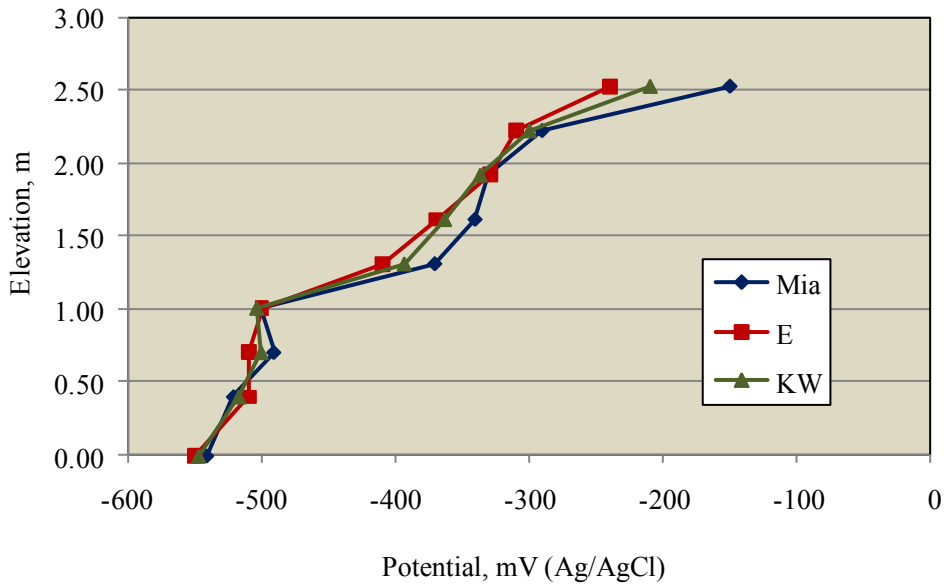


Figure 54: Free corrosion potential data for the east footer/column of Pier 12 as acquired during the August 7, 2007 site visit.

Table 33 lists the instant-off potential at each measurement elevation in comparison to the current-on values and the average of each, and Figure 56 plots the average values versus elevation. This indicates that the difference between the pairs of measurements ranged from -33 to -143 mV at 16 days polarization, was nil at 132 days, and ranged from -95 to -120 mV after 369 days activation. This is in general agreement with data for the other footer/columns.

Table 32: Current-on potential at each of the measurement elevations on the east footer/column of Pier 12 after (a) four hours, (b) 16 days, (c) 132 days, and (d) 369 days activation.

Elevation, m	Potential, mV (Ag/AgCl)			
	Mia	E	KW	Average
2.54	-180	-190	-160	-177
2.24	-240	-270	-280	-263
1.93	-320	-300	-320	-313
1.63	-380	-340	-350	-357
1.32	-500	-460	-430	-463
1.02	-710	-740	-660	-703
0.71	-800	-790	-730	-773
0.41	-900	-880	-910	-897
0.00	-1300	-1300	-1310	-1303

(a)

Elevation, m	Potential, mV (Ag/AgCl)			
	Mia	E	KW	Average
2.90	120	180	260	187
2.59	80	80	160	107
2.29	-230	70	120	-13
1.98	-280	10	80	-63
1.68	-210	-120	-50	-127
1.37	-430	-500	-220	-383
1.07	-470	-510	-450	-477
0.76	-510	-530	-540	-527
0.51	-680	-620	-670	-657
0.00	-810	-800	-790	-800

(b)

Elevation, m	Potential, mV (Ag/AgCl)			
	Mia	E	KW	Average
2.59	-190	-230	-210	-210
2.29	-300	-300	-280	-252
1.98	-340	-350	-320	-280
1.68	-430	-430	-400	-315
1.37	-520	-550	-510	-357
1.07	-750	-830	-730	-426
0.76	-870	-930	-920	-495
0.51	-910	-990	-990	-553
0.00	-1120	-1110	-1080	-614

(c)

Elevation, m	Potential, mV (Ag/AgCl)			
	Mia	W	KW	Average
2.59	-326	-412	-308	-349
2.29	-308	-455	-420	-394
1.98	-410	-523	-505	-479
1.68	-525	-572	-573	-557
1.37	-581	-675	-655	-637
1.07	-680	-820	-786	-762
0.76	-875	-1101	-1160	-1045
0.51	-1160	-1119	-1195	-1158
0.00	-1232	-1250	-1265	-1249

(d)

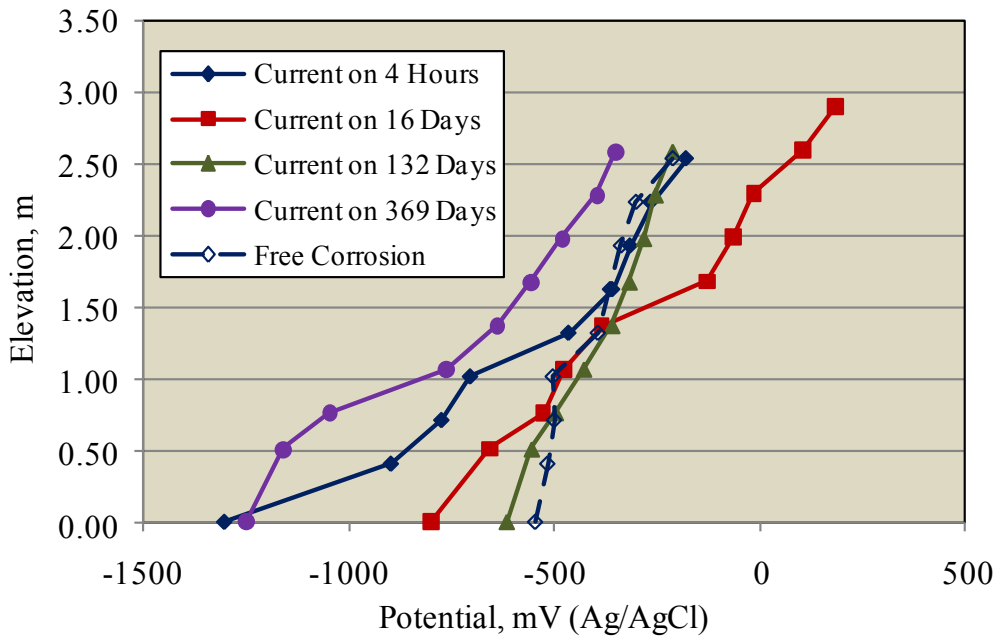


Figure 55 Plot of current-on potentials at each measurement elevation for the east footer/column of Pier 12 for each of the site visits in comparison to the free corrosion values.

Table 34 lists the magnitudes of depolarization for this footer/column at the various elevations and times of disconnection subsequent to activation, and Figure 57 provides a plot of the averages of these data. Both data sets (132 and 369 days activation) indicate greater depolarization after longer disconnection times (24 hours and 45 days) with the effect being particularly apparent at 45 days. The data suggest that some protection was realized to an elevation of 2.5 m. Table 35 lists anode current output for pier 12 as recorded during each of the site visits.

Table 33: Listing of current-on and current-off potentials for the east footer/column of Pier 12 after (a) 16, (b) 132, and (c) 369 days activation.

Elevation, m	Potential, mV (Ag/AgCl)							
	Mia		E		KW		Average	
	On	Off	On	Off	On	Off	On	Off
2.90	120	-	180	210	260	280	187	245
2.59	80	100	80	100	160	180	107	140
2.29	-230	-200	70	90	120	130	-13	107
1.98	-280	-210	10	20	80	100	-63	-27
1.68	-210	-180	-120	10	-50	-20	-127	-73
1.37	-430	-390	-500	-450	-220	-190	-383	-273
1.07	-470	-440	-510	-480	-450	-430	-477	-433
0.76	-510	-470	-530	-500	-540	-500	-527	-480
0.51	-680	-620	-620	-570	-670	-610	-657	-550
0.00	-810	-700	-800	-680	-790	-670	-800	-657

(a)

Elevation, m	Potential, mV (Ag/AgCl)							
	Mia		E		KW		Average	
	On	Off	On	Off	On	Off	On	Off
2.59	-190	-160	-230	-220	-210	-200	-210	-193
2.29	-300	-290	-300	-290	-280	-270	-293	-283
1.98	-340	-330	-350	-340	-320	-310	-337	-327
1.68	-430	-420	-430	-420	-400	-390	-420	-410
1.37	-520	-510	-550	-540	-510	-500	-527	-517
1.07	-750	-730	-830	-820	-730	-720	-770	-757
0.76	-870	-860	-930	-920	-920	-910	-907	-897
0.51	-910	-900	-990	-980	-990	-970	-963	-950
0.00	-1120	-1050	-1110	-1060	-1080	-1040	-1103	-1050

(b)

Elevation, m	Potential, mV (Ag/AgCl)							
	Mia		E		KW		Average	
	On	Off	On	Off	On	Off	On	Off
2.59	-256	-137	-342	-229	-238	-126	-279	-164
2.29	-238	-118	-385	-268	-350	-237	-324	-208
1.98	-340	-225	-453	-341	-435	-322	-409	-296
1.68	-455	-325	-502	-390	-503	-385	-487	-367
1.37	-511	-405	-605	-490	-585	-476	-567	-457
1.07	-610	-485	-750	-637	-716	-599	-692	-574
0.76	-805	-686	-1031	-928	-1090	-975	-975	-863
0.51	-1090	-969	-1049	-1004	-1125	-1005	-1088	-993
0.00	-1162	-1080	-1180	-1045	-1195	-1060	-1179	-1062

(c)

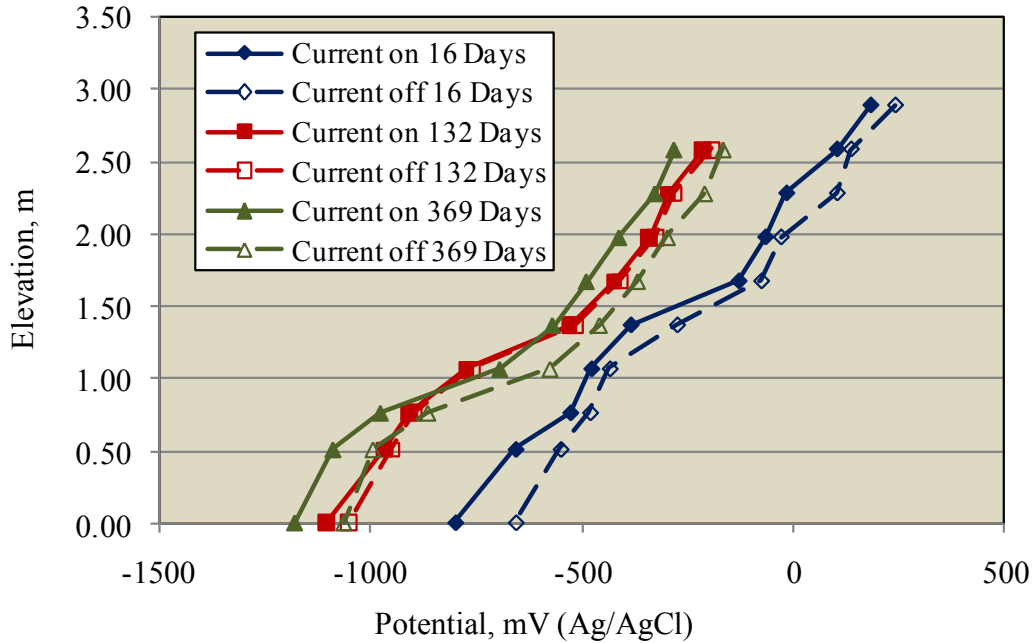


Figure 56: Comparison of current-on and current-off potentials for the east footer/column of Pier 12.

Table 36 lists concrete resistivity data from the three measurement orientation on east footer/column of Pier 12 during three of the site visit, and Figure 58 provides a plot of the August 7, 2007 results. Likewise, Figure 59 shows a plot of the average resistivities. The data generally conform to the trends for the other footer/columns as reported above.

Table 34: Magnitudes of depolarization after (a) 132 days activation and 24 hours depolarization, (b) 132 days activation and 45 days depolarization, (c) 369 days activation and 24 hours depolarization, and (d) 369 days activation and 48 hours depolarization.

Elevation, m	Depolarization, mV			
	Mia	E	KW	Average
2.59	10	-40	20	-3
2.29	-10	-50	0	-20
1.98	-10	-40	-10	-20
1.68	-40	-50	-20	-37
1.37	-50	-70	-40	-53
1.07	-110	-120	10	-73
0.76	-100	-100	-80	-93
0.51	-20	-90	-50	-53
0.00	-80	-90	-60	-77

(a)

Elevation, m	Depolarization, mV			
	Mia	E	KW	Average
2.59	80	-70	-10	0
2.29	-20	-70	-30	-40
1.98	-10	-80	-30	-40
1.68	-70	-110	-70	-83
1.37	-90	-170	-140	-133
1.07	-200	-350	-310	-287
0.76	-280	-310	-300	-297
0.51	-270	-340	-290	-300
0.00	-280	-290	-270	-280

(b)

Elevation, m	Depolarization, mV			
	Mia	E	KW	Average
2.59	-75	-39	-3	-39
2.29	92	-39	4	19
1.98	86	-25	-14	16
1.68	38	-27	-13	-1
1.37	36	-49	-29	-14
1.07	126	-73	-34	6
0.76	172	-132	-202	-54
0.51	-72	-95	-90	-86
0.00	-109	-67	-82	-86

(c)

Elevation, m	Depolarization, mV			
	Mia	E	KW	Average
2.59	-39	-47	-7	-31
2.29	-25	-54	14	-22
1.98	-13	-26	-9	-16
1.68	-12	-46	-29	-29
1.37	-24	-57	-43	-41
1.07	-50	-92	-65	-69
0.76	-119	-171	-226	-172
0.51	-140	-102	-151	-131
0.00	-141	-95	-100	-112

(d)

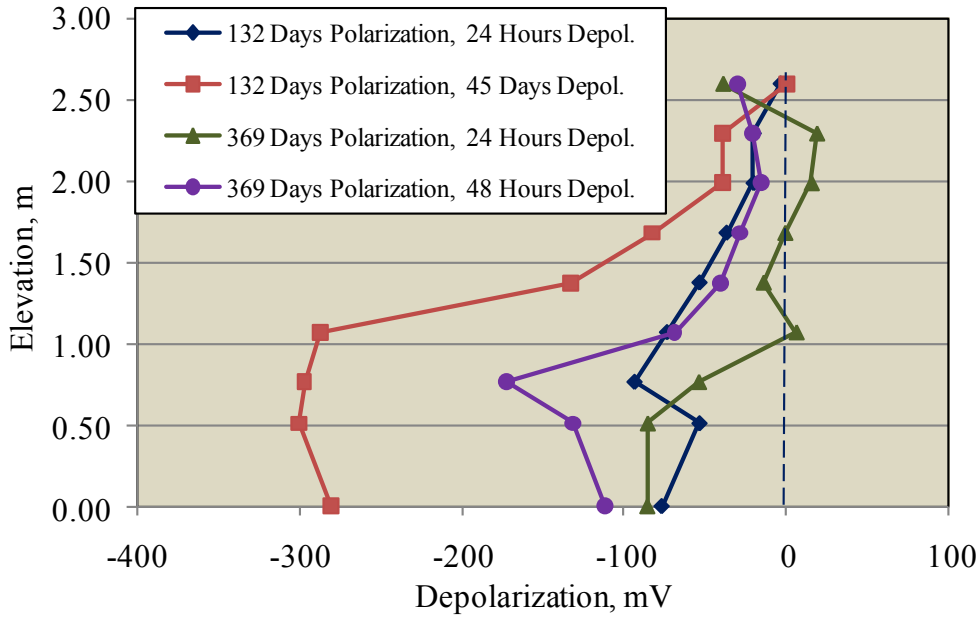


Figure 57: Magnitude of depolarization as a function of elevation after 132 and 369 days activation for the east footer/column of Pier 12.

Table 35: Net current output at different times after anode activation for Pier 12.

Date	Time Since Activation, days	Current, mA
August 8, 2007	0	450
August 24, 2007	16	140
December 18, 2007	132	183
August 12, 2008	369	120

Table 36: Resistivity data acquired from the east footer/column of Pier 12 on each of the three site visits for which measurements were made along with the overall average: (a) 12/07, (b) 2/08, and (c) 8/08.

Elevation, m	Resistivity, kOhm.cm			
	Mia	E	KW	Average
2.44	26.3	23.6	40.0	31.8
2.13	20.25	16.0	41.2	28.6
1.83	23.55	12.6	25.4	19.0
1.52	16.45	10.3	24.3	17.3
1.22	12.95	11.0	37.1	24.0
0.91	-	-	-	-
0.61	2.49	2.2	3.2	2.7
0.30	2.0	2.2	6.2	4.2

(a)

Elevation, m	Resistivity, kOhm.cm			
	Mia	E	KW	Average
2.44	22.0	-	-	22.0
2.13	24.0	36.0	32.0	34.0
1.83	17.0	19.0	26.0	22.5
1.52	13.0	18.0	29.0	23.5
1.22	15.0	20.0	37.5	28.8
0.91	4.0	34.0	11.0	-
0.61	4.0	5.0	5.0	5.0
0.30	5.0	5.6	6.0	5.8

(b)

Elevation, m	Resistivity, kOhm.cm			
	Mia	E	KW	Average
2.44	15.6	21.1	25.4	20.7
2.13	17.6	23.0	22.2	20.9
1.83	21.6	17.5	20.5	19.9
1.52	18.5	18.8	17.5	18.3
1.22	19.2	12.6	15.2	15.7
0.91	12.7	11.4	14.5	12.9
0.61	8.2	34.0	4.5	15.6
0.30	2.1	2.4	2.2	2.2

(c)

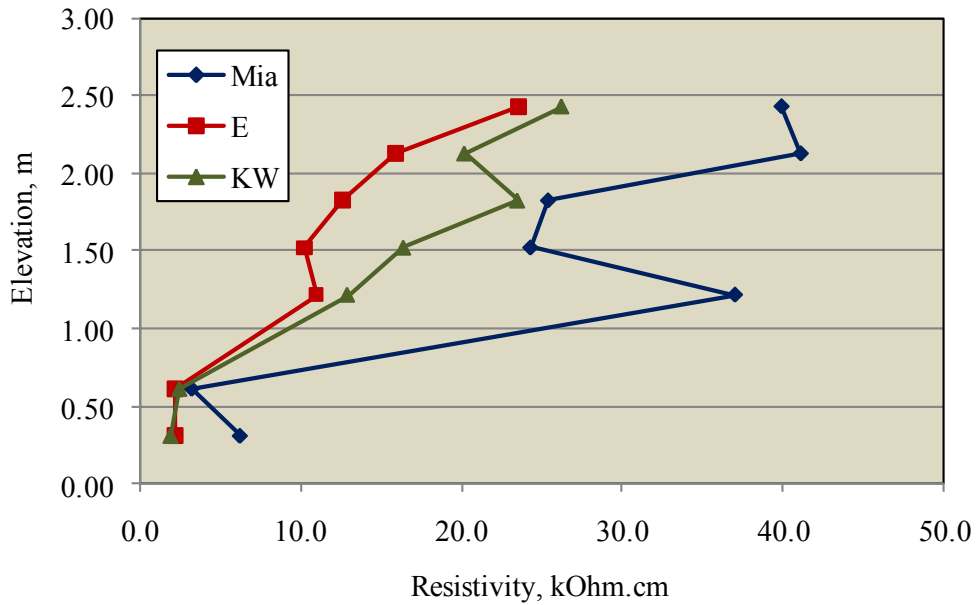


Figure 58: Resistivity data as acquired on the east footer/column of Pier 12 on December 18, 2007.

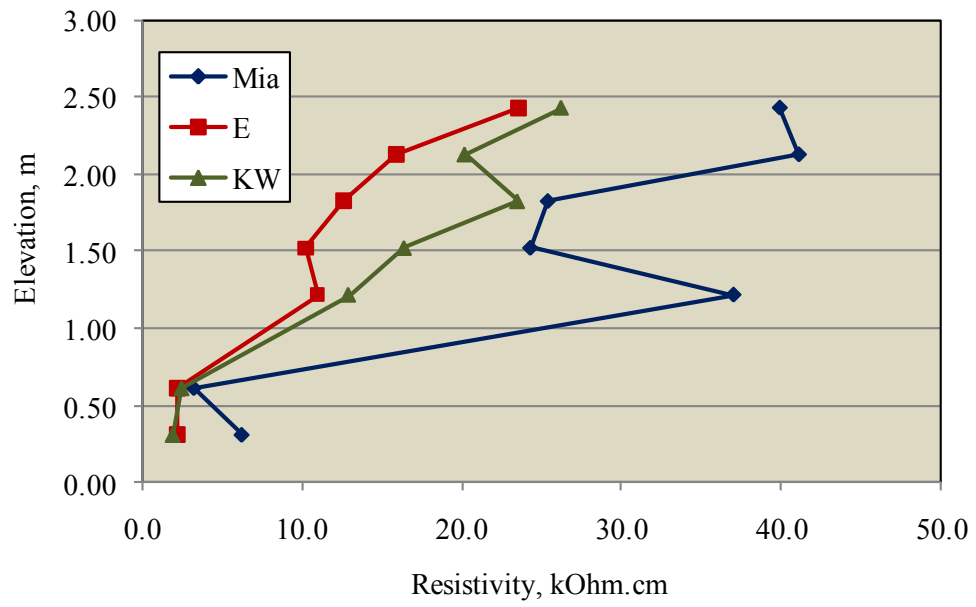


Figure 59: Average resistivity data as acquired on the east footer/column of Pier 12 during each of three site visits.

NUMERICAL MODELING

Bahia Honda Bridge

Modeling for this bridge utilized the commercially available Beasy™ boundary element modeling (BEM) software version 10.0. The program allows input of 1) structure dimensions, 2) assignment of resistivities for the different electrolytes (sea water and concrete in this case with different resistivities being allowed for various concrete components if so desired), and 3) selection of native potentials and polarization characteristics for anodes (ZnSBA in this case) and reinforcement. By so doing, a three-dimensional model of the footer/column reinforcement and concrete was developed along with ZnSBA placement based upon design drawings for the project. Input parameters were as follows:

1. An initial analysis was based on a resistivity of 25 Ω -cm for the sea water, 2.5 k Ω -cm for the footer concrete, and 20 k Ω -cm for the column concrete, consistent with the field results (Figures 24 and 25). Subsequently, an analysis was performed in which all concrete resistivity was that of the footer (2.5 k Ω -cm), as suggested by the highest measurements on the column to apply in cases where gunite repairs have not been made (Figures 24 and 25).
2. The cathodic polarization curve that served as input for polarization behavior for the reinforcement was taken as that experimentally measured by Presuel-Moreno et al.¹⁶ on simulated piling specimens. Figure 60 shows this potential – current relationship along with that for the anode, where the former reflects the rebar surface area that was assumed to be affected. Potential of the anode was taken as constant (non-polarizable or independent of current output) and equal to -1,030 mV. Free corrosion rebar potentials were those listed for Pier 40W-East in Table 2(b) and Figure 21.

Figure 61 shows the BEM results as a color contoured spatial graphic of potential on the external concrete surface and sea water, and Figure 62 provides this same type of view for the anode and reinforcement. An enlarged view of the color coded potential scale from Figure 63. The model projects a potential of -1,003 mV (Ag/AgCl) for the lowest elevation reinforcement which is in the submerged zone and -235 mV (Ag/AgCl) near the column top. Likewise, Figure 64 compares these data with the field survey potential profile for 40W-East, as acquired during the May, 2005 site visit and shows that BEM projects somewhat more positive potentials on the footer and more negative potentials than measured in the column elevation range (1.60 m upward). The latter difference may have been caused by the disbonded gunite having reduced the measured polarization of the column steel. Alternatively, the

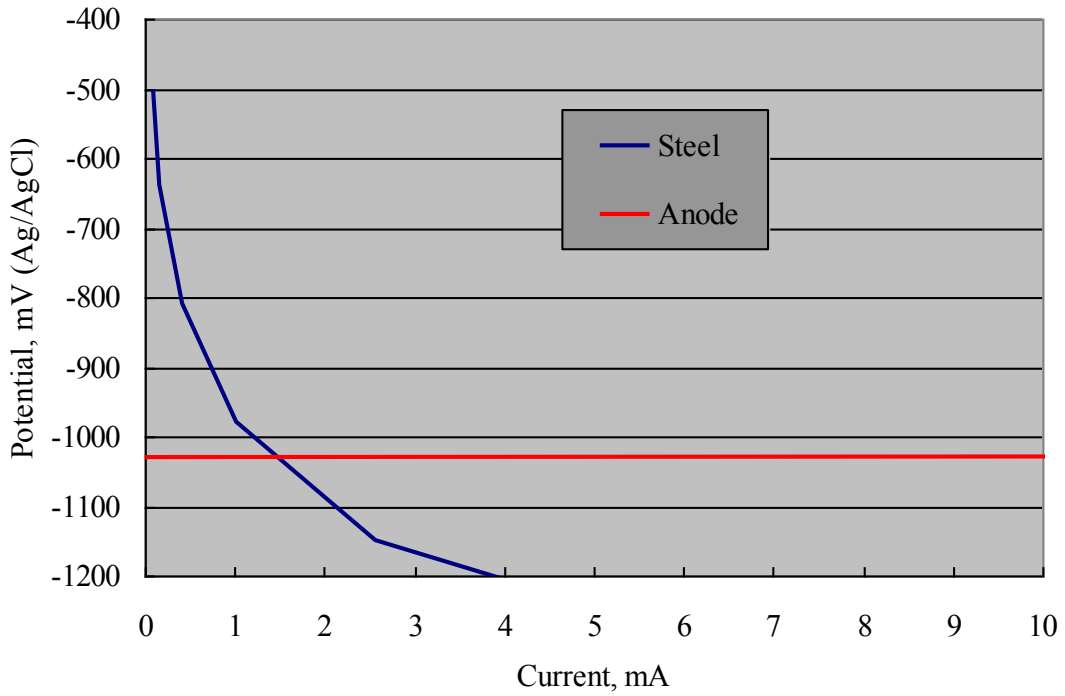


Figure 60: Assumed polarization curve for steel and anode that were employed in the BEM analysis.

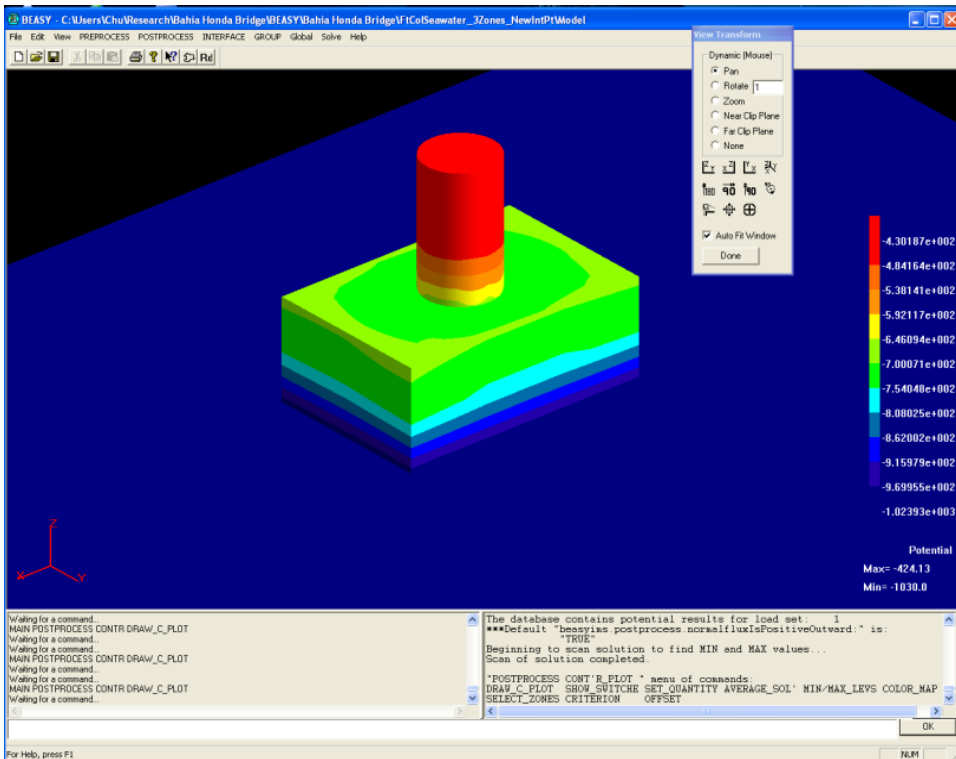


Figure 61: Beasy modeling results for potential on a footer and column of the Bahia Honda Bridge.

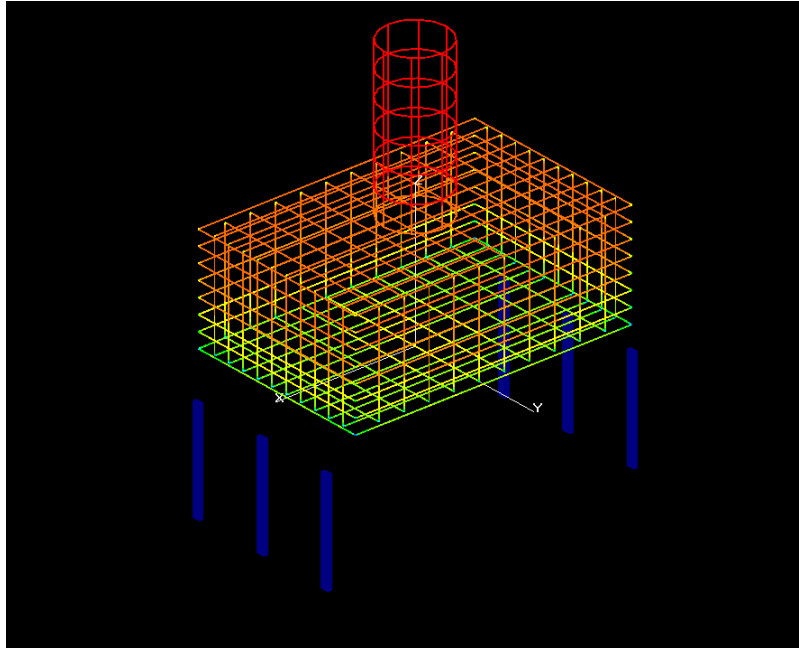


Figure 62: BEM model of the footer and column reinforcement and the submerged bulk anodes on a pier of the Bahia Honda Bridge.

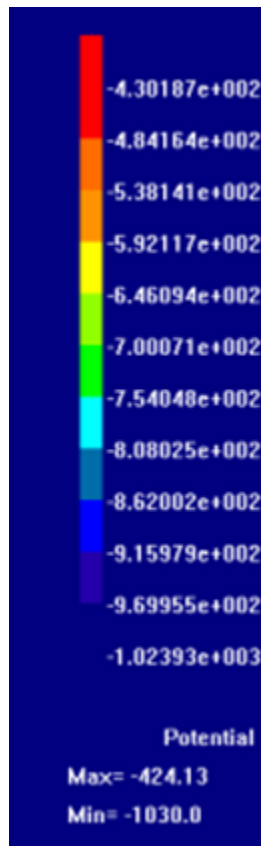


Figure 63: Enlarged view of the color coded potential scale from Figures 61 and 62.

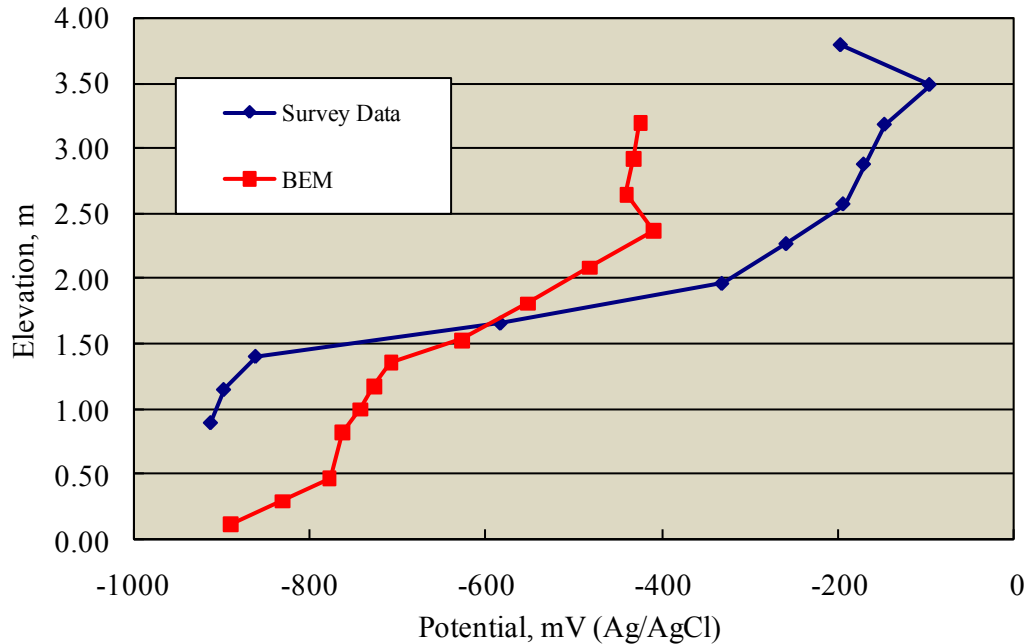


Figure 64: Comparison of the BEM potential versus elevation projection with the field survey results.

reinforcement grid in the footer beneath the column base may have served as a current sink and resulted in reduced current being available to the column steel and reduced polarization here. The BEM projection of greater column steel polarization may have shifted the footer steel potentials to more positive values. If this was the case, then it is more likely that the gunite repair and not the footer steel grid beneath the column was responsible for the differences between measured and BEM values.

As an additional consideration, the analysis was also performed using an operating anode potential of -1,500 mV, which approximates the value for a MgSBA. Results for this are shown in Figure 65 in comparison to results for a ZnSBA. The results indicate that the MgSBA provided about 150 mV greater polarization two meters above the footer base.

Niles Channel Bridge

General

As noted above, two approaches were implemented to model CP on this bridge by MgSBAs: a finite difference two-dimensional (2-D) model, which handled combined activation and concentration cathodic polarization behavior and a simplified one-dimensional (1-D) model. The former closely replicated geometry of the footer/column analytically and was computationally demanding, whereas the latter required fewer computational resources.

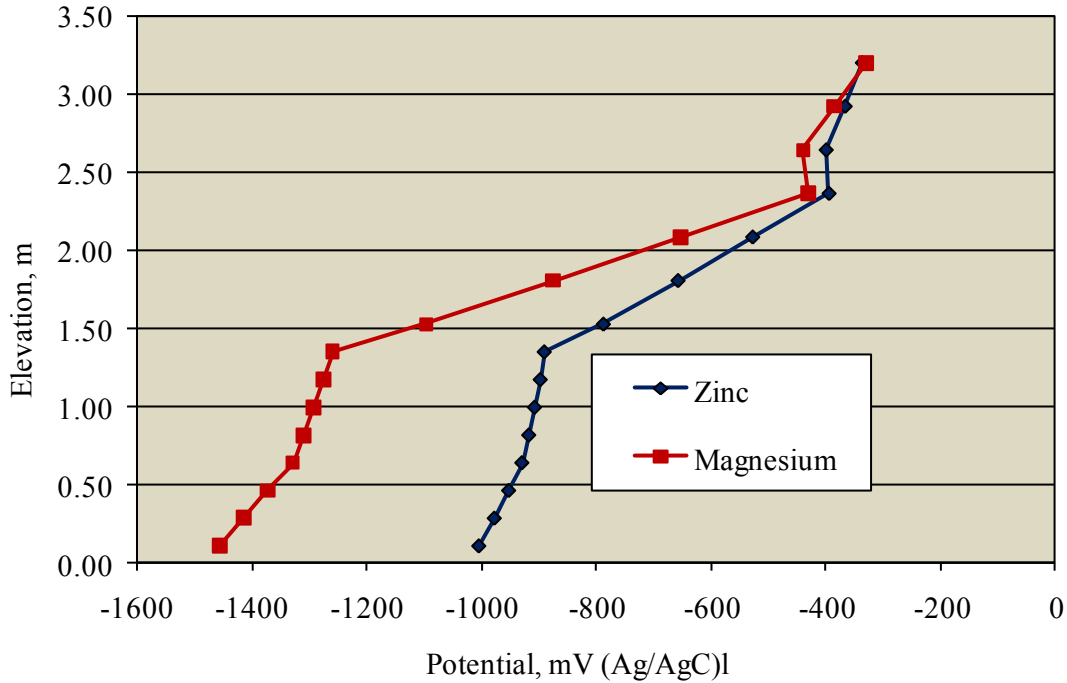


Figure 65: Comparison of the BEM potential versus elevation projections for a MgSBA and ZnSBA

The formulation used to model the electrochemical corrosion process results in two second order partial differential equations, linked by boundary conditions due to polarization at the steel-concrete interface. These difference equations were based on nodes placed on a longitudinal section of the column which represented the concrete and were formulated to account for cylindrical symmetry of the column. The usual central difference scheme was used for computing the potential and concentration values. At points next to the rebar surface the equations were rewritten to account for the fractional spacing. Details of the method are provided elsewhere.²⁰

2D Finite Difference Model

System Dimensions: The model was applied to a cylindrical shape with the lower fourth (1.22 m) submerged in seawater. This geometry approximates the squat prism present in many structures and also in the NC bridge and permits reduction of the problem to two dimensions by assuming angular symmetry. The calculations were performed for a 1.524 m (5.0 ft) diameter by 4.88 m (16.0 ft) high cylinder, with the rebar cage placed such that concrete cover was constant at 10.16 cm (4.0 in) for the external lateral, top, and bottom surfaces. A single mat of rebar was considered with a steel placement density of one m² surface area for each one m² of concrete surface, which approximates typical construction practice. This

geometry is a simplification from the actual structure, and the diameter difference between the footer and column was disregarded.

Concrete Properties. Concrete properties of relevance to the performance of a cathodic protection system include electrical resistivity, ρ , and effective oxygen diffusivity, D . For the purposes of these exploratory calculations both properties were treated as varying only as a function of elevation above the waterline and were assumed constant along the radial direction. Two resistivity profiles, corresponding to the maximum and minimum experimental resistivity profiles, were curve fitted. The region below the waterline and the first 0.45 m above the mean water line were assumed to have constant resistivity. For two meters above this, resistivity increased monotonically to values of either 19 or 44 k Ω -cm, which approximate the minimum and maximum values, respectively, recorded for Pier 2 (see Table 19 and Figures 41 and 42). Resistivity was assumed to be constant above this elevation. The reinforcing steel was assumed to be passive above either 1.83 or 1.52 m above the waterline, corresponding to the low and high resistivity profiles. Only one oxygen diffusivity profile was considered. These profiles are shown in Figure 66. There is little information on effective values of oxygen diffusivity in field structures, but laboratory experiments suggest that concrete nearly saturated with water is expected to have values of D exceeding 10^{-6} cm²/sec. when expressing the oxygen concentration in terms of moles per unit volume of pore water. The value of D increases markedly when saturation is less than complete.^{16,18,19} Accordingly, the assumed profile ranged between values of $D = 10^{-3}$ and 10^{-5} cm²/sec.

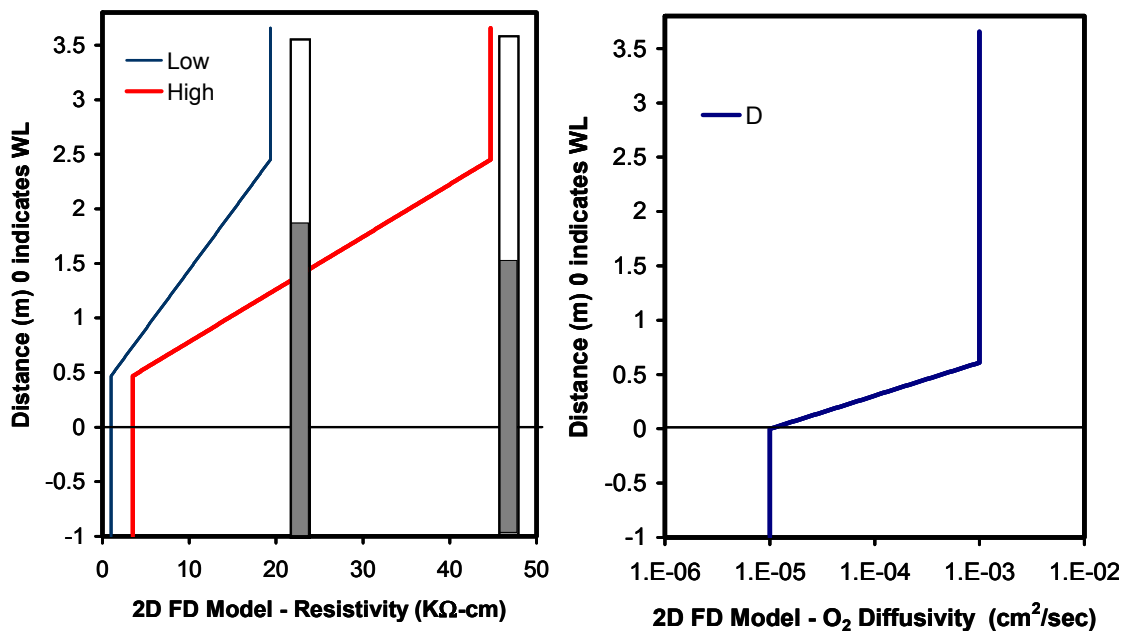


Figure 66: Resistivity and diffusivity profiles assumed for the 2D FD model. Active and passive regions are also indicated.

Electrochemical Variables. The calculations treated only the case of a footer/column that had been in service long enough for severe Cl⁻ contamination over the entire lower portion of the rebar cage so that this steel was active to an elevation of either 1.830 m or 1.524 m above the mean water line. For the higher elevation passive steel, the current density, i_p , was taken as 1×10^{-8} A/cm². The lower active steel dissolution was modeled by assuming Butler-Volmer kinetic control of the reaction $\text{Fe} \rightarrow \text{Fe}^{++} + 2\text{e}^-$ with constant activity for reactant and products. Only one cathodic reaction (oxygen reduction, $\text{O}_2 + 2 \text{H}_2\text{O} + 4\text{e}^- \rightarrow 4 \text{OH}^-$) was considered, with this also obeying Butler-Volmer kinetics but allowing for variation in oxygen activity. The kinetic constants for these reactions are given in Table 37. These assumptions are sweeping simplifications of the actual behavior of reinforcing steel in concrete but represent a reasonable first approximation for the purposes of examining the sensitivity of the cathodic protection scheme to variations in basic system properties. Furthermore, the kinetic constant values were selected to reflect experimentally observed magnitudes and create operating conditions that are representative of conditions often encountered in the field.

Table 37: Kinetic constants for the corrosion reactions.

$i_{0a} = 1.875 \cdot 10^{-2} \mu\text{A}$	$E_{0a} = -780 \text{ mV SCE}$	$\beta_a = 60 \text{ (mV/decade)}$
$i_{0c} = 6.25 \cdot 10^{-4} \mu\text{A}$	$E_{0c} = 160 \text{ mV SCE}$	$\beta_c = 160 \text{ (mV/decade)}$
$C_0 = 2.5 \cdot 10^{-7} \text{ mol / cm}^3$ (assumed O ₂ solubility, in pore water)		

The MgSBA was considered to be large enough to effectively create a fixed potential difference between the rebar cage steel and the sea water immediately in contact with the submerged concrete surface. This condition is reasonable for common commercial anodes since for the cases examined, the total calculated anode currents were mostly less than 300 mA. A value of -1,320 mV (Ag/AgCl) was used as a convenient nominal working anode potential. As the seawater resistivity value ($\rho \approx 20 \Omega \cdot \text{cm}$) is much smaller than was assumed for concrete, the assumption of an equi-potential concrete-seawater interface is also a justifiable approximation.

2D FD Computational Procedure: Numerical calculations were handled by the same scheme used in a previous investigation.²⁰ The model was adapted to have the geometry described above by using a computational grid of 384 nodes in the vertical direction and 60 in the radial direction with a grid spacing of 1.27 cm in both directions.

1-D Model Description and Implementation

The simplified 1-D model retained most of the properties of the Finite Difference 2-D model but required a small fraction of the computational resources. This 1-D model is a modified version of one developed previously for a cathodically polarized substructure element²¹ and was implemented for conditions similar to those modeled with the detailed 2-D model. A major difference between the models was that the 1-D model did not include provisions for oxygen transport nor for a transition between active and passive steel. For this approach, the resistivity profiles were modeled using the maximum, minimum, and averages values for the experimental data (Figure 66). A detailed description of the 1-D model was presented previously,²² and so only a brief review is provided here. The 1.524 m diameter column was assumed to consist of a stack of discrete steel segments in concrete with all segments considered to be net cathodes. A constant potential source simulated a ZnSBA or MgSBA. Figure 67 shows the large-signal electrical equivalent circuit for the case where segments 1 to 9 are net cathodes. Nine segments were used with a segmented thickness, dx , of 0.305 m, thus discretizing a 2.74 m column. The submerged portion was omitted in this model as this region was assumed to have a surface potential equal to that of the SBA potential source. A value for i_{OC} was taken as 2.5×10^{-11} A/cm² in combination with $E_{OC} = 235$ mV (i_{oc} and E_{OC} are the exchange current density and exchange potential, respectively, for the cathodic reaction) with an open circuit potential of ~ -100 mV, which is typical of passive steel. Also, the Tafel parameter, β_c , was taken as 145 mV/decade which is similar to the value used in Reference 17. A constant potential source beneath the lowest column slice component simulated presence of the SBA. As noted above, the potential source value was -1,320 mV. The 1D model assumed a resistive path with cathodic polarization present and that the steel was not corroding.

Results

Figure 68 shows results from the 1D model for the three assumed resistivity profiles compared to the experimental potential profiles measured on Pier 2 four hours after energizing. The potential calculated for the average and low resistivity profiles tend to be more negative than the measured potential values at elevations lower than 0.5 m. For higher elevations, the computed potentials tend to be more noble but still follow the experimentally observed trend. These observations are easier to see when comparing the 1D model versus the average potential (series with symbols and connecting line).

For the 2D FD model, the extent of cathodic protection was examined by observing the potential obtained for the computed cases and comparing this to the average, maximum, and minimum potential profiles from the experimental observations on Pier 2 after four hours of energizing, with the results being as shown in Figure 69. The experimental maximum (more noble) and average potential values appear to

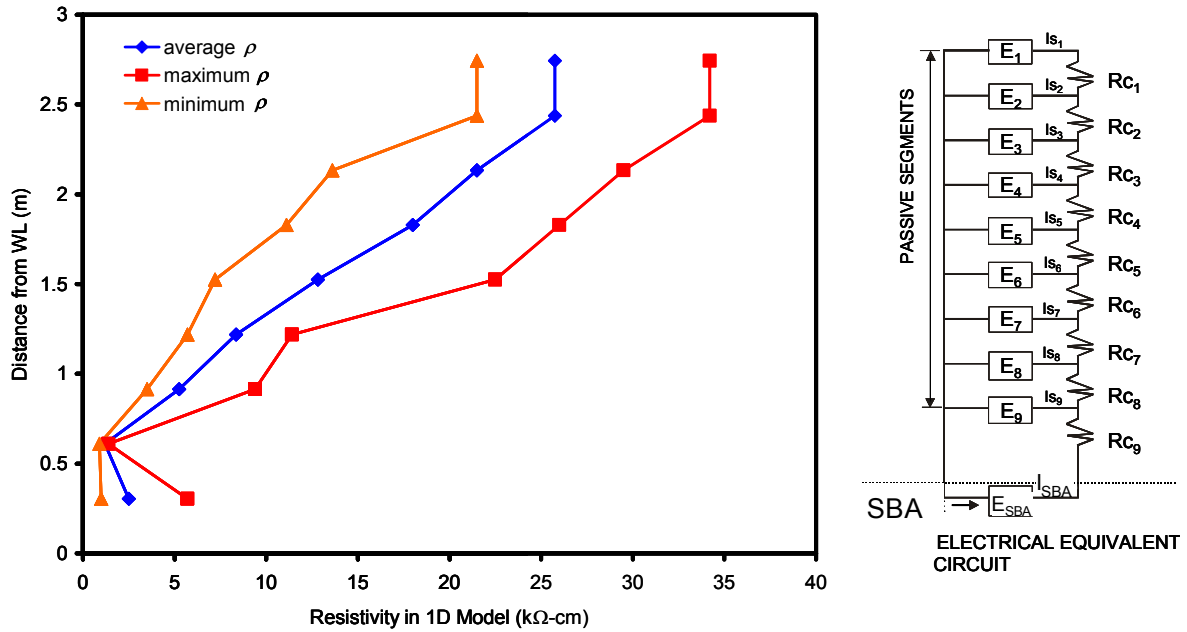


Figure 67: Resistivity profiles used with the 1D model.

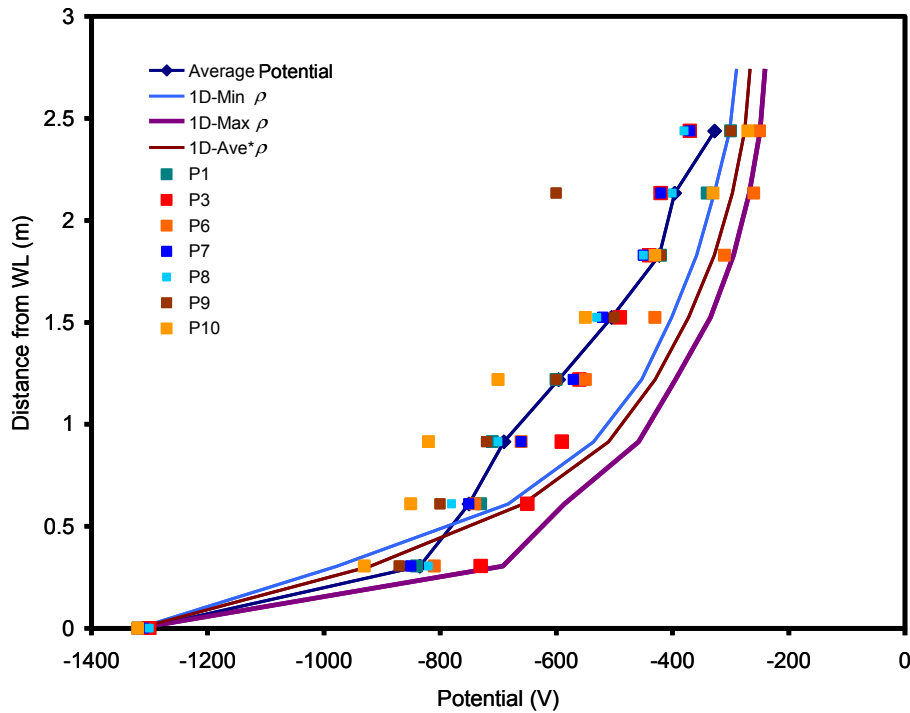


Figure 68: Comparison of 1D model results and experimental potential values after four hours of energizing the system (the average field measurement results are indicated by the series with symbols and connecting line).

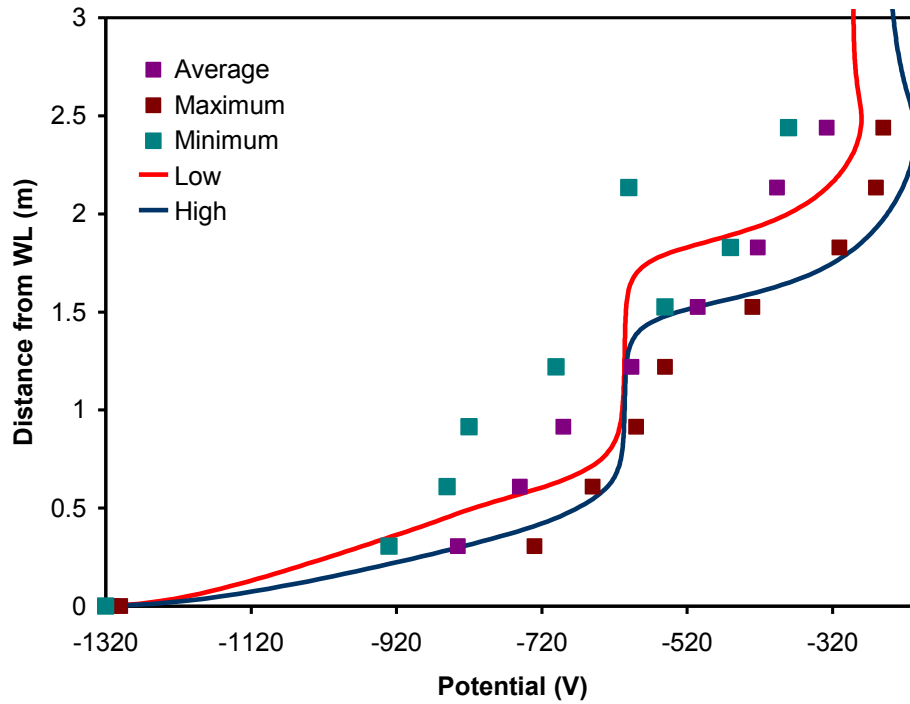


Figure 69: Potential profiles 2D FD versus experimental potential profiles (squares indicate experimental values)

be comprised of two distinctive regions. These are more obvious on the computed potential profiles, where it appears that the lower portion of the pile has different electrochemical kinetics than the upper region. The computed potential profiles when compared to the experimental values suggest that the lower portion of the footer/column is active while the upper portion of the column is passive. Thus, there was reasonable agreement between the experimental measurements and both computational models.

CONCLUSIONS

Field measurements and modeling were performed on two substructure piers each of the Bahia Honda and Niles Channel Bridges in the Florida Keys to characterize the extent to which cathodic polarization and protection can be affected at above-waterline elevations by submerged bulk anodes (SBAs). Reinforcement in the Bahia Honda Bridge is black bar, whereas for the Niles Channel it is epoxy-coated. For the former bridge, Zn SBAs (ZnSBAs) were employed and for the latter Mg SBAs (MgSBAs). In both cases, the physical and electrochemical systems were modeled numerically. For the former bridge (Bahia Honda) this was done using commercially available Beasy™ Boundary Element Modeling software, whereas for the latter both a finite difference two dimensional (2-D) and a simplified one-dimensional (1-D) approach were employed. Findings include the following:

Bahia Honda Bridge

1. A direct relationship was apparent between concrete resistivity and reinforcement-free corrosion potential (higher resistivity, more positive potential).
2. This field study indicated that ZnSBAs affected polarizations greater than 100 mV to the top of the footers (~1m above mean water level). In the columns, polarization decayed sharply above the base and was nil 2.0-2.5 m above the base of the footers. This sharp decay was probably facilitated by the fact that column spalls had previously been repaired by guniting and the added material had disbonded. Polarization probably would have occurred to a higher elevation had the column concrete been sound.
3. Agreement between the field polarization results and boundary element modeling was good but with the latter projecting greater polarization at the column. This probably occurred because the disbonded gunite repair limited polarization from the ZnSBAs. Modeling based upon MgSBA indicated that polarization in excess of 125 mV could be achieved at elevations greater than 2 m above the waterline.
4. Although further study is needed, ZnSBAs appear to be a low cost, technically viable option for affecting corrosion control in situations where 1) protection need not be complete above about 1m MHT or 2) some corrosion is acceptable above this elevation.

Niles Channel Bridge

1. As for the Bahia Honda Bridge, a direct relationship was apparent between concrete resistivity and reinforcement-free corrosion potential (higher resistivity, more positive potential).
2. The submerged bulk galvanic magnesium anodes (MgSBAs) affected polarizations greater than 100 mV to the top of the footers (~1m above mean water level). Results in the columns were mixed but with 100 mV depolarization being achieved in some cases to as high as 2.5 m above mean water. However, there was relatively large data scatter which was attributed to lack of electrical continuity for the epoxy-coated bars.
3. Utility of MgSBAs on piers where thermally sprayed Zn (TSZ) has been applied to the column was limited, apparently because of the Zn serving as a current drain.
4. Agreement between the measured current-on potential profiles and those projected from the two modeling approaches was good. The 1D model projected greater polarization at the lower region of the column for cases involving average and low resistivity, whereas at elevations higher than 0.5 m above the waterline the projected polarization was smaller than the measured values. The 2D model results, which included oxygen concentration polarization at the lower portion of the column and transition of the steel from active to passive with increasing height, better matched the experimentally determined profiles.

Summarizing Conclusions

1. The FDOT should aggressively pursue follow-up field trials to better document the utility of both Zn- and MgSBAs with the former having utility for substructures comprised of prestressed components and the latter where only conventional steel is present. In the case of epoxy coated reinforcement, steps should be taken to ensure that the steel is electrically continuous.
2. Because galvanic cathodic protection systems based upon TSZ, as has been widely employed by the FDOT, are expensive to apply and have a relatively short life, an experimental effort should be developed to explore the utility and means by which residual, expiring TSZ can be removed from columns or alternatively, disconnected from the reinforcement, and protection reinstated using MgSBAs.

3. Results from the numerical modeling portion of the study indicated generally good agreement between this and experimentally acquired data from the field. Using the Boundary Element software involves acquiring a license from BEASY and developing the necessary skills for its application. Alternatively, BEASY provides in-house consulting services that can perform this based upon the requisite geometry and parameter input. Utilization of the Finite Difference approach requires that user friendly software be developed that allows input of structure geometry parameters, concrete resistivity and oxygen concentration, and reinforcement electrochemical properties.

REFERENCES

- ¹ R.G. Powers, A.A. Sagüés, and T. Murase, "Sprayed-Zinc Galvanic Anodes for the Cathodic Protection of Reinforcing Steel In Concrete, Materials Performance and Prevention of Deficiencies and Failures, Ed.: T.D. White, American Society of Civil Engineers, New York, NY, 1992, p. 732.
- ² A.A. Sagüés, R.G. Powers, T. Murase, and I.R. Lasa, "Low-Cost Sprayed Zinc Galvanic Anode for Control of Corrosion of Reinforcing Steel in Marine Bridge Substructures," Final Report, Contract No. SHRP-88-ID024, Strategic Highway Research Program, National Research Council, Washington, DC, 1994.
- ³ J.A. Apostolos, D.M. Parks, and R.A. Carello, "Cathodic Protection Using Metallized Zinc, CORROSION/87, paper no. 137, San Francisco, CA, March 9-13, 1987.
- ⁴ R.J. Kessler, and Powers, R.G., "Zinc Metallizing for Galvanic Cathodic Protection of Steel Reinforced Concrete in a Marine Environment," CORROSION/90, paper no 324, Las Vegas, NV, April 23-27, 1990.
- ⁵ R.J. Kessler, "History and Performance of Marine Substructure Cathodic Protection Systems in Florida," Proceedings International Conference on Corrosion and Rehabilitation of Reinforced Concrete Structures, Orlando, FL, December 7-11, 1998.
- ⁶ B.S.Covino, S.J. Bullard, G.R. Holcomb, J.H. Russell, S.D. Cramer, J.E. Bennett, and H.M. Laylor, Materials Performance, vol. 38(12), 1999, p. 28.
- ⁷ R.J. Kessler, R.G. Powers, and I.R. Lasa, "An Update on the Long Term Use of Cathodic Protection of Steel Reinforced Concrete Marine Structures," CORROSION/02, paper no. 02254, Denver, CO, April 7-11, 2002.
- ⁸ M. Funahashi, S.F. Daily, and W.T. Young, "Performance of Newly Developed Sprayed Anode Cathodic Protection System, paper no. 254, New Orleans, LA, March 10-14, 1997.
- ⁹ J.E. Bennett and C. Firlotte, "A Zinc/Hydrogel System for Cathodic Protection of Reinforced Concrete Structures," CORROSION/96, paper no. 316, Denver, CO, March 25-29, 1996.
- ¹⁰ R.J. Kessler, R.G. Powers, and I.R.Lasa, "Cathodic Protection Using Scrap and Recycled Materials," CORROSION/91, paper no. 555, Cincinnati, OH, March 11-15, 1991.
- ¹¹ R.J. Kessler and R.G. Powers, "Update on Sacrificial Anode Cathodic Protection of Steel Reinforced Concrete Structures in Sea Water," CORROSION/95, paper no. 516, Orlando, FL, March 26-31, 1995.
- ¹² I.R. Lasa, R.G. Powers, and W.H. Hartt, "Jacketing and Jacket-Galvanic Cathodic Protection Systems for Marine Pilings," Proceedings First International Conference on Concrete Repair, Eds.: M. Grantham, F. Rendell, R. Jauberthis, GR Technologies, Ltd., London, 2003.
- ¹³ D.W. Whitmore, "Impressed Current and Galvanic Discrete Anode Cathodic Protection for Corrosion Protection of Concrete Structures, CORROSION/02, paper no. 02263, Denver, CO, April 7-11, 2002.
- ¹⁴ D. Whiting, M. Nagi, and J.P. Broomfield, "Evaluations of Sacrificial Anodes for Cathodic Protection of Reinforced Concrete Bridge Decks," Report No. FHWA-RD-95-041, Federal Highway Administration, Washington, DC, 1994.
- ¹⁵ NACE SP0176-2007, "Corrosion Control of Submerged Areas of Permanently Installed Steel Offshore Structures Associated with Petroleum Production," NACE International, Houston, 2007.
- ¹⁶ F.J. Presuel-Moreno, S.C. Kranc, and A.A. Sagüés, Corrosion, vol 61, 2005, p. 548.
- ¹⁷ A.A. Sagüés, S.C. Kranc, and Presuel-Moreno, F.J., "Advanced Computational Model for Sacrificial Cathodic Protection of Partially submerged Reinforced Concrete Marine Footers," in Repair and Rehabilitation of Reinforced Concrete Structures: The State of the Art, Eds.: W.P. Silva-Araya, O.T. de Rincon, and L. Pumarada O'Neill, American Society for Civil Engineers, Reston, VA, 1998, p. 1.
- ¹⁸ O. Gjorv, O Vennesland, A. El-Busaidy, "Diffusion of Dissolved Oxygen Through Concrete", Materials Performance, vol 25 (12), 1986, p. 39.

-
- ¹⁹ K. Tuutti,, “Corrosion of Steel in Concrete,” Swedish Cement and Concrete Research Institute, Stockholm, Sweden, 1982.
- ²⁰ S.C. Kranc and A.A. Sagüés, “Computation of Reinforcing Steel Corrosion Distribution in Concrete Marine Bridge Substructures”, Corrosion, vol 50, 1994, p. 50.
- ²¹ A.A. Sagüés, H.M. Perez-Duran, and R.G. Powers, “Corrosion Performance of Epoxy-Coated Reinforcing Steel in Marine Substructure Service”, Corrosion, vol 47, 1991, p. 884.
- ²² F.J. Presuel-Moreno, S.C. Kranc S.C., and A.A. Sagüés, “Cathodic Prevention Distribution in Partially Submerged Reinforced Concrete” Corrosion, vol 61, 2005, p 548.